國 立 交 通 大 學

電子工程學系電子研究所

博 士 論 文

提升高速用戶迴路系統性能之研究

Performance Enhancement for DMT-based VDSL

System: Precursor ISI-Free Frame Synchronization,

ISI Cancellation and Optimizing Throughput

研 究 生 ： 林 尚 亭

指 導 教 授 ： 魏 哲 和

中華民國九十四年七月

提升高速用戶迴路系統性能之研究

Performance Enhancement for DMT-based VDSL System: Precursor ISI-Free Frame Synchronization, ISI Cancellation and Optimizing Throughput

研 究 生: 林 尚 亭   Student: Sun-Ting Lin

指導教授: 魏 哲 和 博士   Advisor: Dr. Che-Ho Wei

國 立 交 通 大 學

電子工程學系電子研究所

博 士 論 文

A Dissertation

Submitted to Department of Electronics Engineering

& Institute of Electronics

College of Electrical Engineering and Computer Science

National Chiao Tung University

in Partial Fulfillment of the Requirements

for the Degree of

Doctor of Philosophy

in

Electronic Engineering

July 2005

Hsinchu, Taiwan, Republic of China

中華民國九十四年七月

提升高速用戶迴路系統性能之研究

研究生: 林尚亭　　　　　　　　指導教授: 魏哲和

國立交通大學電子工程學系電子研究所

摘要

DMT (Discrete multitone) 調變技術是目前絕大多數非對稱性用戶迴路 (ADSL)系統所採用的技術，在本論文中，我們首先提出一個觀念，利用增加取樣速度，提升原有非對稱性用戶迴路系統的傳輸速率至高速用戶迴路系統(VDSL)的範圍。 同時我們也提出一些演算法來降低信號相互干擾 (ISI)，以提升系統傳輸效能。

本論文主要分為三部分，第一部分是有關提升原有非對稱性用戶迴路系統的傳輸速率至高速用戶迴路系統的範圍，要達到這個目標，必須要提高使用頻寬。提高使用頻寬可從二方面進行，一是增大 FFT/IFFT 尺寸，另一方面若維持FFT/IFFT 大小不變，則需要增加每一個次通道(sub-channel) 的頻寬，為了探討增加頻寬是否改變原有次通道的特性，即每一個次通道內訊號雜訊比變化不能過大，我們針對每一個次通道內訊號雜訊比變化由原本 4 kHz 頻寬依序倍增到 20 kHz 進行分析，同時也針對在不同長度的電話線在各種干擾和雜訊的影響之下，此

高速用戶迴路系統所能達到的最佳傳輸速率。

　　第二部分則是有關高速用戶迴路系統碼框定位的相關演算法，我們研究一種所謂低複雜度最大可能(low-complexity maximum likelihood)預測演算法，並加以改良，以適合高速用戶迴路系統使用。同時以數學推導証明我們改良的演算法比原有的效能好，因為它能找出傳送資料經過通道影響後真正的碼框起始點，原本的演算法則會因為通道效應影響，後移數個位置到通道強度高峰之處，造成所謂前置信號相互干擾 (precursor ISI)，影響接收端的信號雜訊比。用電腦模擬方式，也可以比較出兩種演算法在接收端的信號雜訊比，我們改良過的演算法表現較佳。

　　第三部分，我們引進一種以遞迴方式，減少殘餘信號相互干擾，降低接收端的數元錯誤率，如此可以減少兩組信號間的防護間隔 (guard interval)，甚至於可以完全不用防護間隔，可提高系統傳輸效能。

Performance Enhancement for DMT-based VDSL System: Precursor ISI-Free Frame Synchronization, ISI Cancellation and Optimizing Throughput

Student: Sun-Ting Lin   Advisor: Dr. Che-Ho Wei

Department of Electronics Engineering

& Institute of Electronics

National Chiao Tung University

Abstract

Discrete multitone (DMT) modulation is the technology selected for most ADSL systems.   In this dissertation, we proposed a concept to upgrade this DMT-based ADSL system to the VDSL transmission data rate by increasing the sampling rate. We also proposed algorithms to improve the performance of this DMT-based VDSL system by minimizing the influence of inter-symbol interference (ISI).

This dissertation is divided into three parts. In the first part, we try to upgrade the transmission data rate of traditional DMT-based ADSL system to the VDSL range by raising the sampling rate. The sub-channel spacing will grow with the same ratio if the

identical FFT is used. The sub-channel flatness and capacity for VDSL test loops are analyzed by varying the symbol rate from 4 kHz to 20 kHz. In this part, we also investigate the throughput of DMT-based VDSL system at high sampling rates under the influence of various noises/interferences. The throughput limitation of the VDSL system is discussed and the optimal solutions of the sampling rates under various test loop lengths and environment conditions are also investigated.

In the second part, a new modified low-complexity maximum likelihood (ML) algorithm for frame synchronization in discrete multitone VDSL transmission system is derived. Computer simulation results are included to show its improvement in Et/N_0 of each tone in the received data. This algorithm estimates the frame boundary at the initial transition edge rather than at the middle peak of a shortened twisted-pair channel response. The timing margin degradation caused by precursor ISI can be reduced significantly, especially when the sub-channels are loaded with more bits.

In the third part, an iterative ISI cancellation algorithm is presented to improve the DMT-based VDSL system by canceling the residual ISI outside the guard interval recursively. The guard interval of the system can be shortened to raise the bandwidth efficiency. In addition, by some modifications, the BER performance can be improved significantly even without any guard interval.

Acknowledgements

First of all, I would like to express my sincere gratitude to my advisor, Dr. Che-Ho Wei, for his patient guidance and profound influence down the road to graduate.

Special thanks to my friends and colleagues for their genuine encouragement, kind help, etc.

Finally, I am deeply indebted to my whole family for their love and supports. This dissertation is dedicated to my grandmother, mother, husband, and daughter. Without their wholehearted care and full support, it is impossible for me to accomplish it.

CONTENTS

List of Tables

List of Figures

Glossary

ADSL	Asymmetric Digital Subscriber Line
ADSL2	Asymmetric Digital Subscriber Line - Second Generation
ADSL2+	Extended Bandwidth ADSL2
ANSI	American National Standards Institute
ATU-C	ADSL Transceiver Unit at Central Office Side
AWGN	Additive White Gaussian Noise
BER	Bit-Error Rate
CAP	Carrierless Amplitude Phase
CO	Central Office
CP	Cyclic Prefix
CPE	Customer Premise Equipment
CSA	Carrier Service Area
DMT	Discrete Multi-Tone
DS	Downstream
DSL	Digital Subscriber Line
ETSI	European Telecommunications Standards Institute
FEQ	Frequency Domain Equalizer
FEXT	Far End Crosstalk
FDD	Frequency Division Duplex
FFT	Fast Fourier Transform
FIR	Finite Impulse Response
HDSL	High Bit Rate Digital Subscriber Line
HDSL2	High Bit Rate Digital Subscriber Line - 2nd Generation

IFFT	Inverse Fast Fourier Transform
IRS	Impulse Response Shortening
ISDN	Integrated Service Digital Network
ITU	International Telecom Union
IIC	Iterative ISI Cancellation
IIC-ZP	Iterative ISI Cancellation with Zero-Padded
ISI	Intersymbol Interference
MMSE	Minimum Mean Square Error
ML	Maximum Likelihood
NEXT	Near End Crosstalk
OFDM	Orthogonal Frequency Division Multiplexing
PSD	Power Spectral Density
QAM	Quadrature Amplitude Modulation
RFI	Radio Frequency Interference
RISIC	Residual ISI Cancellation
SER	Symbol-Error Rate
SIR	Shortened Impulse Response
SISO	Soft Input Soft Output
SNR	Signal to Noise Ratio
TEQ	Time-domain Equalizer
TP	Twisted-Pair
US	Upstream
VDSL	Very-High-Bit-Rate Digital Subscriber Line
VDSL2	Very-High-Bit-Rate Digital Subscriber Line - Second Generation
ZP	Zero-Padding

Chapter 1

Introduction

In the times before the invention of the telecommunication system, all the information interchange between different places had to be carried by people or other trained animals. Therefore, it is hard to imagine the real-time communication system between separate locations. The invention of telephone systems changes our life style significantly. Although there are various types of telecommunication systems, from the telegraph, telephone, to Internet, their essential function is to provide communication facilities between people from all over the world. With the progress of telecommunication system, the formats of the interchange information include from plain text, real time voices to video, etc., and thus the demand of communication bandwidth explodes dramatically. Due to the rapid development of computer and consumer electronics, traditional telephone subscribers are ready for new services based on digital technologies. There is a lot of accessible information on the Internet, the demands of bandwidth by the residential users drive the digital subscriber loop (DSL) systems to become more mature.

There are two candidates for the Internet networks: cable modem provided by cable TV companies, or DSL system provided by traditional telecommunication companies. The details of performance comparisons between these two systems are not covered in this dissertation. In summary, each of them has its advantages and limitations. However, the

DSL system is much more popular in Taiwan because most last-mile twisted-pair telephone wires are short enough for the DSL system to be operated. In addition, the Chung-Hwa Telecommunication company has been very active to establish the DSL network and promote the DSL service since the very beginning.

Actually, the DSL technology has been studied earlier to improve the bandwidth efficiency of the twisted-pair lines, but it is not attended to until the population of the Internet becomes very large. Since the end user usually attend to download or browse a lot of data from the Internet, the technology called asymmetric DSL (ADSL) is selected by most traditional telecommunication company to provide the Internet services. The ADSL system was developed for video-on-demand services since 1991 with a high transmission throughput from a central office to telephone subscribers downstream [1]. The first generation ADSL standards are capable of a downstream transmission throughput of 6.433 Mbits/s over carrier serving area (CSA) distance. For longer telephone subscriber loops confirming the resistance design rule, the downstream transmission throughput is reduced to 1.544 Mbits/s.
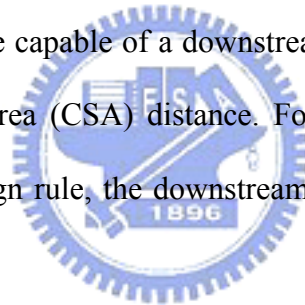
Discrete Multi-Tone (DMT) modulation is the ADSL modem standard approved by ANSI [2]. But DMT is being challenged by the other technology known as Carrierless Amplitude Phase (CAP) modulation. Both systems work very well, according to users at telephone companies that are trialing ADSL before they market the services. There are many discussions on the other advantages/disadvantages of CAP vs. DMT. A reasonably impartial summary of these is [3]:

1. DMT can direct information to sub-carriers and modulate them independently. CAP has a single carrier which has to be treated as a whole, even though channel characteristics vary widely. As a result, DMT may deliver better performance or be more spectrally efficient (i.e., for standard ADSL, DMT only needs roughly two-thirds the bandwidth of CAP).

2. DMT is more complex to initialize and needs more power-up time than CAP.

3. DMT is inherently and straightforwardly rate-adaptive. It delivers the maximum data for any given line. This allows the support of higher rates over shorter loops (8 Mbits/s), or sub-rate connections at very long reach. CAP can support rate adaptation by varying the constellation and the bandwidth, but it requires very careful analog design, and the rates have much lower granularity. DMT steps in 32 kbits/s steps from 64 kbits/s to 8 Mbits/s vs. CAP's 320 kbits/s steps from 320 kbits/s to 7 Mbits/s.

4. DMT has much greater latency; this may actually infringe some specifications for special services such as ISDN.

5. CAP is more resistant to RFI, although DMT can be more adept at coping with multiple or varying RFI sources.

6. CAP has a lower peak-to-average ratio which simplifies the design of the analog stage and reduces its power needs for a given bandwidth and power-spectral-density.

7. It is simple for DMT to meet an arbitrary or variable power mask spectrum for spectral compatibility.

8. Echo-cancellation in DMT is more difficult.

9. Because its symbols are longer, DMT has greater immunity to impulse noise than CAP.

10. CAP can be easier to optimize to a specific application. DMT can be more complex, but it supports more versatility and flexibility. This is important in ADSL with many applications and a wide range of environments.

11. DMT's analysis and measurement functions can be used for diagnostics and testing to detect out-of-specification systems or for preventive maintenance of the copper lines.
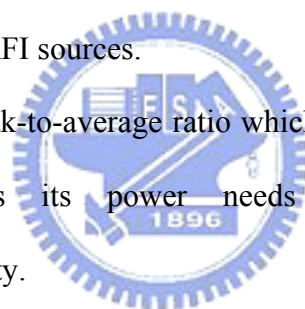
Bellcore (with Bell Telephone and Nynex) organized the "ADSL Olympics" to evaluate and compare three line code contenders from 1993. Trial results indicated that DMT had performed better than CAP and QAM (Quadrature Amplitude Modulation). Consequently, although not unanimously embraced, both ANSI (for the USA) and ETSI (for Europe) adopted DMT, and ANSI T1.413 [2] was born. The standard today is endorsed by the ITU. When we began our research of ADSL transceiver from 1998, DMT-based ADSL system has been popular since it is superior in dealing with line impairments. DMT has since been widely deployed, and proven its value as a successful line-coding approach, therefore, we focus to study and improve the DMT-based ADSL system at first.

Although the transmission throughput of the ADSL system is much more than the traditional dial-up modem (only up to 56 kbits/s), it still needs to be improved to provide more advanced broadband multimedia services. Due to the population increase of fiber on the telecommunication network, the length of twisted-pair line as the last-mile can be gradually reduced. The available frequency spectrum of these short copper wires for transmission becomes much broader and its optimal data rate grows dramatically. A service called very-high-speed DSL (VDSL) [4][5][6][7] has been under study since late 1995, which can provide up to 52 Mbits/s over short telephone line, to meet the requirements for broadband access-network. VDSL can be regarded as an evolution of the ADSL system, which uses the frequency band from a few hundred kilohertz to beyond 10 MHz on some loops.

The standard of VDSL system is under study at ITU-T, ANSI [4], and ETSI at 1998, it is desirable to construct a solution that can support either symmetric or asymmetric transmission. Although the ADSL system was mature in the commercial applications at that time, there are some issues to improve their performance closer to their line capacity limits, such as frame synchronization approach, reducing the inter-symbol interference (ISI) and to increasing the data transmission rate, etc. From those studies, we found a method to extend

the data transmission rate and then improve the DMT-based ADSL system to the performance of VDSL system by increasing the sampling rates. Based on this concept, we proposed a DMT-based VDSL system similar to the structure of the traditional DMT-based ADSL one.

In this dissertation, the performance of DMT-based VDSL system is investigated. The system architecture is introduced at first and then the channel response modeling of the DSL environment is derived in Chapter 2. Chapter 3 is the bit-loading capacity for various channels under different environments. In Chapter 4, a low-complexity frame synchronization method is applied to the DMT-based VDSL system, and a modified approach is also proposed to improve the performance of the whole system. From these studies, it is found that the ISI effect causes serious problem to the whole system. Then an iterative ISI cancellation algorithm for the DMT-based VDSL system is presented in Chapter 5.

1.1 DMT-based ADSL/VDSL System Architecture

DMT modulation is a technique in which a transmission channel is partitioned into a number of independent, parallel sub-channels, and each of them carries a lower-speed QAM signal, as shown in Fig. 1.1 [8]. In wireless applications, it is denoted as orthogonal frequency division multiplexing (OFDM) system [9]. The same modulation scheme is also used in the twisted-pair copper lines for data transmission, this application is denoted as DMT-based ADSL system [1].

POTS

4 KHz

1.1 MHz

e.g. 128-QAM
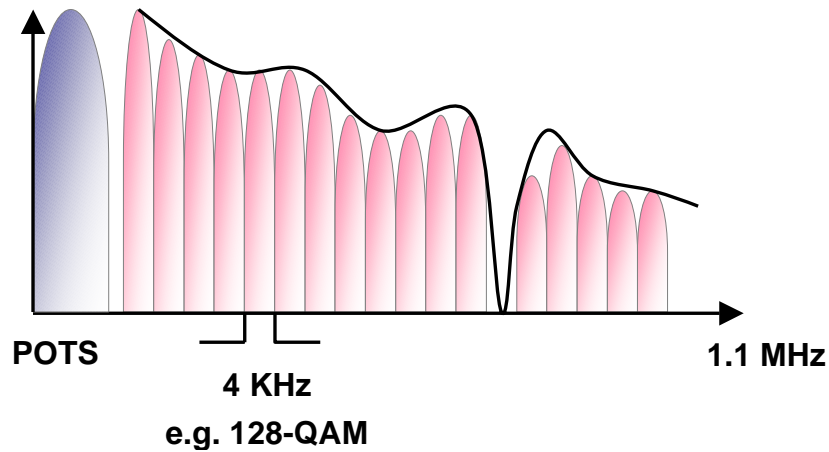
Data rate

= Number of sub-channels x number of bit/sub-channel x modulation symbol rate

Figure 1.1 Discrete multitone line code

From the study of the DMT-based ADSL system, some modifications that can improve the performance of whole system are proposed in this dissertation. These enhancements even can uplift the optimal bit rate to the range of VDSL system by extending the frequency bandwidth. After these ideas are presented in the 2001 IEEE Globecom conference [10], a new system called ADSL2+ [11][12] using double bandwidth was proposed in 2003, which is just similar to our proposed DMT-based VDSL system. In this dissertation, we propose an asymmetric VDSL system, which is upgraded from a DMT-based ADSL system by doubling the sampling rate but remaining the same structure of the DMT symbol.

The VDSL system described in this dissertation is asymmetric with a architecture similar to the ADSL system, as shown in Fig. 1.2 [2]. In this dissertation, we focus on improving the system performance involving modulation, synchronization block, but not the coding parts. The simplified functional blocks of the DMT-based DSL system, including path, noise, transmission and receiver side, are shown in Fig. 1.3.
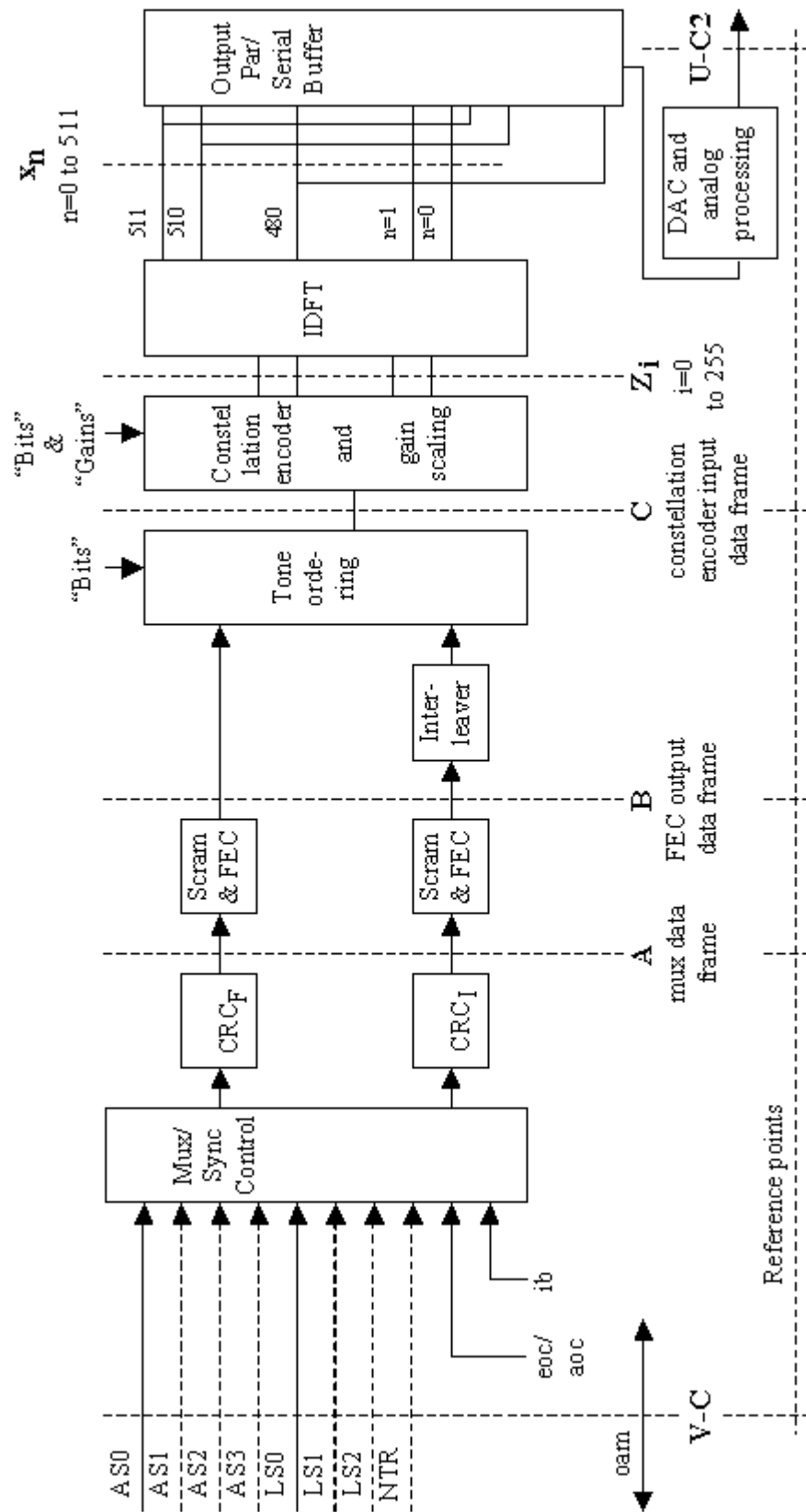
Figure 1.2 Block diagram of an ADSL transceiver unit-central office (ATU-C).
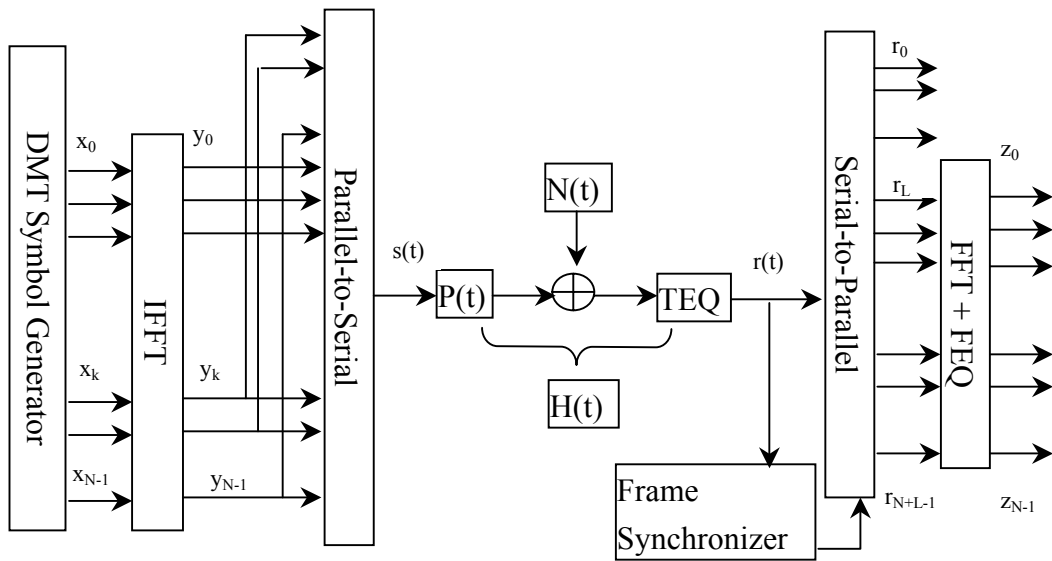
Figure 1.3 Functional block of DMT-based VDSL system.

The maximum transmission data rate supported by this system depends on the characteristics of channel. Therefore, the channel modeling and bit-loading of each sub-channel should be computed. The DMT generator can organize random data into DMT symbols according to these parameters such as the bit-loading of each sub-channel and pilot tone, synchronization symbol, etc. The performance of frame synchronization algorithm is monitored and is measured by calculating the differences between received data and the original one.

The output data of DMT generator, x_k, are used to modulate N sub-carriers by using an inverse Fast Fourier transform (IFFT) to y_k, and the last L samples are copied and put as cyclic prefix to form a frame s_k. P(t) is the channel impulse response of twisted-pair line applied, and H(t) is the transfer function of the system including noise and time-domain equalizer (TEQ). The received data, r(t) is the convolution of s(t) and H(t). In the receiver, after detecting the frame boundary, the first L samples are discarded and the remaining N samples are demodulated by a FFT. A frequency domain equalizer (FEQ) is also applied to

compensate the channel dispersion.

The transmission channel modeling of the twisted-pair lines has played an important role in the engineering of DSL systems. Two sets of test loops employed in this dissertation will be discussed in detail in section 1.2.

The transmission characteristics of these worst-case loops are then simulated with channel impulse responses derived from twisted-pair cable primary parameters. Most twisted-pair phone lines can be well-modeled for transmission at frequencies up to 30 MHz by using the well-known two-port modeling or "ABCD" theory [1][13][14]. The procedure for generating the channel modeling includes transmission-line RLCG characterization, RLGC to ABCD parameters conversion, multiple ABCD section integration, and transfer characteristics of a subscriber loop calculations. According to the parameters and equations mentioned in [15], we have developed a set of MATLAB programs to generate the channel modeling of the twisted-pair lines.

The DMT technique applied to a transmission line can be viewed as a set of independent frequency-indexed sub-channels with center frequency f_i. Each sub- channel is approximately flat that no transmission distortion is evident, and the overall capacity is the summation of the sub-channels. The number of bits per symbol carried by the ith tone (sub-channel) can be calculated using the formula given in reference [1].

1.2 Topology of VDSL Test Loops

There are 8 test loop topologies listed in the VDSL draft standard, namely, from VDSL0 to VDSL7, and their purposes of test are summarized in Table 1.1 while their topologies are shown in Fig. 1.2. Table 1.2 enumerates short, medium, and long-range values for a nominal length variable in VDSL1 through VDSL4 [4]. In order to study the effect of loop length to the whole system, anther set of loops with length from 100 m to 1500 m is the second test set.

In this section, the DMT-based DSL system description and topology of VDSL test loops are introduced. The characteristics of these twisted-pair lines can be modeled by a mathematical method described in the next section.

Table 1.1 VDSL test loops

No.	Rationale
VDSL0	Null loop
VDSL1	Range stress limit, underground cable
VDSL2	Flat-wire vertical drop, horizontal aerial cable on other section
VDSL3	Reinforced-wire vertical drop, horizontal aerial cable on other section
VDSL4	Bridged tap, horizontal aerial cable
VDSL5	Short loop test with bridged taps and various crosstalk
VDSL6	Medium loop test with bridged taps and various crosstalk
VDSL7	Long loop test with bridged taps and various crosstalk

Table 1.2 Nominal length for asymmetric VDSL loops

Variable Name	Short Reach	Medium Reach	Long Reach
x(VDSL1)	1000 ft. (304.8 m)	3000 ft. (914.4 m)	4500 ft.(1.3716 km)
y(VDSL1)	1500 ft. (457.2 m)	3000 ft. (914.4 m)	4500 ft.(1.3716 km)
z(VDSL2)	1500 ft. (457.2 m)	3000 ft. (914.4 m)	4500 ft.(1.3716 km)
u(VDSL3)	1500 ft. (457.2 m)	3000 ft. (914.4 m)	4500 ft.(1.3716 km)
v(VDSL4)	1000 ft. (304.8 m)	3000 ft. (914.4 m)	4500 ft.(1.3716 km)

FP flat untwisted pair

TP1   0.4mm or 26-gauge

TP2   0.5mm or 24-gauge

TP3   DW10

VDSL0

2m TP2
_____

VDSL1

x(=305/913/1372m) TP1
_____

VDSL2

z-76.2 m TP2   76.2m FP

VDSL3

u-76.2m TP2   76.2m TP3

S4_2 = 91.4m, S4_3 = 45.7m, S5_2 = 15.2m TP2

VDSL4

v-91.4m TP1   S4_2   S4_3

VDSL5

                              S5_2

167 m   30.4m   76.2m

TP2   TP2   TP2

VDSL6

503m   198m

TP1   TP2   VDSL5

VDSL7

503m   701m

TP1   TP2   VDSL5
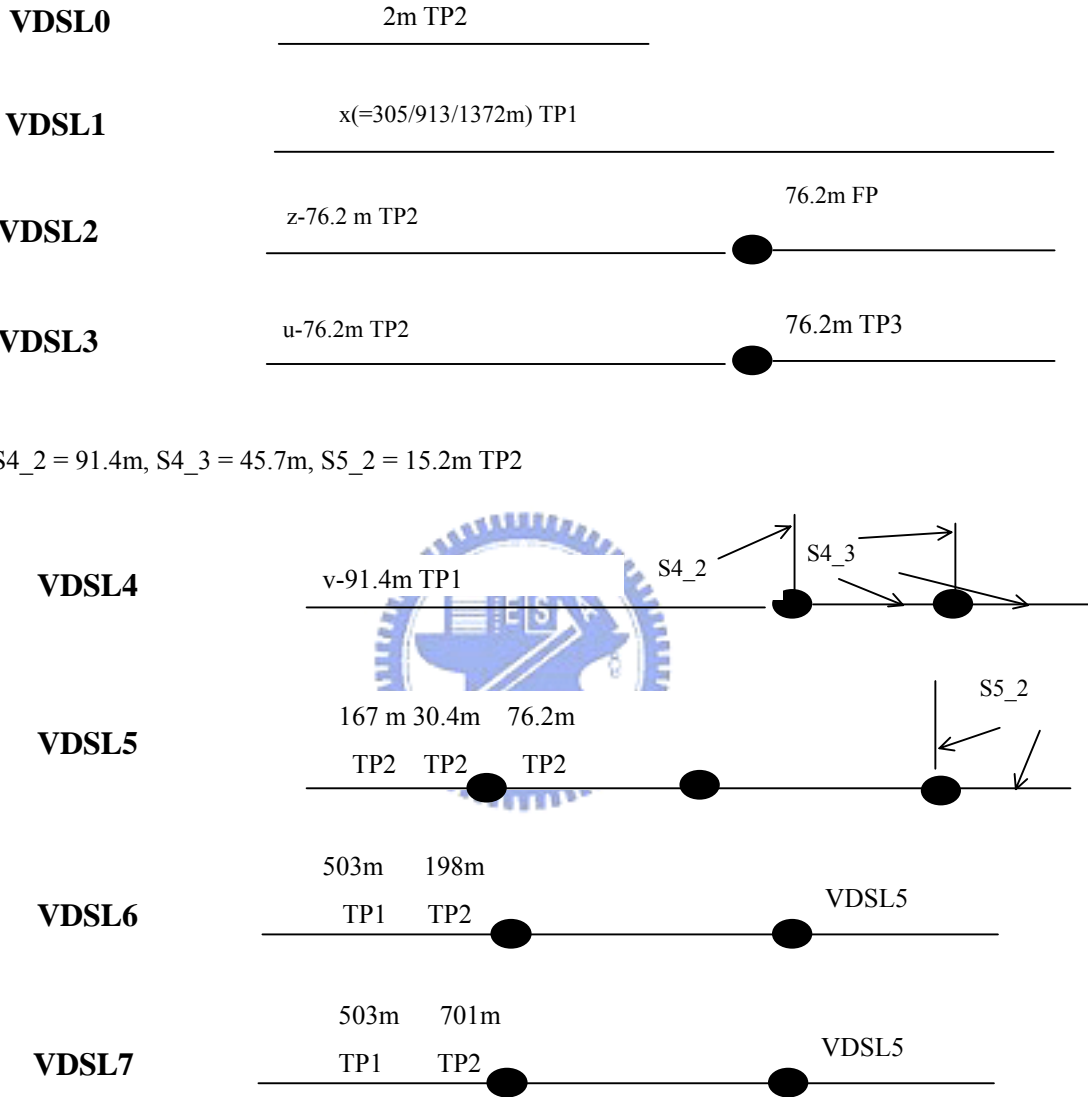
Figure 1.4 Topologies of VDSL test loops.

Chapter 2

Channel Modeling

Most twisted-pair phone lines can be well-modeled for transmission at frequencies up to at least 30 MHz by using what is known as two-port modeling or "ABCD" theory [1][13][14][15][16]. The procedure for generating the channel modeling includes transmission-line RLCG characterization, RLGC to ABCD parameters conversion, multiple ABCD section integration, and transfer characteristics of a subscriber loop calculations, etc. In this chapter, the basic theory of the channel modeling and their computer simulation results are included as well as the relative noise models such as crosstalk and background noises are introduced in this chapter.

2.1 Transmission-line RLCG Characterization

The R, L, C, and G parameters represent resistance, inductance, capacitance, and conductance per unit length of the transmission line, respectively. The two-port characterization of a transmission line can be derived from the per-unit length two-port model in Fig. 2.1.
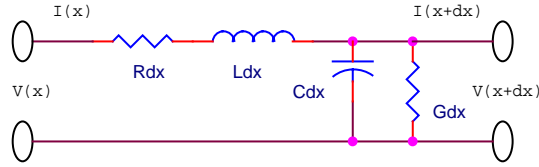
Figure 2.1 Incremental section of twisted-pair transmission line.

The RLCG can be fitted to the measured values which are frequency dependent. The other coefficients in the models are related to the types of twisted-pair lines and can be looked up in reference [1][14]. The curve-fitting RLCG values are listed as

$$R(f) = \cfrac{1}{\cfrac{1}{\sqrt[4]{r_{0c}^4 + a_c \times f^2}} + \cfrac{1}{\sqrt[4]{r_{0s}^4 + a_s \times f^2}}}$$ ……………………………………..(2.1)

$$L(f) = \frac{l_0 + l_\infty \times (f/f_m)^b}{1 + (f/f_m)^b}$$ ……………………………………..(2.2)

$$C(f) = c_\infty + c_0 \cdot f^{-c_e}$$ ……………………………………..(2.3)

$$G(f) = g_0 \cdot f^{+g_e}$$ ……………………………………..(2.4)

where r_{0c} (kΩ/kft) is the copper-line DC resistance; a_c is characterizing the rise of resistance with frequency in the "skin" effect; l_0 (mH/kft) and l_∞ (mH/kft) are the low- and high- frequency inductance, respectively; f (MHz) is the frequency at which R and L are calculated; f_m (MHz) and b are characterizing the transition between low and high frequencies in the measured inductance values.

In this section, the transmission-line RLCG characterization is defined and the curve-fitting formulae of the RLCG parameters for twisted-pair line are also introduced. These parameters can be converted to ABCD matrix parameters.

2.2 Conversion of RLGC to ABCD Parameters

In this section, we introduce how to convert the RLGC to ABCD parameters and the multiple ABCD section integration.

2.2.1 Two-Port Network and ABCD Parameters
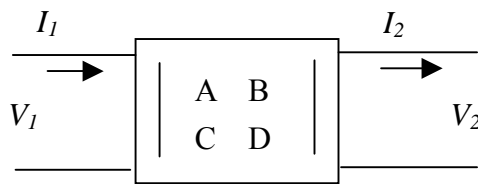
Figure 2.2 Two-port network model.

Fig. 2.2 shows a transmission model of two-port linear circuit. The terminal voltages and currents will be defined by the matrix relationship given by

$$\begin{bmatrix} V_1 \\ I_1 \end{bmatrix} = \begin{bmatrix} A & B \\ C & D \end{bmatrix} \cdot \begin{bmatrix} V_2 \\ I_2 \end{bmatrix} = \Phi \cdot \begin{bmatrix} V_2 \\ I_2 \end{bmatrix}$$ ....(2.5)

Where Φ is a 2x2 matrix of 4 possibly frequency-dependent parameters, A, B, C, and D. All these parameters depend only on the network and not on external connections. For example, ABCD parameters for a simple two-port network consisting of a series impedance, as shown in Fig. 2.3, can be derived as follows

$$\begin{bmatrix} A & B \\ C & D \end{bmatrix} = \begin{bmatrix} 1 & Z \\ 0 & 1 \end{bmatrix}$$ ....(2.6)
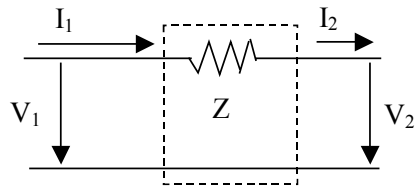
Figure 2.3 A series impedance as a two-port network.
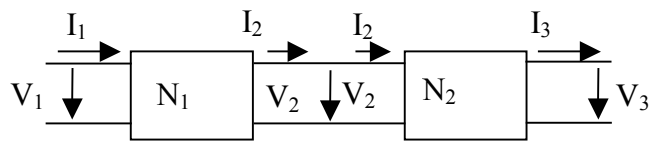
Figure 2.4 Two two-port networks in series.

The ABCD parameters of two two-port networks in series can be obtained by equating the voltage and current of the first two-port network to that of the following network, as shown in Fig. 2.4. For two two-port networks in series, the input and output voltage and current relationship is represented as follows

$$\begin{bmatrix} V_1 \\ I_1 \end{bmatrix} = \begin{bmatrix} A_1 & B_1 \\ C_1 & D_1 \end{bmatrix} \begin{bmatrix} V_2 \\ I_2 \end{bmatrix}$$

$$\begin{bmatrix} V_2 \\ I_2 \end{bmatrix} = \begin{bmatrix} A_2 & B_2 \\ C_2 & D_2 \end{bmatrix} \begin{bmatrix} V_3 \\ I_3 \end{bmatrix}$$
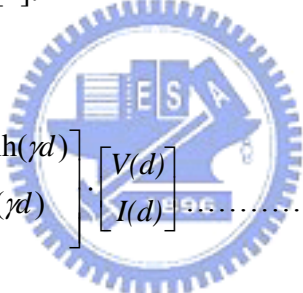
and

$$\begin{bmatrix} V_1 \\ I_1 \end{bmatrix} = \begin{bmatrix} A_1 & B_1 \\ C_1 & D_1 \end{bmatrix} \begin{bmatrix} A_2 & B_2 \\ C_2 & D_2 \end{bmatrix} \begin{bmatrix} V_3 \\ I_3 \end{bmatrix}$$ ……………………………………………………(2.7)

To derive the relationship between "RLCG" and "ABCD" parameters, some new variables have to be introduced. First, the impedance per unit length, Z, is defined as R+jwL and the admittance per unit length, Y, is G+jwC. By taking equations (2.6) and (2.7) into Fig. 2.1, the ABCD parameters of a unit-length twisted-pair line are expressed by

$$\begin{bmatrix} V(x) \\ I(x) \end{bmatrix} = \begin{bmatrix} 1 & Z \\ 0 & 1 \end{bmatrix} \begin{bmatrix} 1 & 0 \\ Y & 1 \end{bmatrix} \begin{bmatrix} V(x+dx) \\ I(x+dx) \end{bmatrix} = \begin{bmatrix} A & B \\ C & D \end{bmatrix} \begin{bmatrix} V(x+dx) \\ I(x+dx) \end{bmatrix} \dots\dots\dots\dots\dots\dots\dots\dots\dots\text{(2.8)}$$

The incremental section of twisted-pair transmission line is calculated by evaluating the voltage and currents at x=0 in terms of those at x=d. The following two-port representation is then obtained [4].

$$\begin{bmatrix} V(0) \\ I(0) \end{bmatrix} = \begin{bmatrix} \cosh(\gamma d) & Z_0 \cdot \sinh(\gamma d) \\ \frac{1}{Z_0} \cdot \sinh(\gamma d) & \cosh(\gamma d) \end{bmatrix} \cdot \begin{bmatrix} V(d) \\ I(d) \end{bmatrix} \dots\dots\dots\dots\dots\dots\dots\dots\dots\text{(2.9)}$$

where the propagation constant γ and characteristic impedance Z_0 of the transmission line are defined, respectively, by

$$\gamma = \sqrt{(R+jwL)\cdot(G+jwC)} = \sqrt{Z \cdot Y} \dots\dots\dots\dots\dots\dots\dots\dots\dots\dots\dots\dots\dots\text{(2.10)}$$

$$Z_0 = \sqrt{\frac{(R+jwL)}{(G+jwC)}} = \sqrt{\frac{Z}{Y}} \dots\dots\dots\dots\dots\dots\dots\dots\dots\dots\dots\dots\dots\text{(2.11)}$$

The "ABCD" parameters are related to the propagation constant γ, characteristic impedance Z_0, and length of a transmission line d. However, a subscriber loop is usually constructed by combining several different lines. In the next section, multiple ABCD section integration and the characteristics of bridged-tap are introduced.

2.2.2 ABCD Parameters of Multiple Sections and Bridged-taps

Since the ABCD matrix of a composite network consisting of two-port networks in series is obtained by the product of these two ABCD parameters matrices as shown in equation (2.7). A cascade of two-port networks has an equivalent two-port matrix that is the product of the component ABCD matrices, in order, as shown by

$$
\begin{bmatrix} V_1 \\ I_1 \end{bmatrix} = \Phi_1 \cdot \Phi_2 \cdots \Phi_{N-1} \cdot \begin{bmatrix} V_N \\ I_N \end{bmatrix} = \Phi \cdot \begin{bmatrix} V_N \\ I_N \end{bmatrix} \quad \text{...(2.12)}
$$
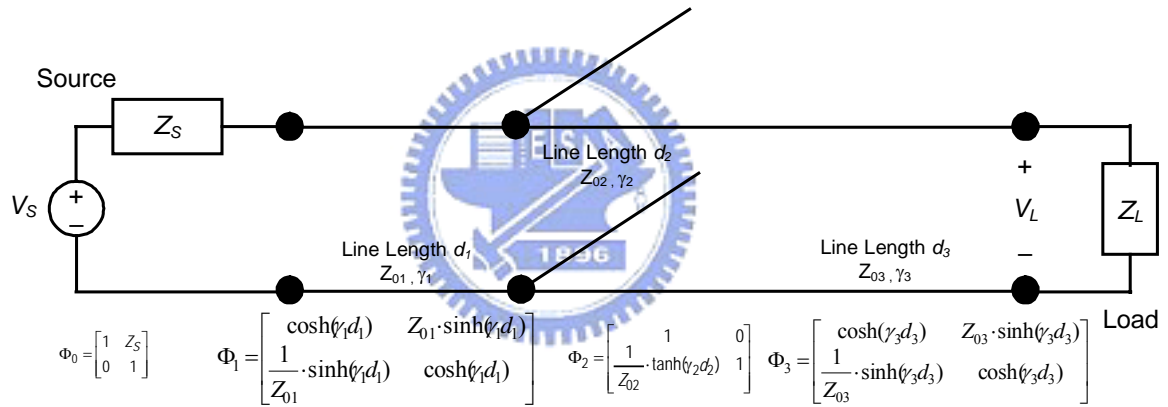
Figure 2.5 Example of two-port cascades for twisted-pair line configurations.

Another more general configuration of loops with bridged-taps and various types of twisted-pair lines is shown in Fig. 2.5. The transmission matrix can be expressed as

$$
\begin{bmatrix} V_S \\ I_S \end{bmatrix} = \Phi_0 \cdot \Phi_1 \cdot \Phi_2 \cdot \Phi_3 \cdot \begin{bmatrix} V_L \\ I_L \end{bmatrix} = \Phi \cdot \begin{bmatrix} V_L \\ I_L \end{bmatrix} \quad \text{...................................(2.13)}
$$

where

$$\Phi_0 = \begin{bmatrix} 1 & Z_s \\ 0 & 1 \end{bmatrix} \quad \dotfill (2.14)$$

$$\Phi_1 = \begin{bmatrix} \cosh(\gamma_1 d_1) & Z_{01} \cdot \sinh(\gamma_1 d_1) \\ \dfrac{1}{Z_{01}} \cdot \sinh(\gamma_1 d_1) & \cosh(\gamma_1 d_1) \end{bmatrix} \quad \dotfill (2.15)$$

$$\Phi_2 = \Phi_t = \begin{bmatrix} 1 & 0 \\ \dfrac{1}{Z_{02}} \cdot \tanh(\gamma_2 d_2) & 1 \end{bmatrix} \quad \dotfill (2.16)$$

$$\Phi_3 = \begin{bmatrix} \cosh(\gamma_3 d_3) & Z_{03} \cdot \sinh(\gamma_3 d_3) \\ \dfrac{1}{Z_{03}} \cdot \sinh(\gamma_3 d_3) & \cosh(\gamma_3 d_3) \end{bmatrix} \quad \dotfill (2.17)$$

where Z_s is the source impedance and Z_t is the characteristic impedance of the bridged-tap section.
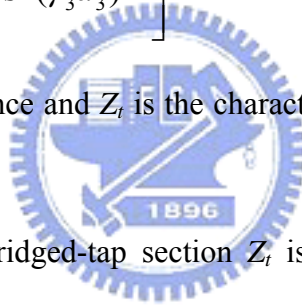
The impedance of the bridged-tap section Z_t is computed according to the above formula, as a parallel (shunt) impedance, for the input impedance of a section of transmission line terminated with an open circuit ($Z_L = \infty$). The overall two-port matrix is simply the product of the 4 two-port matrices shown in Fig. 2.5 and equations (2.13) to (2.17). Circuits with multiple bridge-taps can be calculated by similar procedures as multiplying multi-section of two-port networks. The impedance of previous section then becomes a termination impedance for the next section working backwards towards the main transmission pair of interest. The calculation process is straightforward and recursive to build the whole loop models.

2.3 Transfer Characteristics of a Subscriber Loop

The computation of the transfer functions for twisted-pair transmission lines with multiple sections then simply becomes a process of multiplying the corresponding ABCD matrices of the cascaded two-port sections. The source voltage divider is modeled by equation (2.18) and the final output voltage, current and load are V_L, I_L, and Z_L, respectively. The transfer function, H, is computed from the ratio of V_L and V_s, as shown in equation (2.19).

$$H(f) = \frac{V_L}{V_s} = \frac{Z_1}{Z_s + Z_1} \cdot T(f)$$ ....(2.18)

, where $T(f)$ is the ratio of V_L and V_1, and

$$T(f) = \frac{1}{\cos(\gamma d) + (\frac{Z_0}{Z_L}) \cdot \sinh(\gamma d)}$$ ....(2.19)

$$Z_1 = Z_0 \frac{Z_L + Z_0 \cdot \tanh(\gamma d)}{Z_0 + Z_L \cdot \tanh(\gamma d)}$$ ....(2.20)

$$H(f) = \frac{Z_0 \cdot \sec h(\gamma d)}{Z_s \cdot \left[\frac{Z_0}{Z_L} + \tanh(\gamma d)\right] + Z_0 \cdot \left[\frac{Z_0}{Z_L} + \tanh(\gamma d)\right]}$$ ....(2.21)

In DSL case, the source impedance is matched to the characteristic impedance (which equals the input impedance of the line when the line is long) and all impedances are real over the higher frequency range for DSL transmission. In this case, the transfer function is simply 6 dB lower than the insertion loss. The transfer function, H, is called the channel modeling of a twisted-pair line. Usually, its form can be represented both in frequency-domain and time-domain by applying proper sampling time. A program to

generate the time- domain transfer function of xDSL implemented according to the theory mentioned above is developed, and some of the results used in VDSL are shown in the next section.

2.4 Simulation Results of the Channel Characteristics

In this section, some simulation results of the DSL channel characteristics will be illustrated. In the first test set, the VDSL test loops, VDSL0 to VDSL7 in Table 1.1, Table 1.2, and Fig. 1.4 in Chapter 1 are studied. The other test set is the TP1 (gauge #26) line with length from 100 m to 1500 m since the VDSL system limits its twisted-pair loop length up to 1500 m. This set of test loops is simulated to observe the relationship between channel characteristics and its length. In Fig. 2.6 and 2.7, the channel responses of VDSL0 to VDSL7 of short reach in Table 1.2 (about 300 to 450 m) are illustrated in both time-domain and frequency-domain. While the channel responses of the second test set are shown in Fig. 2.8 and Fig. 2.9.

From the simulation results, it can be seen that the time-domain channel response of VDSL4, which has two bridged-taps, contains several peaks, with a broader main peak. In addition, its frequency-domain channel response contains some notches. The SNR values at those notches are reduced and the number of bits carried are also decreased.

In general, the longer the loop, the broader the response will be. In addition, the delay becomes greater while the loop length gets longer.
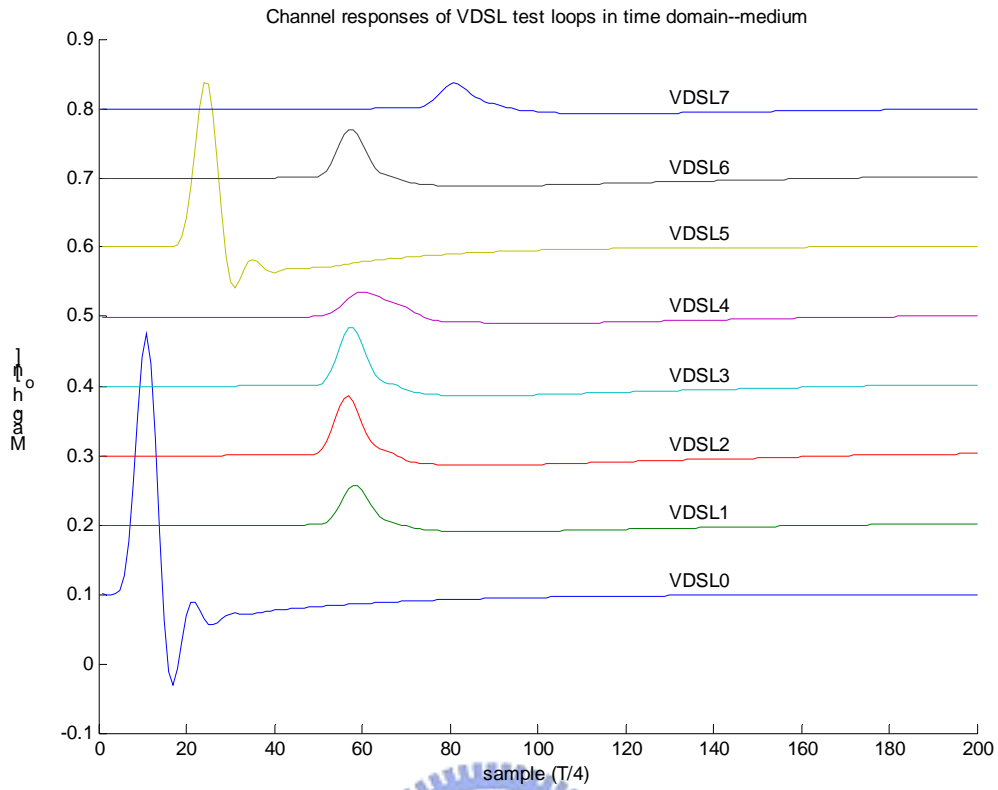
Figure 2.6 Time domain channel responses of VDSL0 to VDSL7.
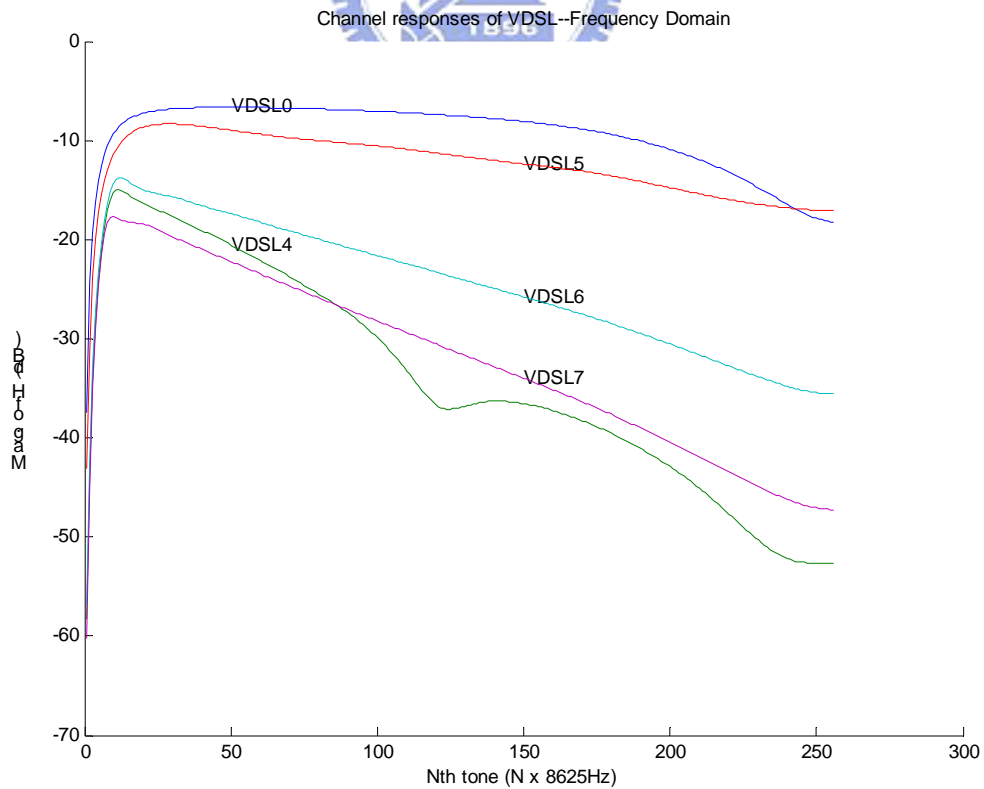

Figure 2.7 Frequency domain channel responses of VDSL0 to VDSL7.

21
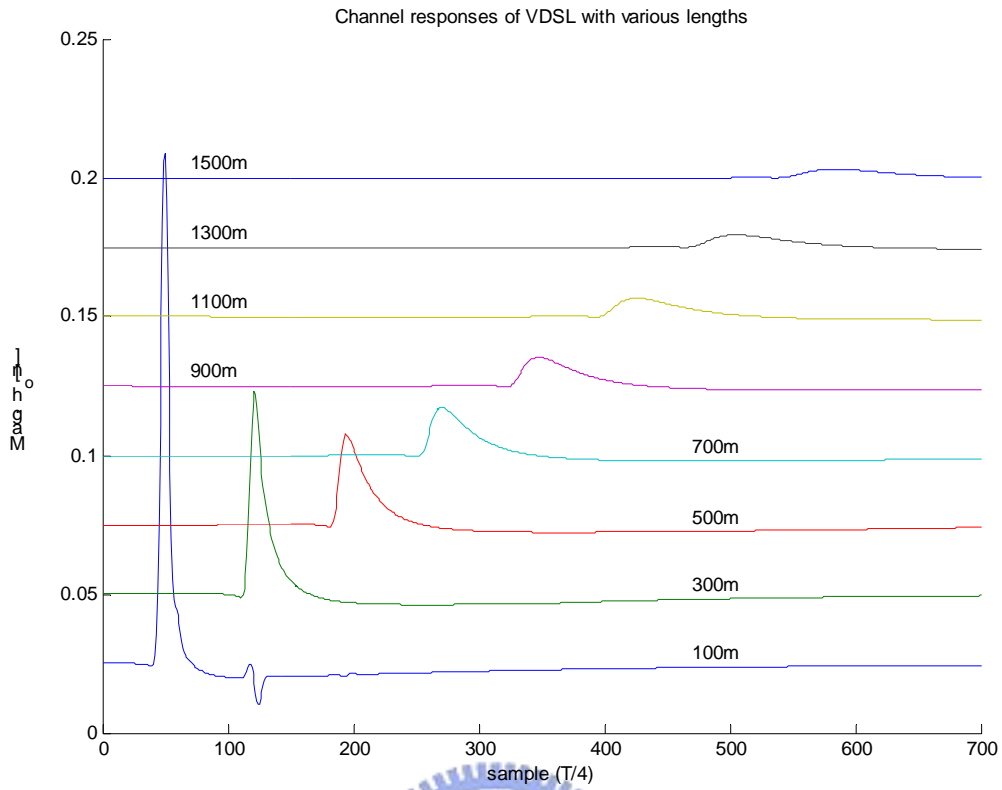
Figure 2.8 Time domain channel responses of TP1 lines of various lengths.
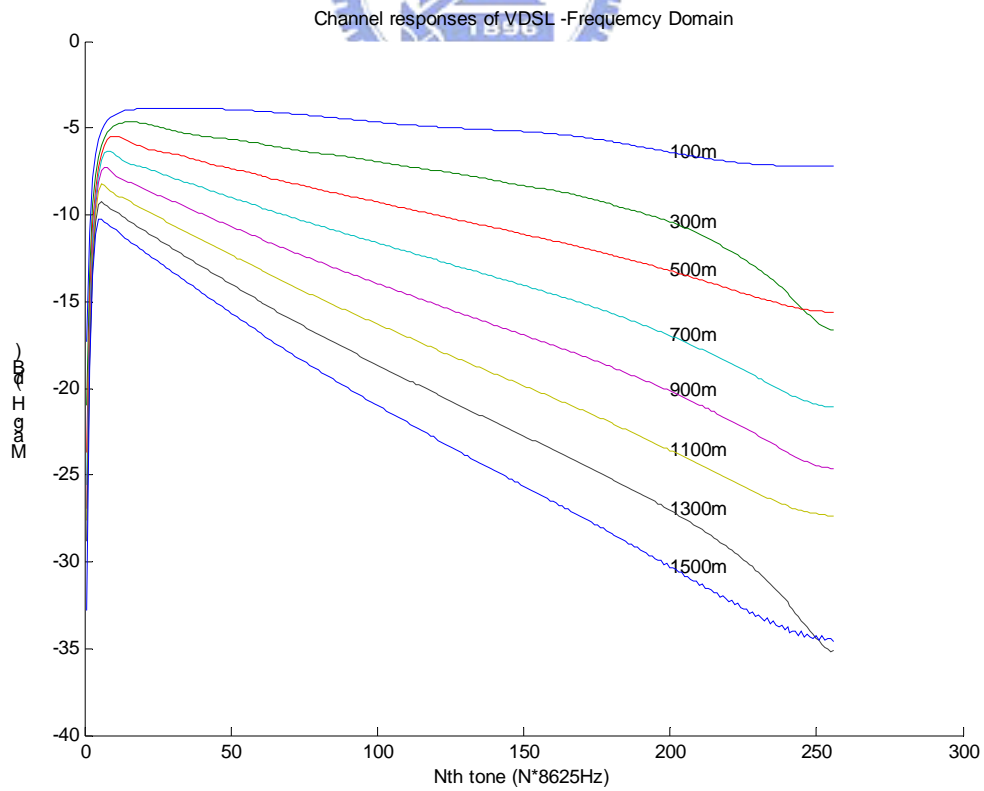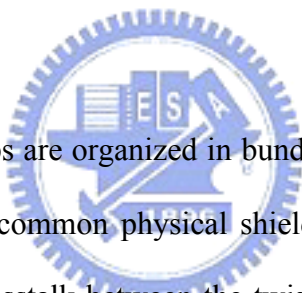
Figure 2.9 Frequency domain channel responses of TP1 lines of various lengths.

2.5 Interference and Noise Models

In the above sections, the channel responses of the twisted-pair lines are derived. However, in the real DSL operating environment, there are other effects, such as crosstalks, noises, etc. that will lower the performance of the DSL system. Besides the natural limitation of thermal noise, there are three other types of interference or noise that affect the performance of DSL system, i.e., crosstalk [17][18][19][20][21][22][23], impulse noise [17][24][25][26], and background noise [1].

2.5.1 Crosstalk

Telephone subscriber loops are organized in bundle groups of 10, 25, or 50 pairs, and several binder groups share a common physical shield in a cable. Due to capacitive and inductive coupling, there is crosstalk between the twisted-pair lines even though pairs are well insulated at DC. For DSL system, in which the signal bandwidth is much broader than that of voice frequency, the crosstalk becomes a dominant limitation to the whole transmission throughput.

Crosstalk coupling loss models have been developed for far end crosstalk (FEXT) [19] and near end crosstalk (NEXT) [18][20][21] with the consideration of different number of disturbers. These crosstalk coupling loss models are based on twisted-pair lines within the same cable of significant length, usually longer than 300 m. The effect of crosstalk could be different if only a portion of twisted-pair lines are within the same cable. In this subsection, the formula of power spectrum density (PSD) of ADSL downstream are introduced and their induced FEXT and NEXT to the system are also discussed and simulated.

$$PSD_{\text{ADSL-Disturber}} = K_{\text{ADSL}} \times \frac{2}{f_o} \times \frac{\left[\sin\left(\frac{\pi f}{f_o}\right)\right]^2}{\left(\frac{\pi f}{f_o}\right)^2} \times |LPF(f)|^2 \times |HPF(f)|^2 \ , \ 0 \le f < \infty \quad \cdots (2.22)$$

, where $f_0 = 2.208 \times 10^6$ Hz, $K_{\text{ADSL}} = 0.1104$ Watts

This equation gives the single sided PSD, where K_{ADSL} is the total transmitted power

in Watts for the downstream ADSL transmitter before shaping filters, and is set such that

the ADSL PSD will not exceed the maximum allowed PSD. f_0 is the sampling frequency in

Hz.

$$|LPF(f)|^2 = \frac{f_h^\alpha}{f^\alpha + f_h^\alpha} \ , \ f_h = 1.104 \times 10^6 \, Hz, \ \alpha = \frac{36}{10\log(2)} = 11.96 \quad \cdots\cdots (2.23)$$

LPF is a low pass filter with a 3 dB point at 1104 kHz and 36 dB/octave rolloff.
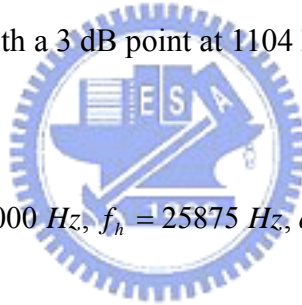
$$|HPF(f)|^2 = \frac{f^\alpha + f_l^\alpha}{f^\alpha + f_h^\alpha} \ , \ f_l = 4000 \, Hz, \ f_h = 25875 \, Hz, \ \alpha = \frac{57.5}{10\log\frac{f_h}{f_l}} = 7.09 \quad \cdots\cdots (2.24)$$

HPF is a high pass filter with 3 dB points at 4 kHz and 25.875 kHz and 57.5-dB

attenuation in the voice band, separating ADSL from POTS. With this set of parameters the

PSD_{ADSL}-Disturber is the PSD of a downstream transmitter that uses all the sub-carriers.

A. FEXT Coupling Configurations

FEXT [1][2][19] is defined as the crosstalk effect between a receiving path and a

transmitting path of DSL transceiver at opposite ends of two different subscriber loops

within the same twisted-pair cable, as shown in Fig. 2.10.
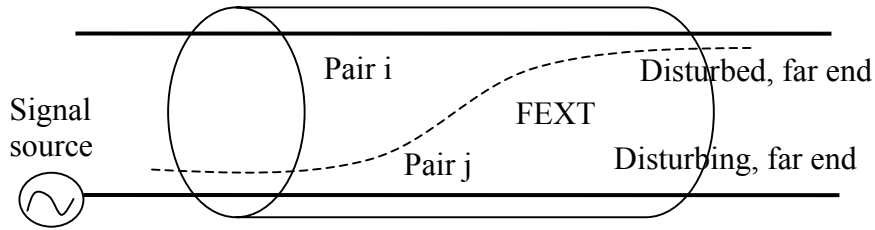
Figure 2.10 Illustration of FEXT.

The FEXT loss model is given by [2]

$$\left| H_{FEXT}(f) \right|^2 = \left| H_{channel}(f) \right|^2 \times k \times l \times f^2 \quad\ldots\ldots\ldots\ldots\ldots\ldots\ldots\ldots\ldots\ldots\ldots\ldots\ldots(2.25)$$

where $H_{channel}$ (f) is the channel transfer function, k is the coupling constants, l is the coupling path length and f is the frequency. k is $8.0 \times 10^{-20} \times (n/49)^{0.6}$ for n<50, 1% worst-case disturbers with the coupling path length l in feet. If the meter of length is used, then the coupling constant k is changed to $2.44 \times 10^{-20} \times (n/49)^{0.6}$ for n<50.

The FEXT noise PSD is therefore given by

$$PSD_{ADSL-FEXT} = PSD_{ADSL-Disturber} \times \left| H_{FEXT}(f) \right|^2 \quad\ldots\ldots\ldots\ldots\ldots\ldots\ldots\ldots\ldots\ldots\ldots(2.26)$$

In Fig. 2.12, the magnitude of these FEXT noises are shown in frequency domain.

B. NEXT Coupling Configurations

NEXT [1][2][18][19] is defined as the crosstalk effect between a receiving path and a transmitting path of DSL transceivers at the same end of two different subscriber loops with in the same twisted-pair cable, as shown in Fig. 2.11.
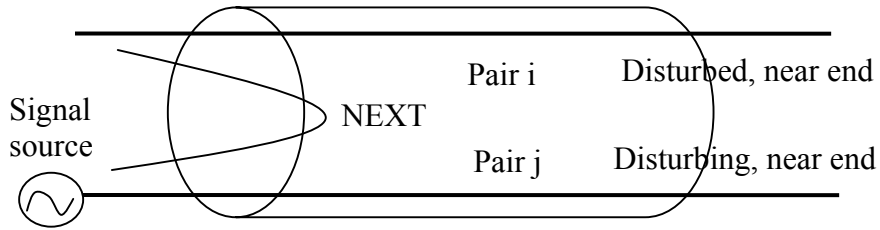
Figure 2.11 Illustration of NEXT.

The PSD of the ADSL NEXT coupling into the upstream is defined as [2]

$$PSD_{ADSL-NEXT} = PSD_{ADSL-Disturber} \times \left(x_n \times f^{3/2} \right) \qquad for\ 0 \le f < \infty,\, n < 50 \ldots\ldots..(2.27)$$

where $x_n = 8.818 \times 10^{-14} \times (n/49)^{0.6}$ or equivalently, $x_n = 0.8536 \times 10^{-14} \times n^{0.6}$. The integration of the induced NEXT over the band from 0 to 1.104 MHz for n=49 is −25.4 dBm.
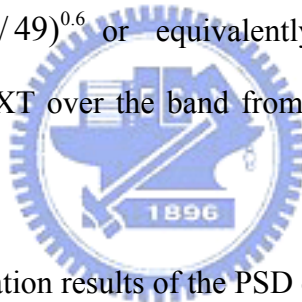
Fig. 2.12 shows the simulation results of the PSD of 10-disturber downstream ADSL NEXT into the upstream as well as ADSL and VDSL FEXT with 300 m loop length.
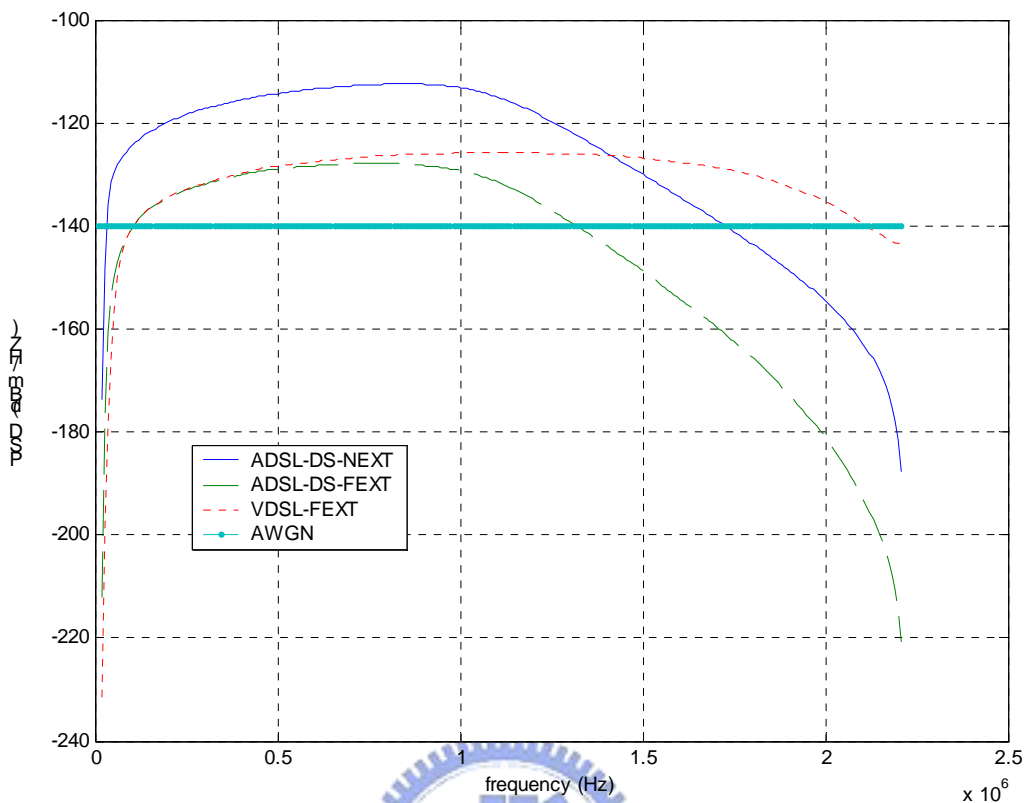
Figure 2.12 Simulation results of the PSD of 10-disturber downstream ADSL NEXT coupling into the upstream as well as ADSL and VDSL FEXT.

2.5.2 Impulse Noise

The origin of impulse noise is usually difficult to locate. It could come directly through some connections to the telephone subscriber loop or come from the influence of an electromagnetic field. Impulse noise is characterized as a random pulse waveform whose amplitude is much higher compared with the Gaussian-like background noise. Impulse noise is a major impairment for DSL system, especially due to the heavy DSL subscriber loop loss. While crosstalk and background noises impose a limit on transmission throughput over the twisted-pair telephone subscriber loop, the error caused by impulse

noise can be corrected with forward error correction codes. The required error correction coding overhead could reduce a small portion of the transmission throughput.

2.5.3 Background Noise

The loop plant noise level or the receiver front-end noise level becomes a limiting factor for the performance of a DSL system. The analysis of transmission performance over the twisted-pair subscriber loop has been based on the assumption of a received signal over an AWGN channel. The probability density of the background noise is very close to a Gaussian distribution. The histograms of the background noise are very similar to Gaussian density, except that they have short tails. Therefore, the Gaussian noise assumption is still valid.

Based on the results of noise survey, the background noise level for the twisted-pair telephone loop plant has been assumed to be -140 dBm/Hz. It is assumed that the loop plant background noise level is higher than the thermal noise of a receiver front-end electronic circuit whose noise power density is around -174 dBm/Hz.

In this chapter, the characteristics of twisted-pair line and some related interfaces and noises are studied to model their responses in both time-domain and frequency-domain, these responses are used thereafter to calculate the system performance.

Chapter 3

Bit Loading and Optimal Throughput of

DMT-based VDSL System

In this chapter[1], the bit-loading [1][27] and throughput of a DMT-based VDSL system is studied to investigate its system performance. In the first section, the formulae of bit-loading calculations at each tone are given. In those formulae, the factors that affect the bit-loading of each tone can be well defined. Finally, the throughput of this system is computed. In the second section, two methods to increase the throughput of DMT-based VDSL systems, extending the FFT size or increasing the symbol rate, are discussed. The computer simulation results of optimal throughput vs. various sampling rate under different types of noise environments, such as AWGN noises, crosstalk, bridged-taps[28][29], etc., are then discussed.

---

[1] Part of the content in this chapter has been published in:

S. T. Lin and C. H. Wei, "Optimal Channel Capacity Analysis for DMT VDSL System of Various Symbol Rates," *Proc. IEEE Globecom'01, San Antonio, U.S.A.*, pp.389-393, Nov. 2001

3.1 Bit Loading Calculations

The procedures of calculating the system bit-loading and its throughput are to compute the sub-channel SNRs first, then the number of bits per sub-channel, and the total system throughput.

The DMT-based system includes a set of independent sub-channels. And the overall capacity is the summation of each sub-channel. A subscript index, 'i', is used for recognizing the quantities of the ith sub-channel, such as C_i, SNR_i, etc. The number of bits per symbol carried by the ith tone (sub-channel) can be calculated by [1][27]

$$b_i = \log_2\left(1 + \frac{SNR_i}{\Gamma}\right) = \log_2\left(1 + \frac{P}{\Gamma\sigma^2}|H(d,f)|^2\right) \quad\text{..(3.1)}$$
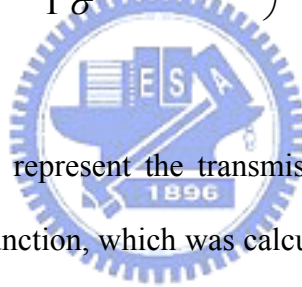
The variables P and σ^2 represent the transmission and noise power, respectively. H(d,f) is the channel transfer function, which was calculated in Chapter 2. The variable, Γ, is called SNR gap, which is dependent on the error rate, system margin γ_m (6 dB), and coding gain γ_c (3 dB), as defined in (3.2) with error rate of 10^{-7}[1][27].

$$\Gamma = 9.8 - \gamma_c + \gamma_m \text{ dB} \quad\text{...(3.2)}$$

The channel capacity of a loop can be calculated by applying its channel modeling into the above equations and obtained by summarizing the bits carried by each tone, as shown below.

$$C_{total} = \sum_{i=1}^{N/2} b_i = \sum_{i=1}^{N/2} (1 + \frac{SNR_i}{\Gamma}) \quad\text{..}(3.3)$$

From the previous derivation, the throughput of the DMT-based DSL system depends on the length of loop and the bandwidth used, as shown in the above equations. If the same FFT size (N=512) of the DMT system is maintained, the bandwidth of each sub-channel is proportional to its symbol rate. However, it becomes saturated after the symbol rate being increased to a certain value, as shown in reference [10]. It can also be observed from Fig. 2.7 and Fig. 2.9 that the magnitude of the channel response H(f) decreases in high frequency range especially for long loop.

To observe the relationship between the channel response and its capacity, the scaled channel response magnitude in frequency domain vs. the corresponding bit-loading is shown in Fig. 3.1. We use gauge #26 twisted-pair line with 1200 m as an example, the dotted line is the magnitude of the channel response "H(f)". The solid line as a down-stair curve represents the bit-loading of each tone, its value depends on the signal-to-noise ratio (SNR), which is the corresponding magnitude of channel response represented as the dotted line. The channel capacity can be calculated by multiplying the total bit-loading of each tone with the symbol rate. All the test loops introduced in the first chapter are simulated. In Fig. 3.1, the result of 1200 m TP1 loop is illustrated as an example. As shown in Fig. 3.1, the SNR curve cause the numbers of bits loaded in each sub-channels decrease in decent order.
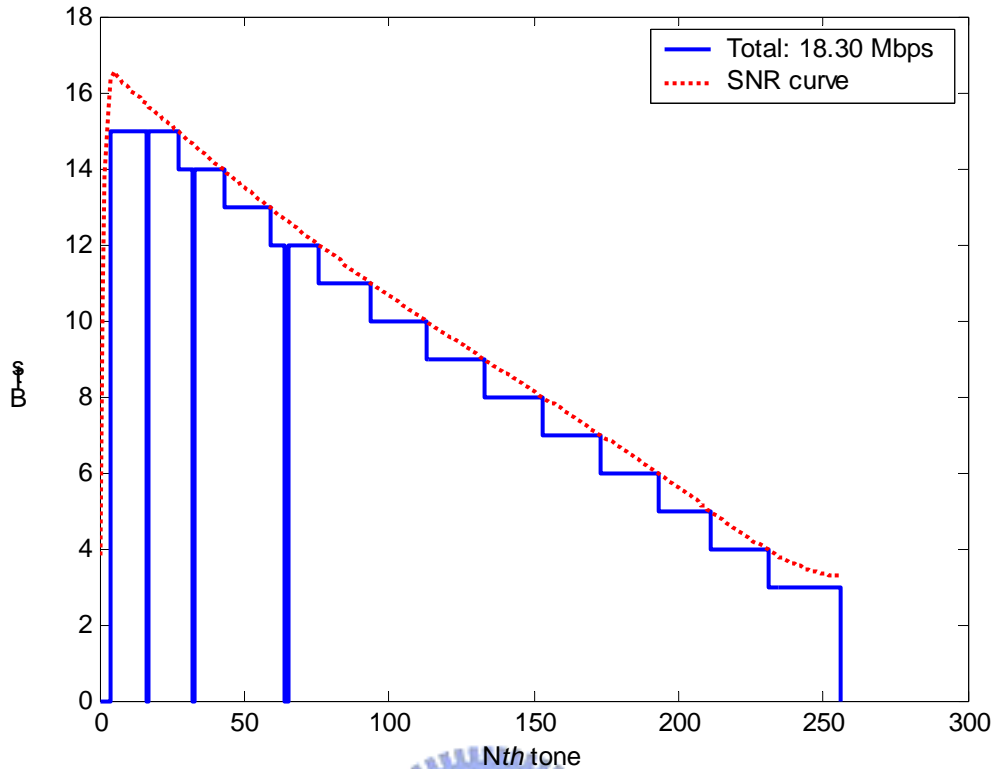
Figure 3.1 Channel capacity of gauge #26 twisted-pair line with 8 kHz symbol rate.
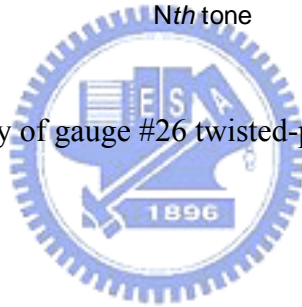
Since the magnitude of the channel response decreases at high frequency, the bits carried are lowered in those corresponding sub-cannels. Those tones with bit-loading smaller than 2 are not activated; therefore, the channel capacity has its limitation even though the symbol rate can be increased much higher.

Currently, due to the increased population of fiber on the telecommunication network, the last mile of twisted-pair line can be gradually reduced to below 1.5 km, especially in the urban areas. The available frequency spectrum of these short copper wires for transmission becomes much broader and its channel capacity grows dramatically. For example, VDSL system can provide up to 52 Mbits/s over short telephone line to meet the broadband access-network requirements. It can be regarded as an evolution of the ADSL system. Several VDSL system architectures have been proposed [4][5][6][7]. These systems use the

frequency band from a few hundred kHz to beyond 10 MHz over some loops.

In [7], we propose an asymmetric VDSL system, which is upgraded from a DMT-based ADSL system by multiplying the symbol rate. Its architecture and symbol format are the same as the original ADSL system except that both clock rate and frequency bandwidth are increased in the same ratio. Recently, the new standard for ADSL2 [13] has been announced, which also doubles the traditional ADSL bandwidth and FFT size to upgrade the throughput. No matter which method is selected, to improve the throughput of the whole system, the sampling rate should be increased to a certain ratio, which is proportional to the frequency bandwidth extension. In this chapter, the optimal channel capacity of this proposed system is analyzed over VDSL test loops at various sampling rates. This optimal channel capacity has its upper-bounded limitation due to the characteristics of the twisted-pair channel. In addition, some interference or noise types such as crosstalks and other background noises, are taken into consideration and analyzed also in this section.
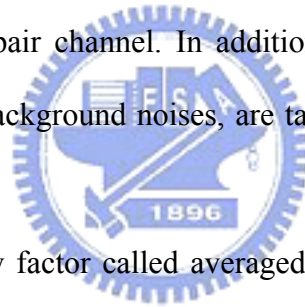
In this dissertation, a new factor called averaged sub-channel power spectral density (PSD) flatness is defined and calculated over VDSL test loops with various symbol rates. This factor is computed to make sure that the DMT technology can be applied at higher symbol rate if the length of twisted-pair line is shorter, such as VDSL system.

Sub-channel PSD flatness factor in this dissertation is defined as the magnitude difference (in dB) of two consequent sub-channels in frequency domain. This factor indicates the variation of PSD in each sub-channel. It should be approximately flat in the region that no transmission distortion is evident, a basic assumption of DMT system. The averaged PSD sub-channel flatness is obtained by taking the average of all used sub-channel PSD flatness. In traditional ADSL system, the averaged sub-channel PSD flatness difference between adjacent sub-channels varies from 0.23 to 0.35 dB for the eight loops in T1.413. This factor depends on the length and topology of a tested loop as well as the bandwidth of a

sub-channel. In our proposed VDSL system, both the symbol rate and the bandwidth of each sub-channel are increased, thus the magnitude difference of two consequent sub-channels is increased also. If the difference varies too much, some of the sub-channel may not be used, and the DMT system performance degrades.

The VDSL test loops set 1, as shown in Table 1.2 and Fig. 1.4, can be grouped into three types: short, medium, and long loops. The short group includes VDSL1~4 of length x equal to 300 m and VDSL5, and they are represented as test loop 1 to 5 in Fig. 3.2. The medium group includes VDSL 1~4 of length 1000 m and VDSL6, while the long one includes VDSL1~4 of length 1500 m and VDSL7, and they are represented as test loop 6 to 10, and 11 to 15 in Fig. 3.2. VDSL0 is used as a reference for the limitation of performance since its length is only 2m, very close to a null loop. The symbol rate varies from 4 kHz to 20 kHz, and so is the bandwidth of a sub-channel. The magnitudes of averaged PSD flatness vs. VDSL test loops with different symbol rate are displayed in Fig. 3.2.
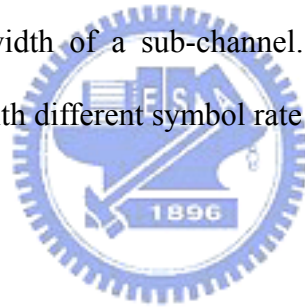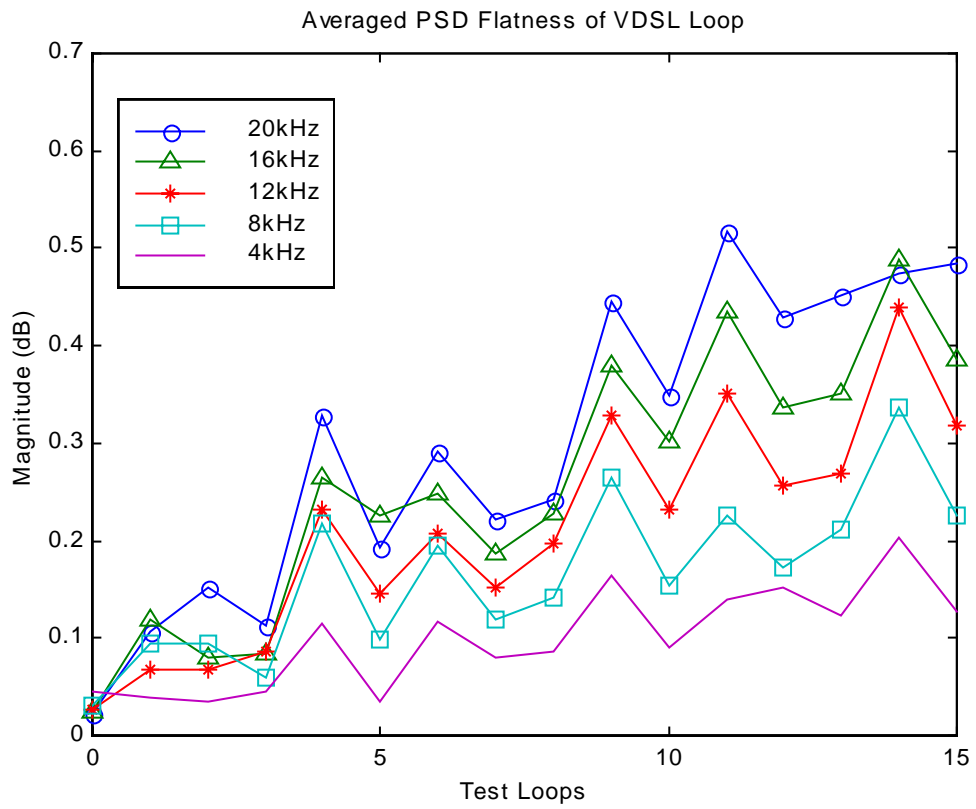
Figure 3.2 Averaged PSD flatness of VDSL loops.

3.2 Channel Capacity vs. Symbol Rate or FFT Size

In the previous discussion, one method to expand the used bandwidth is increasing the symbol rate with fixed FFT size. The other method is fixing the symbol rate but increasing the FFT size, which will increase the bandwidth at the same ratio. Therefore the total channel capacities will be close if the same bandwidth is used. Fig. 3.3 shows the relationship of FFT size and symbol rate vs. frequency bandwidth usage. Fig. 3.4 shows the simulation results of the AWGN cases with different symbol rates or FFT sizes. The dashed lines are results for FFT size extension and the solid lines are symbol rate upgrading. The variable N is the number of sub-channels for data-carrying, and the FFT size is 2N to maintain the output signal to be real instead of complex number [1][30][31].
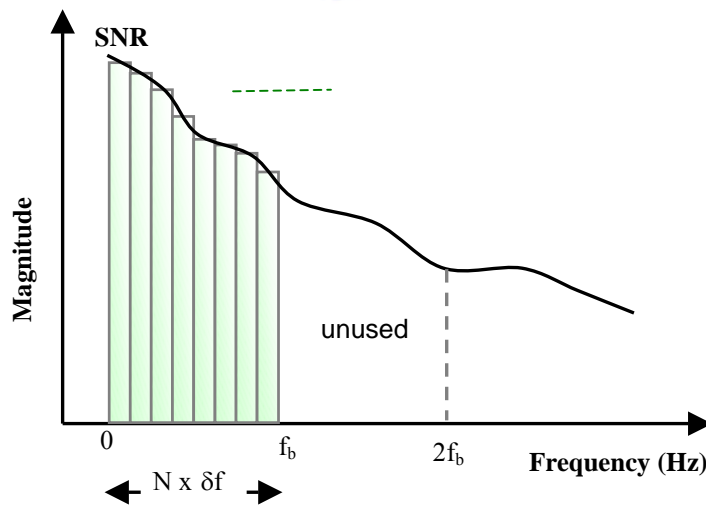
(a)
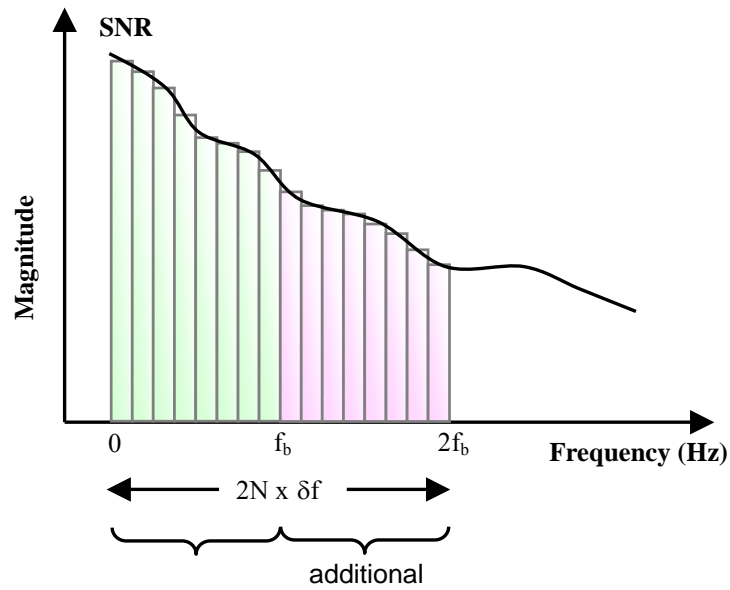
(b)
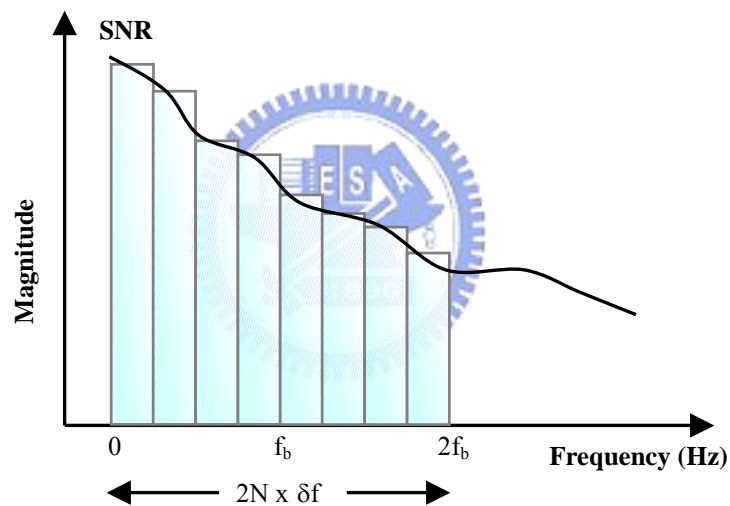
Figure 3.3 FFT size and symbol rate vs. frequency bandwidth usage.

(a) original (b) double FFT size (c) double symbol rate

From the simulation results, it can be seen that if the same bandwidth is used, the total throughputs of DMT- based systems are similar no matter by expanding the FFT size or by increasing the sub-channel bandwidth. For hardware based FFT implementation, if the FFT size is increased, the system complexity will increase significantly for both the FFT and IFFT blocks.
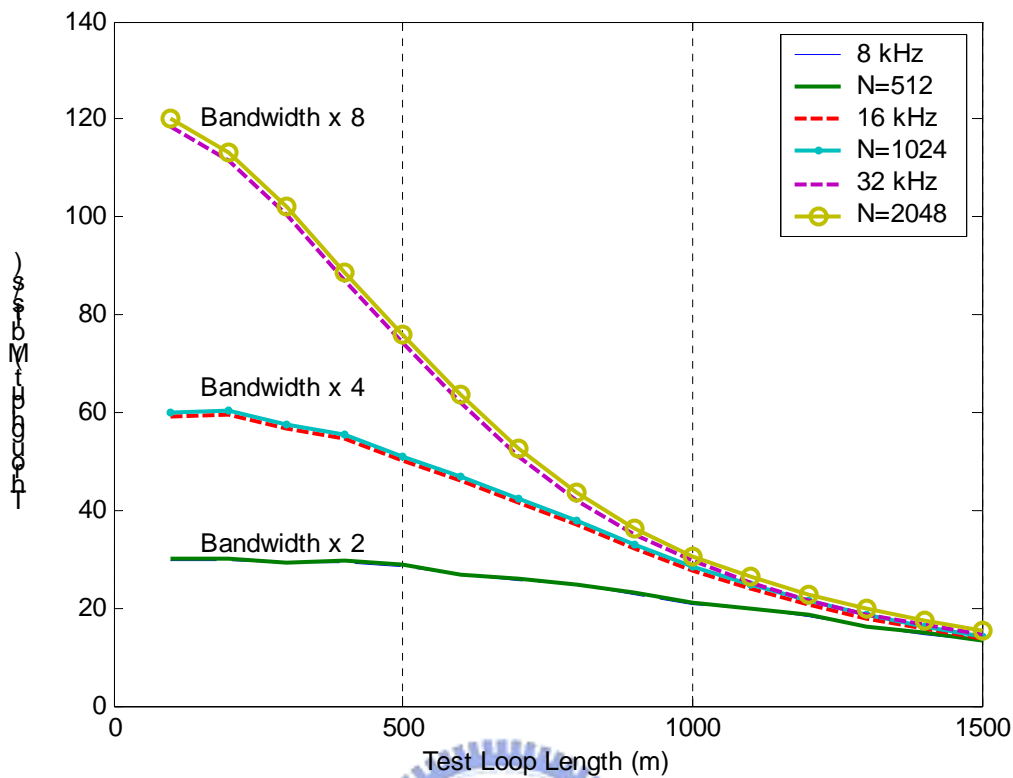
Figure 3.4 Channel capacities of VDSL system with various bandwidths (4.4, 8.8 and 17.6 MHz).

For the current ADSL system, the symbol rate is only 4 kHz, and it is not difficult to increase the symbol rate by the current VLSI technology. For DSP-based FFT implementation, variable FFT block can be easily realized without additional effort only if the total computations can be completed in 232 μs [32]. Currently, the new ITU-T standard chooses the various FFT size solutions [32][33][34]. No matter which method is selected, the sampling rate should be increased by the same ratio as the bandwidth extension. For example, for the original ADSL DMT-based system with bandwidth of 1.104 MHz, the sampling rate should be 2.208 MHz to complete sampling the 512 FFT outputs plus additional 40 cyclic prefix data for a 4 kHz symbol. If the bandwidth is doubled, either by increasing the symbol rate to 8 kHz or doubling the FFT size to 1024, the sampling rate should be 4.416 MHz. The other sampling rate upgrade, such as four times or more, also expand the same bandwidth ratio. In next section, the optimal sampling rate for DMT-based

system under various loops and noise conditions are studied.

3.3 Computer Simulations

To verify the analysis of the relationship between channel capacity and sampling rate, some computer simulations are performed. By using the simulation results, the parameters and facts that degrade the channel capacity, such as background noise and crosstalk, are analyzed.

3.3.1 Maximum Channel Capacity vs. Sampling Rate in AWGN Channel

First, the maximum channel capacity vs. symbol rate under AWGN and system margin of various loop lengths are illustrated in Fig. 3.5 In this figure, it can also be seen that the channel capacity becomes saturated while the symbol rate is increasing to a certain value. We define the optimal sampling rate as the first point whose througput becomes more than 99% of the final maximum throughput.
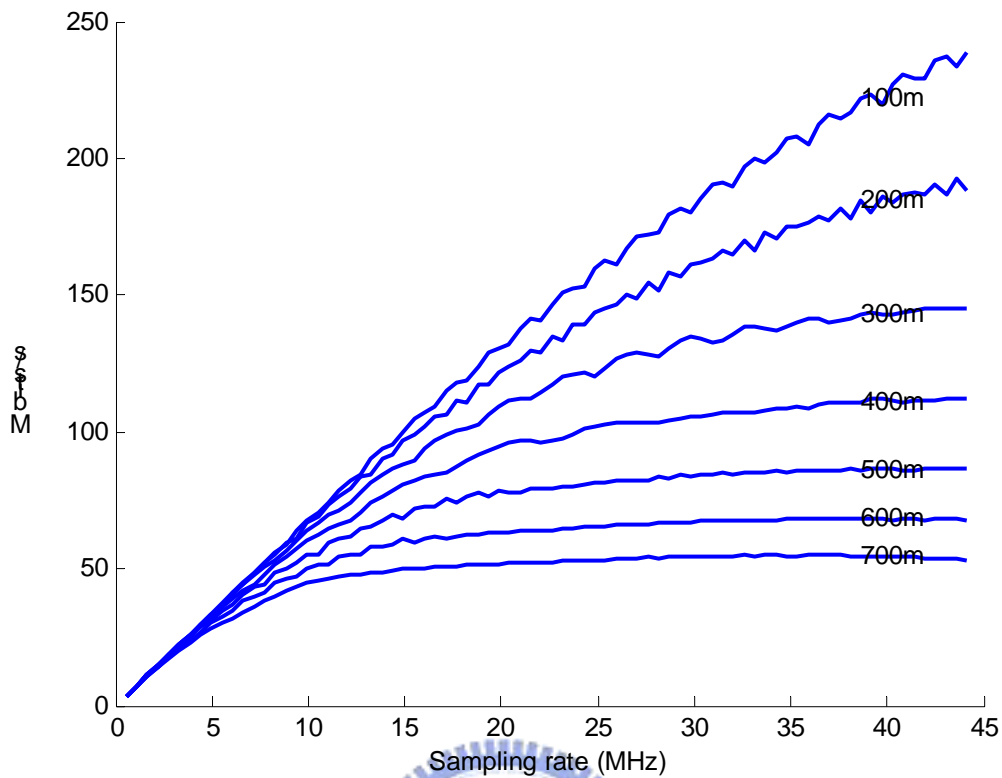
Figure 3.5 Maximum throughput of a DMT-based VDSL system under various sampling rates.

In Fig. 3.6, the theoretical maximum channel capacity vs. real system throughput with constraints are shown. The green dotted line is the theoretical value, while the blue solid lines represent the channel under system constraints. It can be seen that the degradations after considering the system constrains are in certain ratios to the ideal channel capacity. In other words, shorter loop length or higher symbol (sampling) rate results in larger loss. The optimal sampling rate also depends on the loop length. For example, if the loop length is 400 m, the sampling rate above 22 MHz would not improve the system performance much. However, for that of 700 m, the optimal sampling rate lowers to less than 11 MHz.
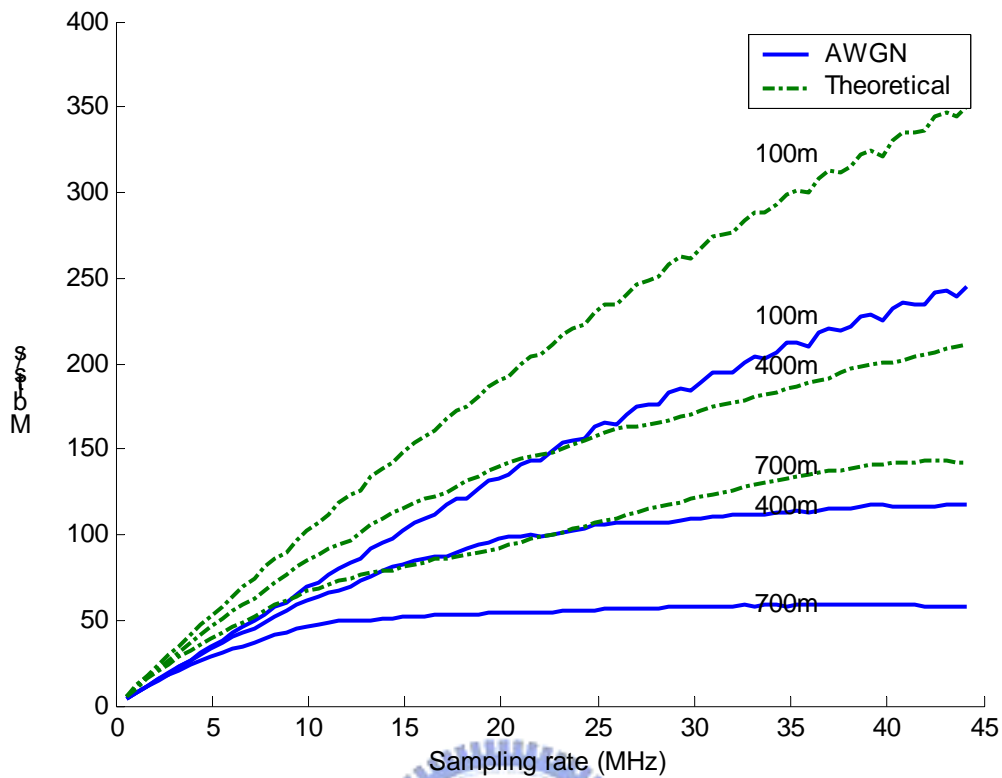
Figure 3.6 Performance comparison of AWGN with system margin to theoretical one.

The optimal sampling rate here is defined as the frequency at which the curve is turning to the saturation state. It can be seen that before the saturation state occurs, the channel capacity increases with the sampling rate linearly. In current DMT-based ADSL system, the sampling rate is 2.208 MHz only. If it is raised to 11.04 MHz, the channel capacity can be increased from 15 Mbits/s to nearly 50 Mbits/s at loop length of 700 m. If the loop length becomes shorter, the improvement is even higher.

The curves of the simulation results are lower than those in reference [1] since the SNR gap, which depends on some system parameters, such as bit error rate, coding gain, and system margin, is considered. However, the trend is the same that the channel capacity becomes saturated at high frequency, as shown in Fig. 3.6.

3.3.2 AWGN vs. VDSL Noise

In VDSL standard, two types of color noise mask are included[4]. These two noise masks located at certain frequency part (below 1.1 MHz), therefore, the maximum throughput is smaller than the AWGN case with a system margin of certain amount. The simulation results for noise type A and type B are shown in Fig. 3.7 and 3.8, respectively.

It can be observed that the degradation increases with the loop length. The reason is that the channel response magnitude of a longer loop is smaller but the noise density is the same, and therefore the degradation ratio increases.
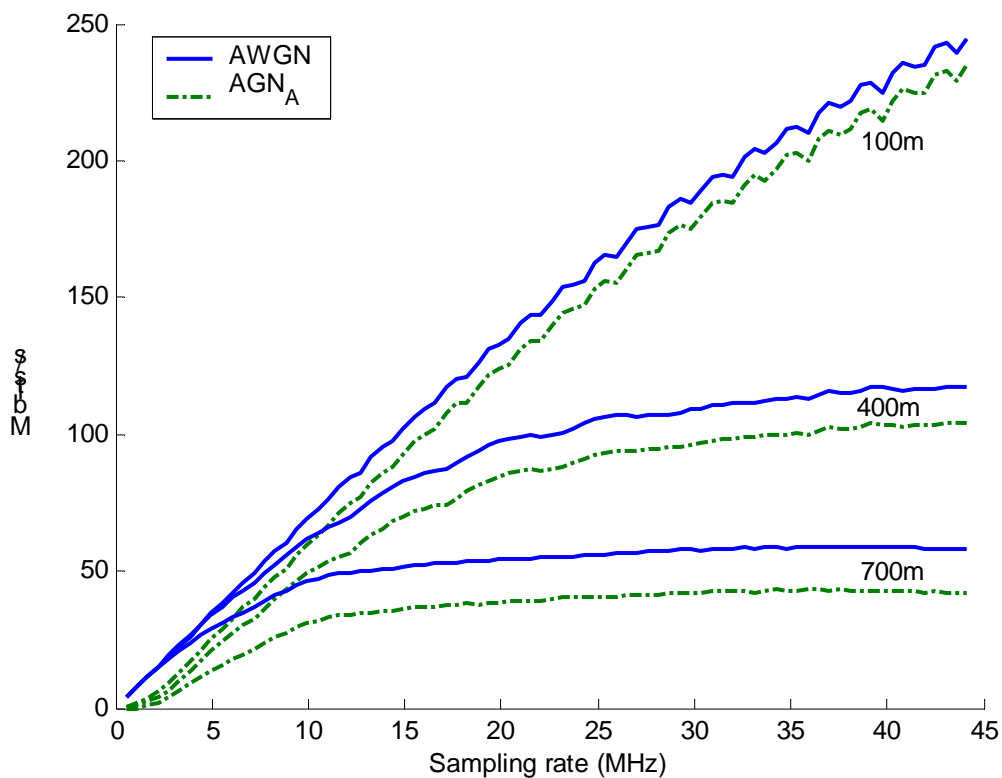
Figure 3.7 Performance comparison of noise type A with AWGN.
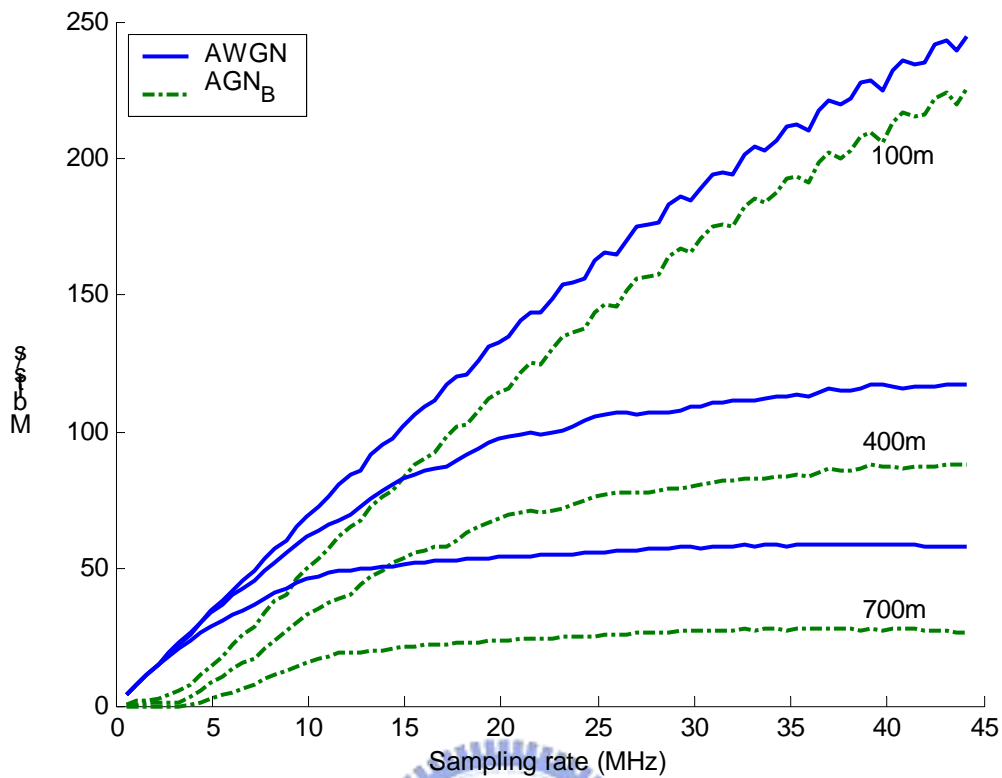
Figure 3.8 Performance comparison of noise type B with AWGN.
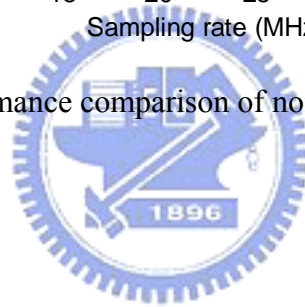
3.3.3 AWGN vs. Various Crosstalk

In this subsection, different crosstalk noise are simulated, such as HDSL and ADSL NEXT and VDSL FEXT, etc[35]. In general, NEXT noise is much larger than FEXT, therefore, only the NEXT of other DSL system will be dominant. Fig. 3.8 shows the HDSL NEXT case, the degradation is less than 5% because its bandwidth of power spectrum is concentrated below 400 kHz. For the 512-FFT and symbol rate of 10 kHz VDSL system, its bandwidth is 5 MHz. Therefore, its effect is not so significant. The second one is the ADSL downstream NEXT case, its power spectrum bandwidth is up to 2.2 MHz and has more effect on the system performance, as shown in Fig. 3.10.
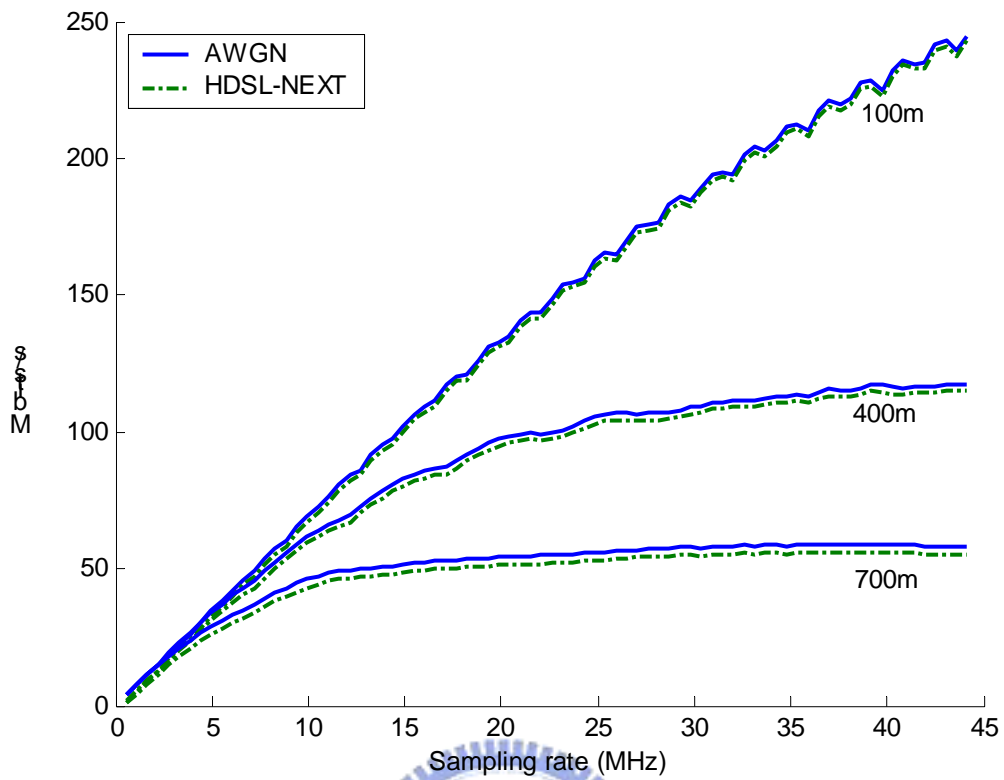
Figure 3.9 Performance comparison of HDSL NEXT crosstalk with AWGN.
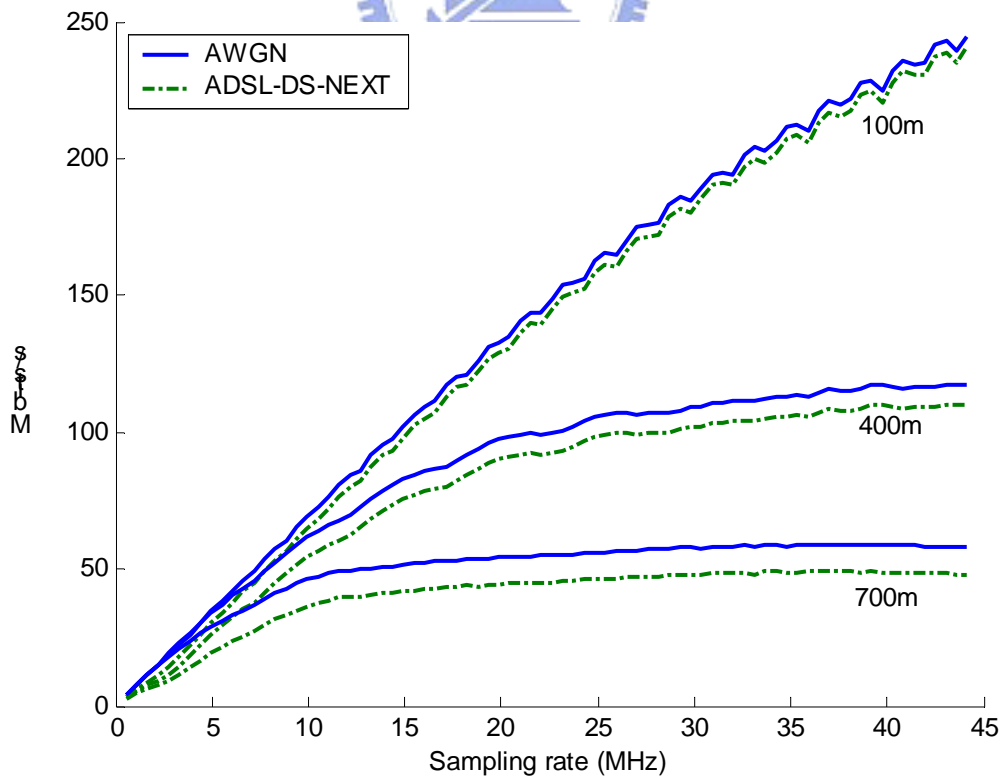
Figure 3.10 Performance comparison of ADSL NEXT crosstalk with AWGN.
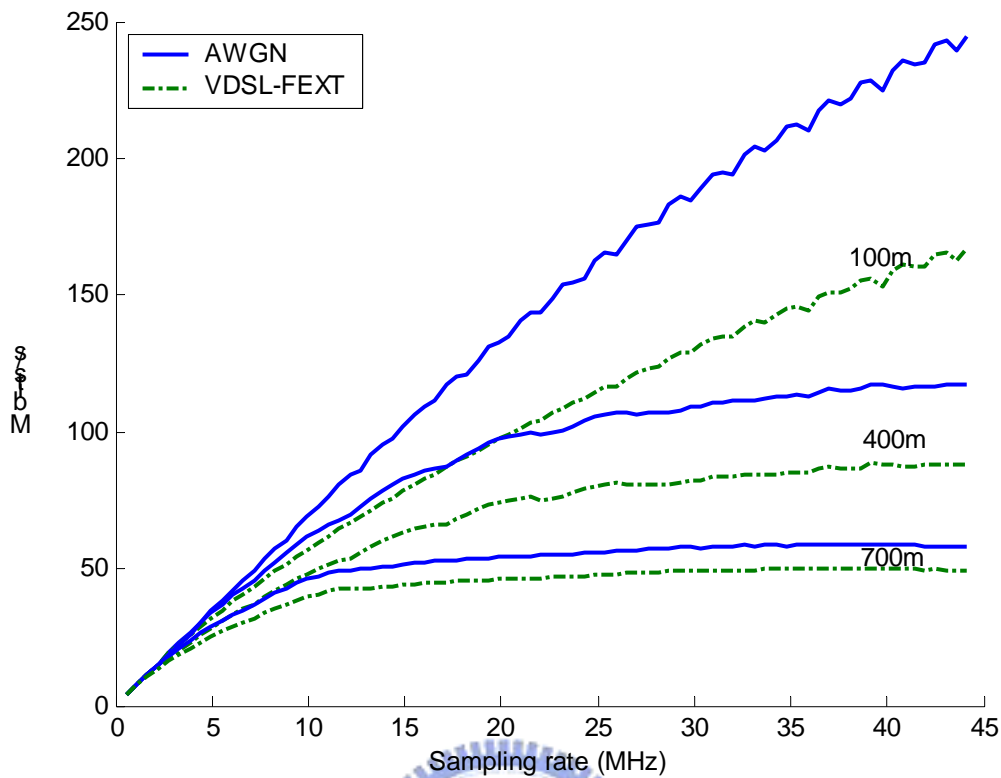
Figure 3.11 Performance comparison of VDSL FEXT crosstalk with AWGN.

In DMT-based VDSL system, if the synchronous system is used, the NEXT problem can be discarded. Therefore, only the FEXT should be considered. It is clear that this FEXT depends on the loop length. The shorter the loop is, the larger the degradation will be, as shown in Fig. 3.11. This result is reasonable because the crosstalk coupling from the far end will decay more through the long loop length.

3.3.4 AWGN vs. Bridged-taps

In general, the bridged-taps can cause notches for VDSL length loops. If some bridged-taps of various lengths are added into the middle of a tested loop, the shortest bridged tap causes the deepest null [1][5]. In our test case, we use the bridged-tap type as shown in [3], and the simulation results are shown in Fig. 3.12.
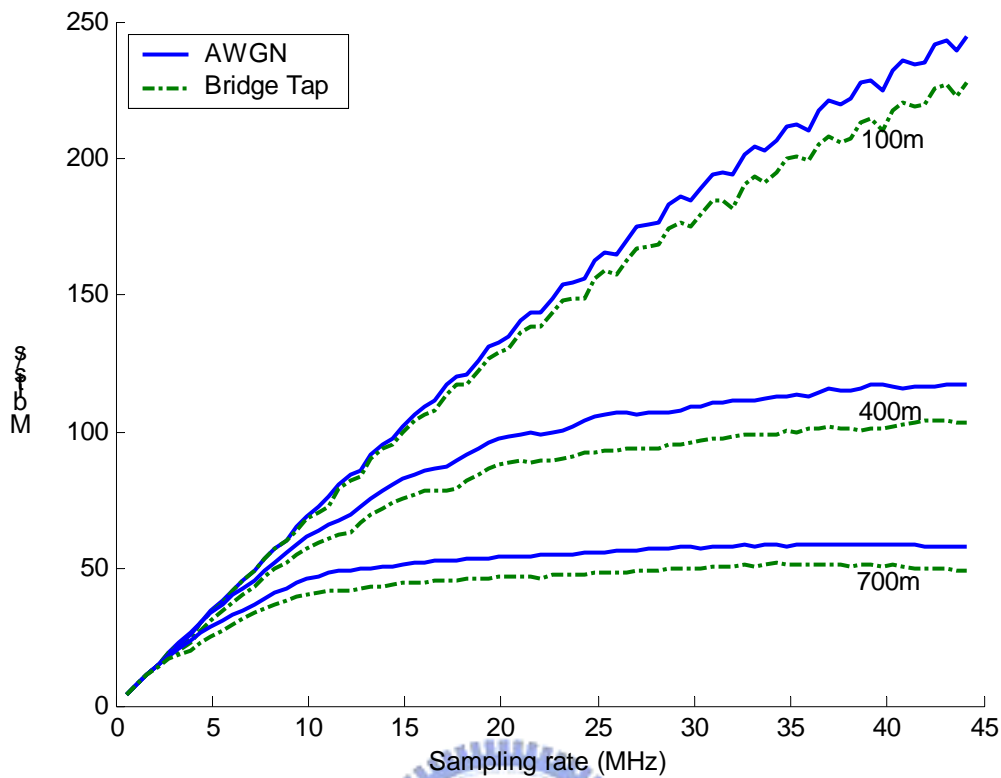
Figure 3.12 Performance comparison of tested loops with and without bridged-taps.

3.3.5 Analysis of Maximum Throughput

From previous discussions, we simulate all the different effects which lower the maximum throughput of the whole system. In this section, we compare all of these effects that lower the system performance. The significances of these effects depend on the loop lengths as well as the symbol rates. In Fig. 3.13, all the effects discussed in section 3 are plotted together under various symbol rates. It is seen that some effects such as bridged-taps and VDSL-FEXT are more sensitive to the system symbol rate. In other words, the degradation of the throughput increases with the sampling rate. However, the background noises decrease the throughput in a certain amount, the ratio to the total throughput increases with the loop length. In Fig. 3.14, the percentages of the channel capacities under those effects are illustrated.

(a)
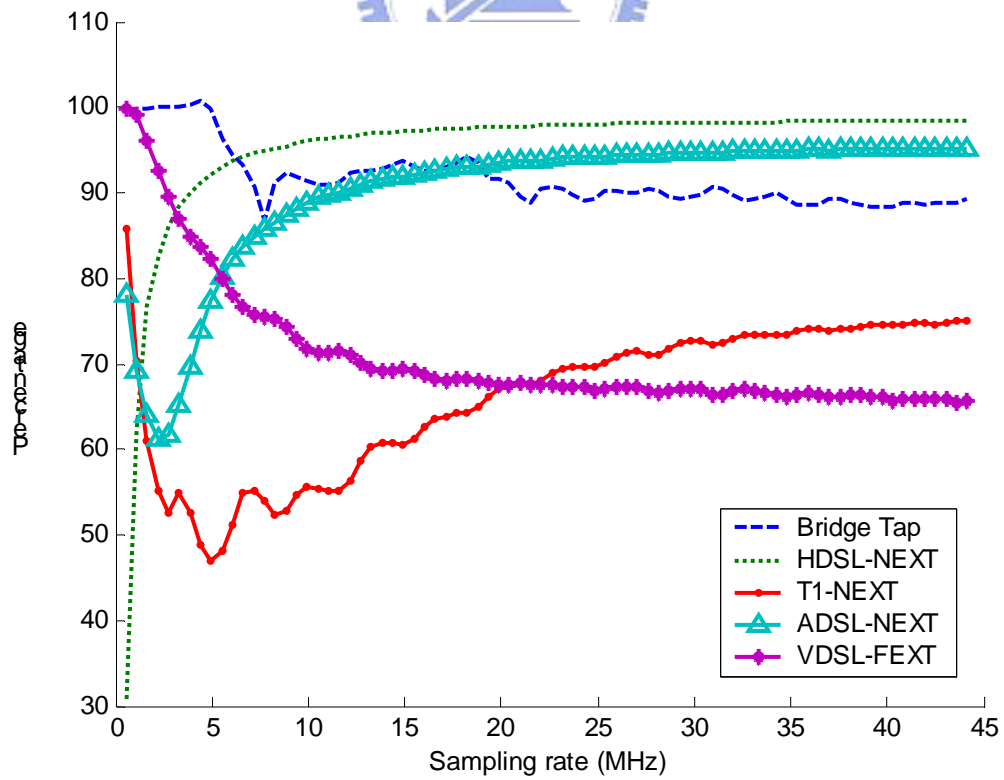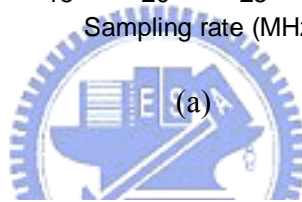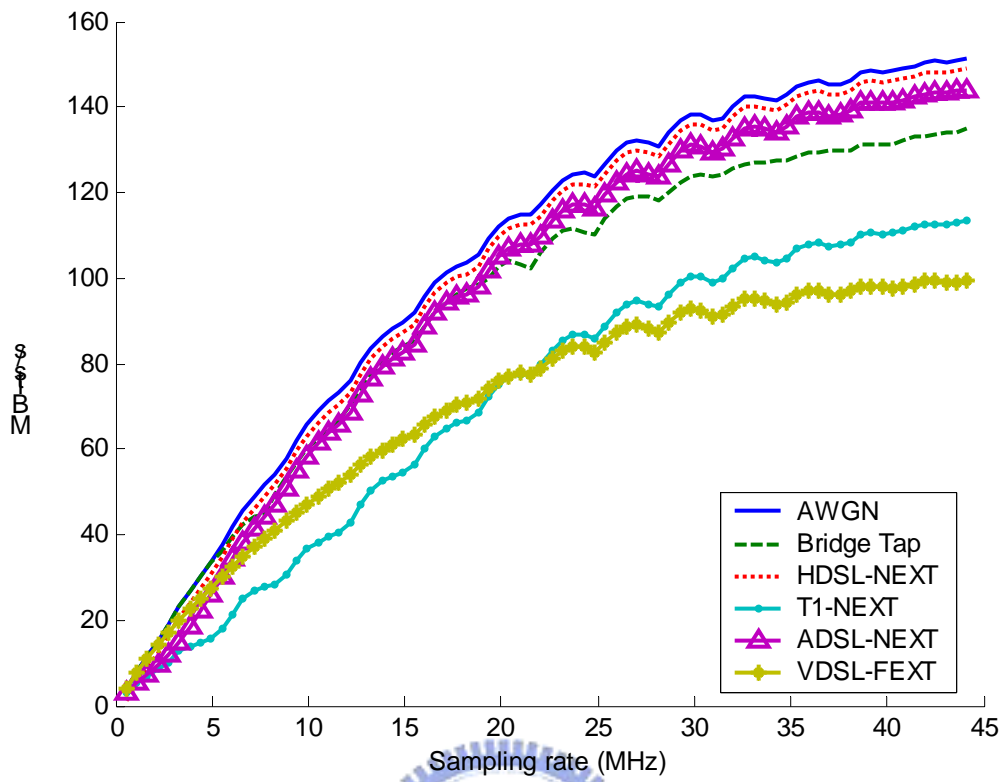
(b)

Figure 3.13 (a) Performance and (b) Throughput comparison of tested loop 300 m.
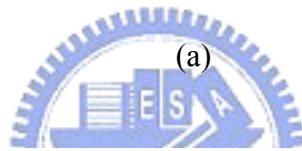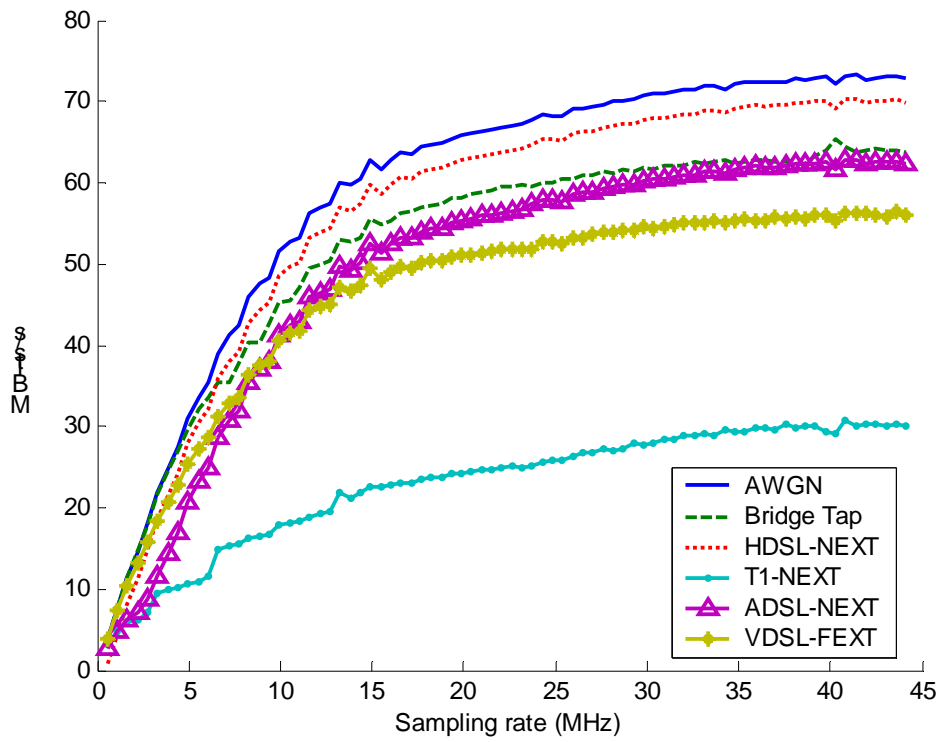
(a)
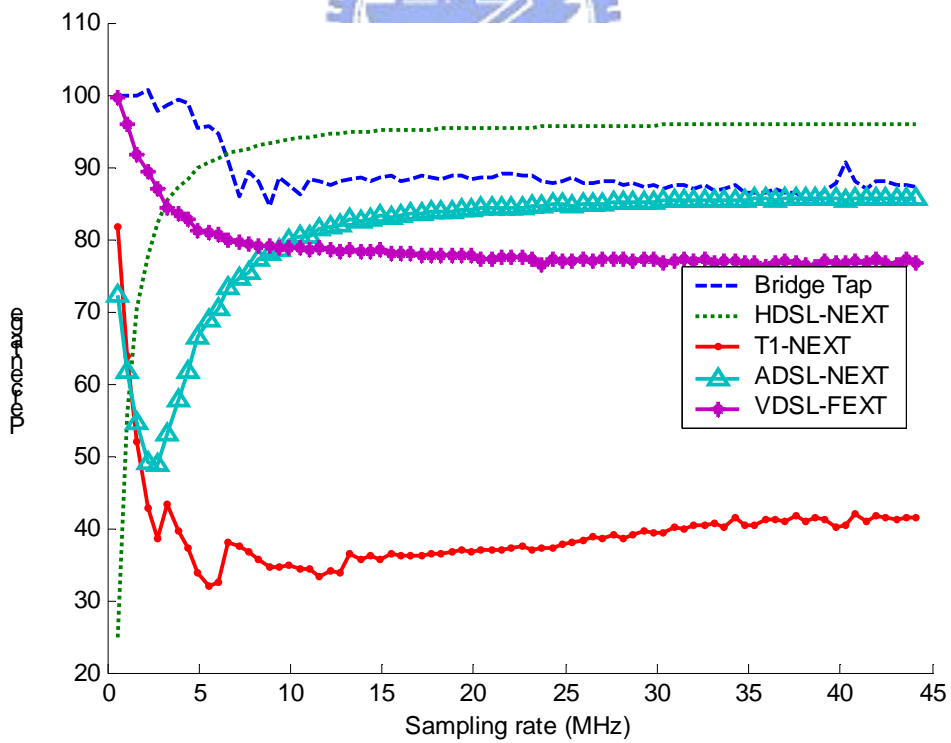
(b)

Figure 3.14 (a) Performance and (b) Throughput comparison of tested loop 600 m.
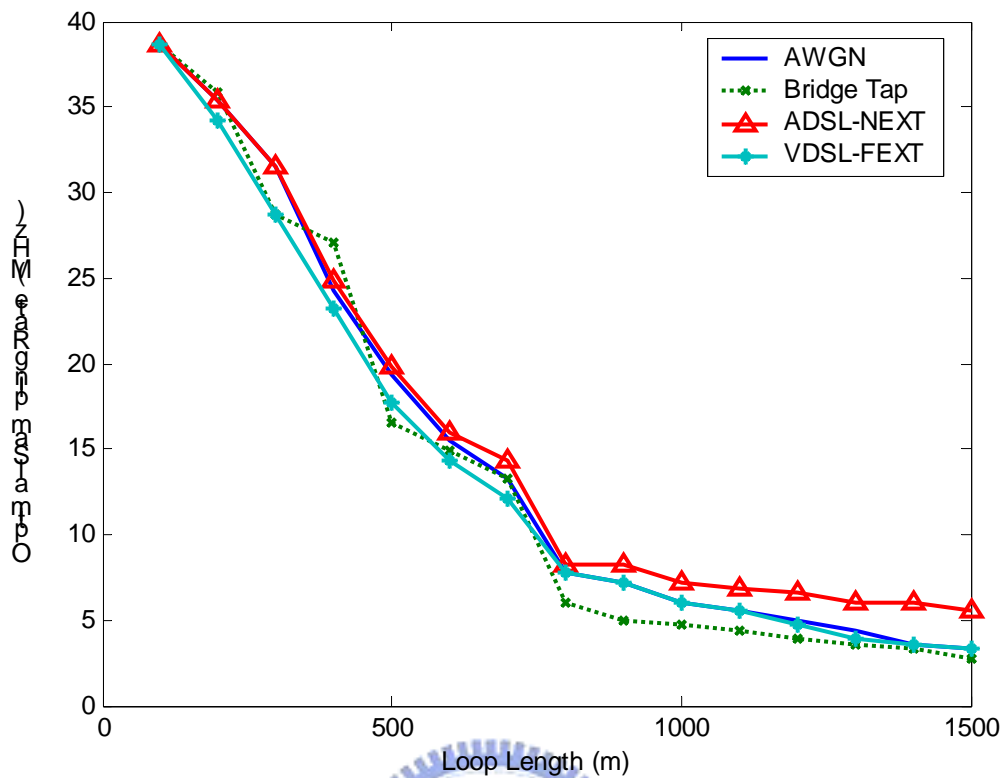
Figure 3.15 Optimal sampling rate of DMT-based VDSL test loop.

In Fig. 3.15, the optimal sampling rate of the system is selected by finding the minimum sampling rate of a test loop with the throughput up to 97% of its optimal value. The influence of HDSL system is small and can be ignored. The influence of T1 system to the VDSL one is so significant that it is not practical to bundle these two types of services together.

From the simulations, if the loop length is below 800 m, increasing the sampling rate will improve the system performance significantly. The optimal sampling rate for the VDSL system varies from 5.5 to 40 MHz if the loop length is below 800 m, as shown in Fig. 4. Otherwise, for the loop length above 800 m, 4.4 MHz sampling rate is good enough to reach the optimal performance of a DMT-based VDSL system. The optimal throughput of the DMT VDSL system also depends on the loop length.

3.4 Summary

In this chapter, the maximum throughputs of a DMT-based VDSL system under various constraints, such as the effects of crosstalks and bridged taps, are analyzed. It is seen that raising the sampling rate can improve the system throughput, especially when the loop length is short. However, this method has its limitations as shown in the previous simulations, and the optimal solutions are calculated according to the defined constraints. From our simulation results, if the loop length is below 800 m, increasing the sampling rate will improve the system throughput significantly. Otherwise, for the loops with length above 800 m to 1500 m, 4.4 MHz sampling rate is good enough to reach the optimal throughput of the DMT-based VDSL system, which is the value selected in ADSL 2 standard.

Chapter 4

Frame Synchronization by Cyclic Prefix

In the previous chapter, the maximum transmission data rate is calculated based on the optimal bit-loading capability of the twisted-pair line. However, in the receiver side, the overall performance depends on the equalization algorithm, frame synchronization, etc. Since the channel responses of these test loops have been calculated, the well-trained coefficients of TEQ [36] and FEQ can be applied to those simulations directly.

In this chapter[2][37], the theory of maximum likelihood (ML) algorithm for frame synchronization will be discussed, and a modified algorithm to improve the performance is then proposed to obtain the optimal estimation.

4.1 ML Algorithm for Frame Synchronization

In the transmitted data sequence of DMT system, the cyclic prefix causes non-zero correlation between some pairs of samples. A maximum-likelihood estimator for frame synchronization derived in [38][39][40] employs the special characteristic of cyclic prefix. Fig. 4.1 shows that the last L samples, I', are copied to the guard interval, I, at the beginning of each DMT symbol of length N+L (from θ-L+1 to N+θ). We assume that the

---

length of cyclic prefix is L and the size of IFFT is N, 2(N+L) samples of two consecutive received symbols are observed. The variable θ is defined as the start position of a frame in the observed data, i.e., the θth sample is placed as the first element in the FFT operation. The maximum likelihood estimation of θ, given the received signal r(k), can be formulated as [38]

$$\hat{\theta} = \max_{\theta} \Lambda_r = \sum_{k=\theta-(L-1)}^{\theta} 2\{r(k)r(k+N)\} - \rho \cdot \left(|r(k)|^2 + |r(k+N)|^2\right) \quad \ldots\ldots\ldots\ldots\ldots\ldots(4.1)$$

where $\rho = \dfrac{\sigma_s^2}{\sigma_s^2 + \sigma_n^2}$, σ_s^2 and σ_n^2 are signal power and noise power, respectively.

If we define the "correlation" in term of the Euclidean distance between two constellation points, a low complexity ML algorithm [40] is obtained. When signal-to-noise ratio is high, i.e. 'ρ' is close to unity, the estimated result is similar to the ML algorithm.
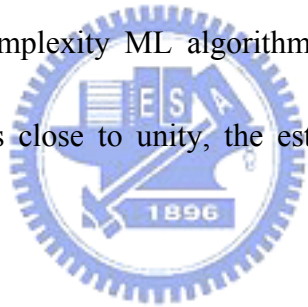
$$\hat{\theta} = \max_{\theta} \Lambda_r(\theta) = \max_{\theta} \sum_{k=\theta-(L-1)}^{\theta} -\{r(k) - r(k+N)\}^2 \quad \ldots\ldots\ldots\ldots\ldots\ldots\ldots\ldots\ldots(4.2)$$

All the above algorithms are based on the assumption that the channel is ideal. In other words, the received signals, r(k), are assumed identical to r(k+N) in the cyclic prefix period. However, the twisted-pair channel is dispersive, therefore, an algorithm to minimize the ISI should be considered. In Fig. 1.3, a DMT symbol can be sent after parallel-to-serial conversion as $\mathbf{Y}$= {y_{N-L}, y_{N-L+1},…, y_{N-1}, y_o, y_1, y_2, … ,y_{N-1}}. Denote that y_{N-L+k} = a_k for simplicity. If the length of the channel response $\mathbf{P}$ is shortened to M, M<L, by a time-domain equalizer (TEQ), then the shortened channel response $\mathbf{H}$ is represented by {h_o,

$h_1, h_2, \ldots h_{M-1}\}$. The received signal vector **R** is the convolution of transmitted signal **Y** and channel response **H**, i.e., **R=H·Y**.

$$
\mathbf{R} = \begin{bmatrix}
h_{M-1} & h_{M-2} & \cdots & h_1 & h_0 & 0 & \cdots & & & & & 0 \\
0 & h_{M-1} & \cdots & h_2 & h_1 & h_0 & 0 & \cdots & & & & 0 \\
\vdots & \vdots & & \vdots & & & \vdots & & & & & \vdots \\
0 & \cdots & 0 & h_{M-1} & \cdots & & & h_0 & 0 & \cdots & & 0 \\
\vdots & & & & & & & & & & & \\
0 & \cdots & & & & 0 & h_{M-1} & \cdots & h_0 & 0 & \cdots & 0 \\
\vdots & & & & & & & \vdots & & & & \vdots \\
0 & \cdots & & & & & 0 & h_{M-1} & \cdots & & h_0 & \cdots & 0 \\
\vdots & & & & & & & & \vdots & & \vdots & & \vdots \\
0 & \cdots & & & & & & & 0 & h_{M-1} & \cdots & h_1 & h_0
\end{bmatrix}
\begin{bmatrix}
a_{L-M+1}^{j-1} \\
a_{L-M+2}^{j-1} \\
\vdots \\
a_{L-1}^{j-1} \\
a_0^{j} \\
\vdots \\
a_{L-1}^{j} \\
y_0^{j} \\
\vdots \\
a_0^{j} \\
\vdots \\
a_{L-1}^{j}
\end{bmatrix}
\quad ..(4.3)
$$

The representation of r(k) can be expressed as:

$$
r(k) = \begin{cases}
\sum_{i=0}^{k} a_{k-i}^{j} \cdot h_i + \sum_{i=k+1}^{M-1} a_{k+L-i}^{j-1} \cdot h_i & 0 \le k < M\text{-}1 \\
\sum_{i=0}^{M-1} a_{k-i}^{j} \cdot h_i = \sum_{i=0}^{M-1} y_{N-L+k-i}^{j} \cdot h_i & M\text{-}1 \le k < L \\
\sum_{i=k-L+1}^{M-1} a_{k-i}^{j} \cdot h_i + \sum_{i=0}^{k-L} y_{k-L-i}^{j} \cdot h_i & L \le k < L+M\text{-}1 \\
\sum_{i=0}^{M-1} y_{k-L-i}^{j} \cdot h_i & M\text{-}1+L \le k < M+N\text{-}1 \\
\sum_{i=0}^{M-1} a_{k-N-i}^{j} \cdot h_i = \sum_{i=0}^{M-1} y_{k-L-i}^{j} \cdot h_i & M\text{-}1+N \le k < L+N \\
\sum_{i=k-N-L+1}^{M-1} a_{k-N-i}^{j} \cdot h_i + \sum_{i=0}^{k-N-L} a_{k-N-L-i}^{j+1} \cdot h_i & L+N \le k < L+N+M\text{-}1
\end{cases}
\quad ......(4.4)
$$

Note that, when $M-1 \le k < L$, r(k) is equal to r(k+N). Assuming that the length M of the shortened channel impulse response is shorter than the cyclic prefix length L, then only the Mth to L^{th} samples are identical to the $(M+N)^{th}$ to $(L+N)^{th}$ samples, respectively. If the number of summation terms of the estimation function is reduced to less than (L-M), the estimated value is much more likely located at the initial transition edge of the channel

impulse response. Thus we formulate a new modified ML algorithm by defining the

estimate of θ as:

$$\hat{\theta} = \max_{\theta} \Lambda_r(\theta) = \max_{\theta} \sum_{k=\theta-(L-M-1)}^{\theta} -\{r(k) - r(k+N)\}^2 \quad \dots\dots\dots\dots\dots\dots\dots\dots\dots\dots(4.5)$$

From the matrix analysis listed above, it can be proved theoretically that equation (4.5)

gives better estimation value over a dispersion channel. The detailed derivation is described

in the following section.

4.2 Modified ML Algorithm
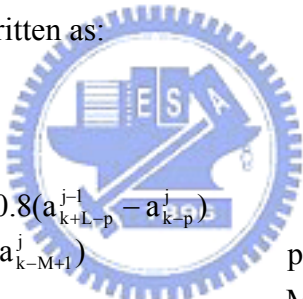
In order to prove that equation (4.5) performs better than equation (4.2), a new variable,

u(k), is defined by the difference between r(k) and r(k+N), i.e., u(k)=r(k)-r(k+N). By

applying the previously defined r(k) and r(k+N), u(k) can be expressed as:

$$u(k) = \begin{cases} \sum_{i=k+1}^{M-1} a_{k+L-i}^{j-1} \cdot h_i - \sum_{i=k+1}^{M-1} a_{k-i}^{j} \cdot h_i & 0 \le k < M-1 \\ 0 & M-1 \le k < L \\ \sum_{i=0}^{k-L} y_{k-L-i}^{j} \cdot h_i - \sum_{i=0}^{k-L} a_{k-L-i}^{j+1} \cdot h_i & L \le k < L+M-1 \\ \vdots & \vdots \end{cases} \quad \dots\dots\dots\dots\dots\dots\dots\dots\dots(4.6)$$

Then r(k) is used in equations (4.2) and (4.5) to find the maximum estimation value. If

some elements in the summation window are nonzero; i.e., r(k) is not equal to r(k+N), their

squared values are greater than zero. Therefore, the result is negative if some elements are

nonzero. Otherwise, if r(k) equals to r(k+N) for all elements in the summation window, the result will equal to zero, which gives the maximum value.

When the summation window length is shorter than (L-M) as in equation (4.5), the summation is zero, if k=L. Therefore, the estimated value, θ, is equal to L, which locates the frame boundary. Since the Lth to $(N+L)^{th}$ elements of r(k) contains only the jth symbol, then no ISI exists. However, if the summation window length equals to L as in equation (4.2), the estimated value will be located at the peak of the channel response. To reduce the complexity of derivation, we assume a simple channel model with $h_0=0.1$, $h_p=0.8$, and $h_{M-1}=0.1$. Then u(k) can be rewritten as:

$$u(k) = \begin{cases} 0.1(a_{k+L-M+1}^{j-1} - a_{k-M+1}^{j}) + 0.8(a_{k+L-p}^{j-1} - a_{k-p}^{j}) & 0 \leq k < p \\ 0.1(a_{k+L-M+1}^{j-1} - a_{k-M+1}^{j}) & p \leq k < M-1 \\ 0 & M-1 \leq k < L \\ 0.1(y_{k-L}^{j} - a_{k-L}^{j+1}) & L \leq k < L+p \\ 0.1(y_{k-L}^{j} - a_{k-L}^{j+1}) + 0.8(y_{k-L-p}^{j} - a_{k-L-p}^{j+1}) & L+p \leq k < L+M-1 \\ \vdots & \vdots \end{cases} \quad \ldots\ldots\ldots\ldots(4.7)$$

If the summation window length is L as that in equation (4.2), the maximum value should be obtained when k = (L+p), with a delay "p" from the previous value, where "p" is the peak position of the channel response. Since the $(N+L)^{th}$ to $(N+L+p)^{th}$ elements of r(k) contains the jth as well as $(j+1)^{th}$ symbol, thus ISI is introduced. Fig. 4.1 is used to demonstrate the previous derivations. From these derivations, it is seen that equation (4.2)

estimates the frame boundary at the channel peak instead of its initial rising edge; therefore,

ISI is introduced and it degrades the system performance [41].

(a) Original DMT data sequence

(b) Channel response

(c) Received data convoluted with channel response and offset with N samples

(d) Received data convoluted with channel response

(e) Equation (4.5) output by applying modified ML algorithm

(f) Equation (4.2) output by applying ML algorithm
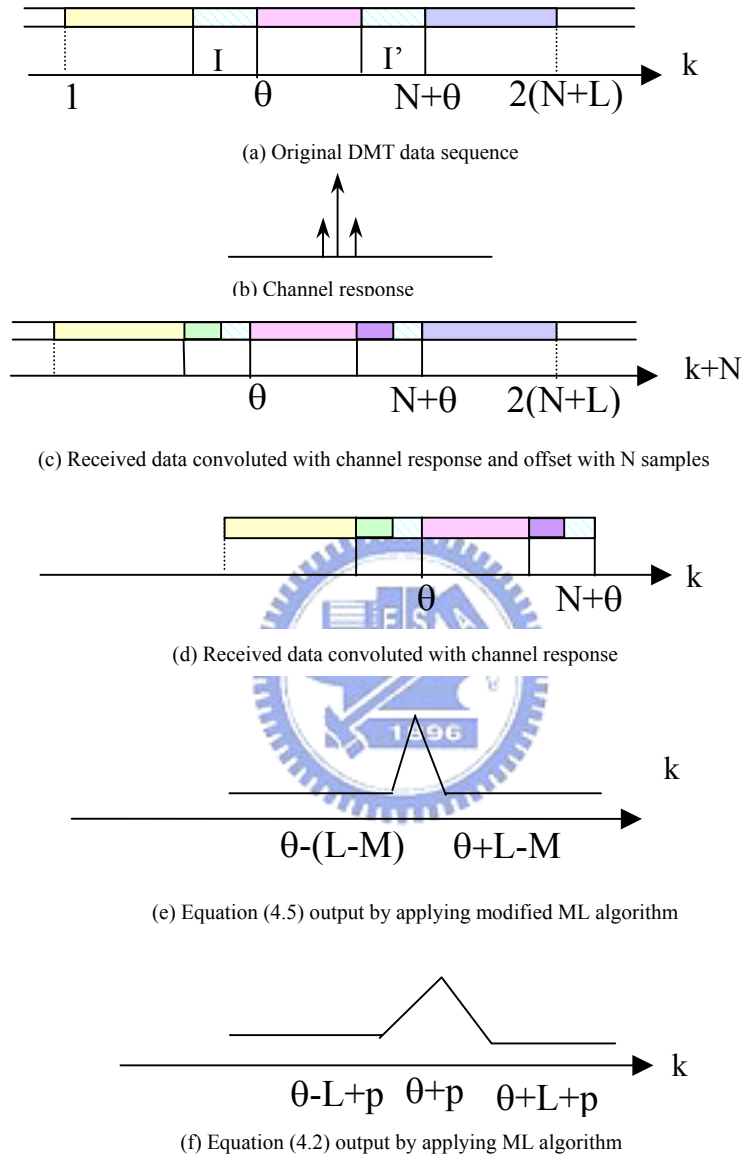
Figure 4.1 Illustration for equation derivation.

4.3 Computer Simulations

To evaluate the performance of this modified algorithm, some computer simulations are performed. First, the simulation environment is introduced, and then a new term, called Et/N_0, is defined as a parameter to indicate the performance of these algorithms. From the simulation results, it is seen that the performance is strongly dependent on the bit-loading of each tone. Therefore, the relationship between these two parameters is studied in the second subsection. Then the test procedures are applied to a simple loop with various lengths to compare the performance of two algorithms as well as the loop characteristics. Finally, all VDSL test loops, VDSL0 to VDSL7 in reference [4], are simulated to study the performance of these algorithms over various types of loop topology.
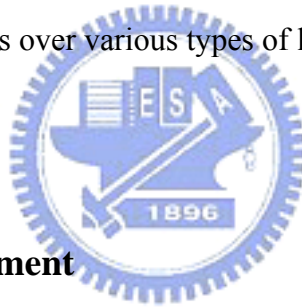
4.3.1 Simulation Environment

The complexity of the modified ML algorithm is the same as the conventional one. However, it provides better estimation for frame synchronization of the DMT system. A test environment is built to perform the evaluation of these algorithms. This simulation program includes several modules: the DMT symbol generator, channel models, and receiver. The DMT symbol generator assigns random data into N/2 sub-channels continuously. The bit number of each sub-channel is assigned by the bit-loading table, which is calculated according to the transfer functions of the corresponding loops. A look-up table is also set up to contain the QAM constellations of various sizes, ranging from 2 bits to 15 bits with normalized signal power. Each DMT symbol is converted to the corresponding time-domain samples by using N-point IFFT, parallel-to-serial converter, and adding cyclic

prefix. These data are then convoluted with the channel modeling in time domain to simulate the data at the receiver side. In the analysis, the AWGN noise is taken into consideration and the transmission power is –60 dBm/Hz in the amateur radio bands.

The received data are processed by a TEQ such that the tail of the impulse response is shortened to less than that of cyclic prefix. Subsequently, the frame synchronization algorithm is applied to locate an FFT symbol so that a precursor ISI-free demodulation can be obtained. A one-tap per sub-channel FEQ is used to equalize the channel distortion so that the transmitted QAM signal can be recovered. The function of performance monitor program is to calculate the difference between the received data and its original source.

Currently, most of the DMT xDSL system uses a TEQ[36] plus FEQ structure for channel equalization. Since the channel response of a twisted-pair line is longer than hundreds of taps, a TEQ is used to reduce the length of impulse response. In our simulation, the coefficient of TEQ is calculated by using the Impulse Response Shortening (IRS) algorithm[36] with 32 zeroes and 16 poles in downstream direction. It can generate a shortened impulse response (SIR) with length shorter than that of cyclic prefix for each test loop in our system. The coefficient of FEQ is calculated by an inverse function of the product of TEQ and original channel response. Since the topologies of test loops are known, their impulse responses and corresponding TEQ and FEQ coefficients can be calculated directly without any training process.

The simulation environment has been built by creating the functional blocks as shown in Fig. 1.3. All topologies of test loops, VDSL0 to VDSL7 as well as a simple loop with length varying from 100 m to 1500 m, have been applied in the performance test simulations. The estimated value θ by the ML and modified ML algorithms are calculated first. If the block of each frame is selected according to the calculated frame boundary, and passed through the FFT and FEQ blocks frame by frame. Finally, the results are compared with the original transmitted data. Due to the channel effect, the received data are scattered

around the original constellation point. The deviation of the noisy data determines the performance of the system. If the deviation is larger than half the distance between two consecutive constellation points, the received data may be decoded incorrectly. We define a new parameter, called Et/N_0, to indicate the normalized energy of two constellation points over the noise power. The distance between two constellation points is reduced if the QAM size grows, and thus is more sensitive to the noises.

4.3.2 Performance Comparison of ML and Modified ML Algorithms

The computer simulations of two synchronization algorithms are applied on all the test loops to obtain the Et/N_0 of each tone in the receiver side. From the simulation results, it is observed that the performance of Et/N_0 is strongly dependent on the number of bits per sub-channel. Loop VDSL 1200 m is selected to demonstrate this relationship because its bit-loading curve varies like going-downstairs step by step from 15 bits to 3 bits, as shown in Fig. 4.2. The performance monitor module calculates the average of Et/N_0 (dB) for each tone over 100 symbols under various transmission power and noise, as shown in Fig. 4.3.

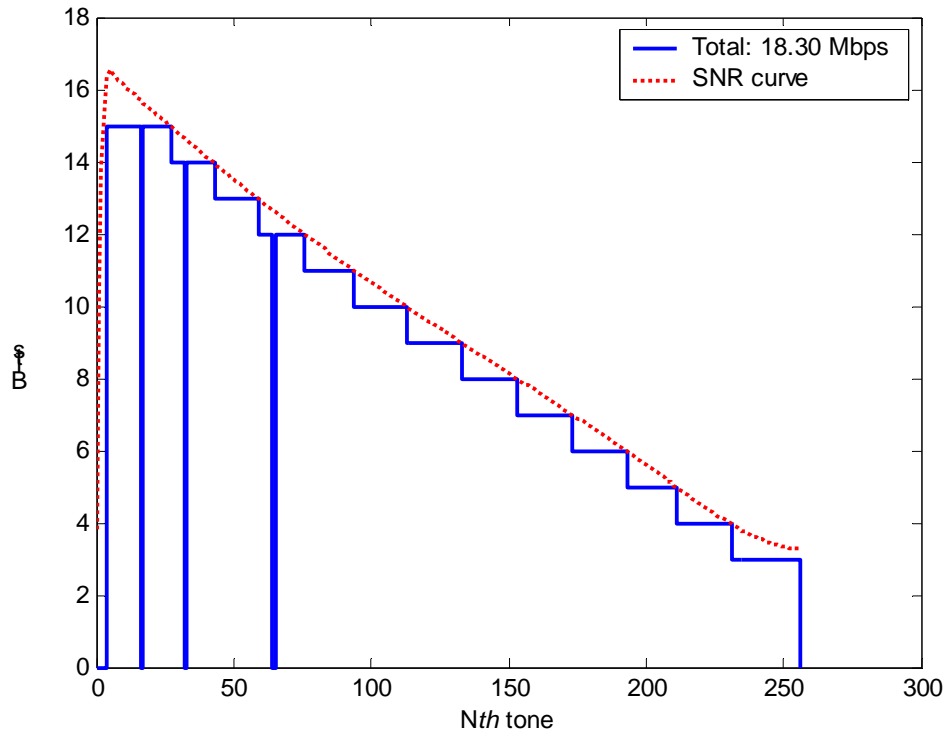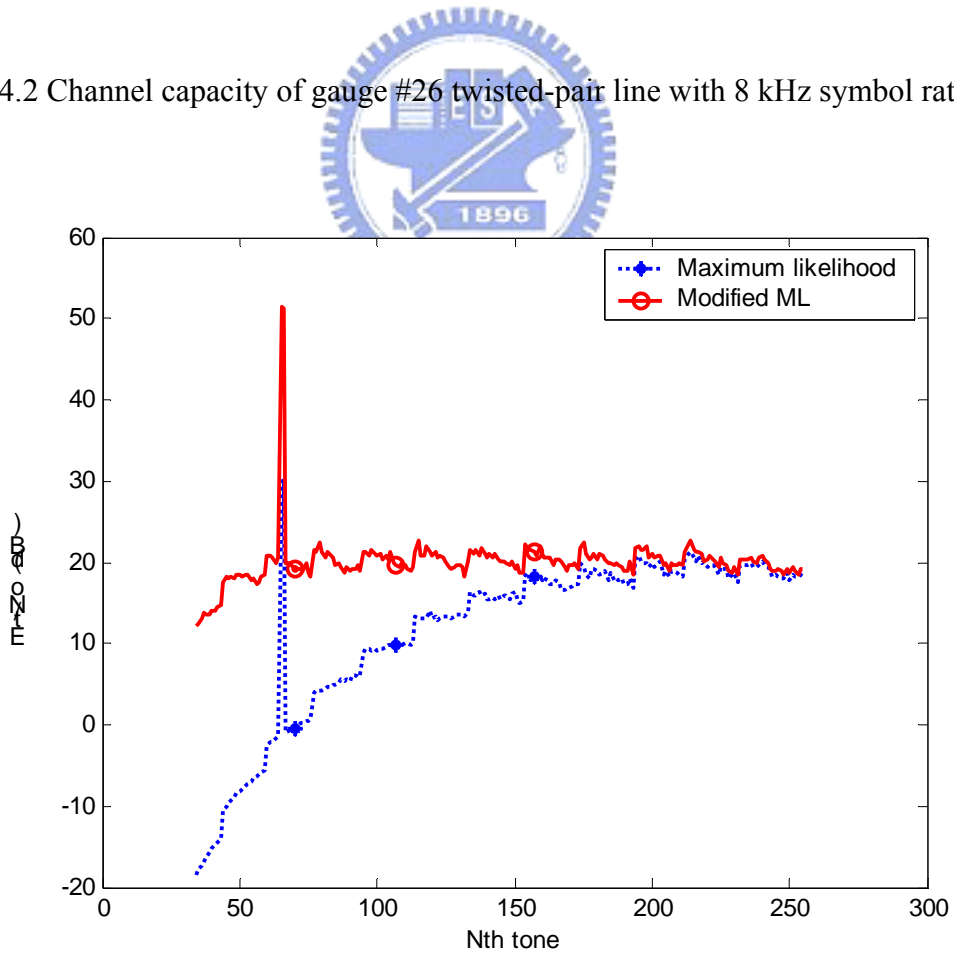Figure 4.2 Channel capacity of gauge #26 twisted-pair line with 8 kHz symbol rate.

(a)
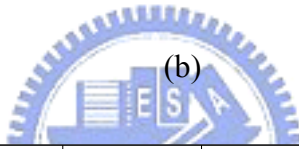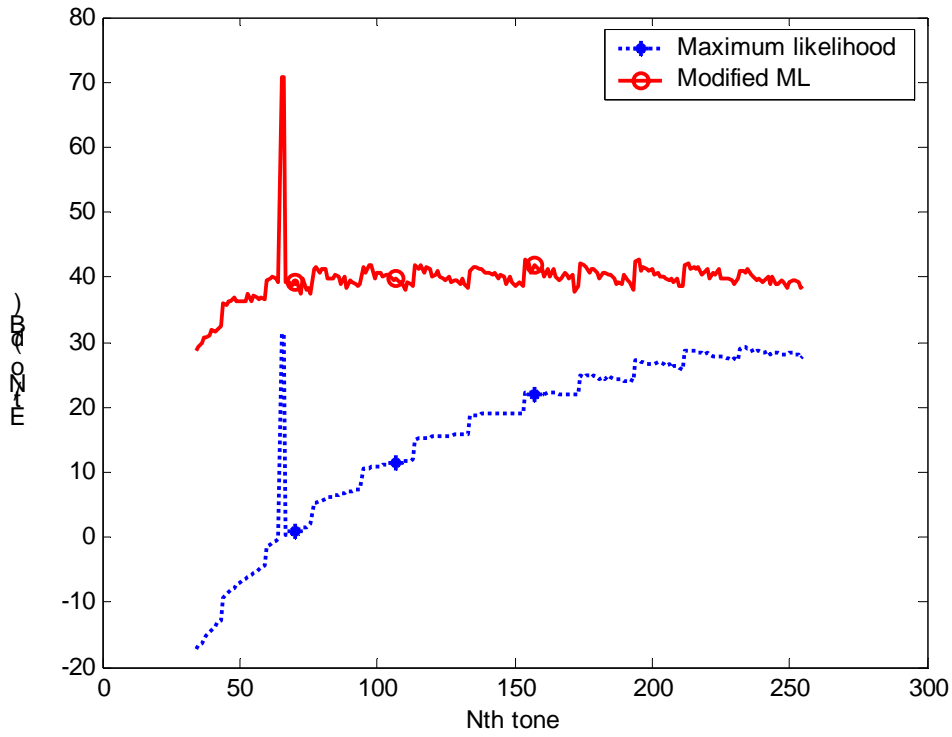
(b)
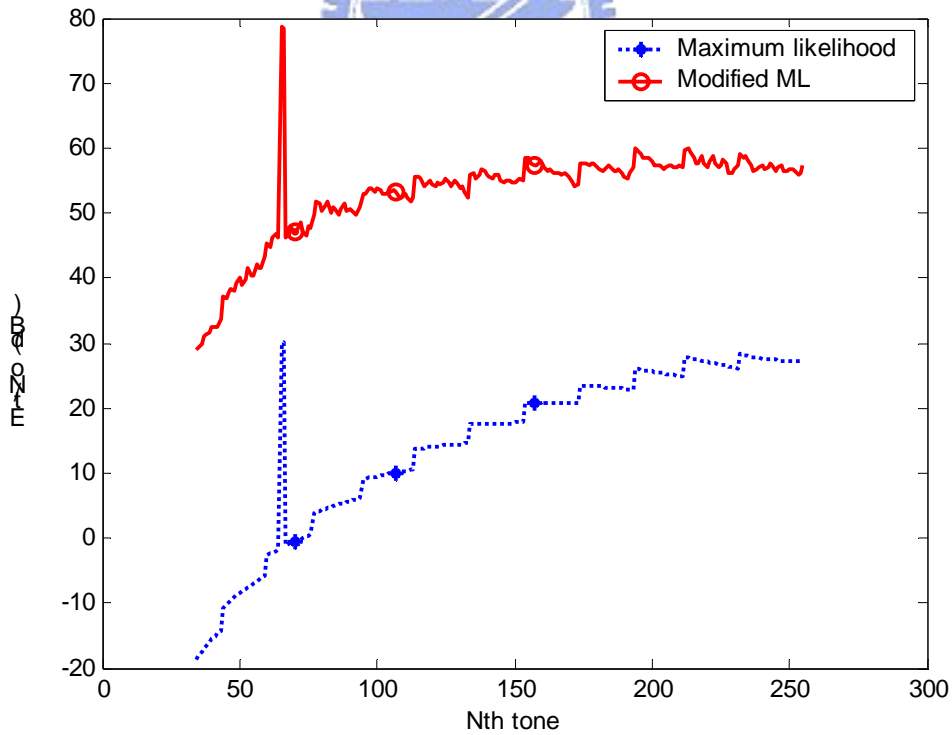
(c)

Figure 4.3 Performance of frame synchronization algorithms with various transmission power (a) -60 dBm/Hz (b) -40 dBm/Hz (c) without AWGN -140 dBm/Hz

For conventional maximum likelihood estimator, the obtained values of E_t/N_0 are 0, 12, and 20 dB for 12-, 10-, and 7-bit constellation, respectively. However, the value of E_t/N_0 maintains around 20 dB respectively for the modified ML method while the transmission powere is around -60 dBm/Hz. If the transimission power is raised to -40 dBm/Hz, the value of E_t/N_0 is raised around to 40 dB for the modified ML method. If the AWGN noise of -140 dBm/Hz is not added into the receiving signal, the value of E_t/N_0 can be raises to even around 50 dB. It is clear to see the performance degradation caused by precursor ISI, especially for high-level QAM. The peak in each case occurs at the 64th sub-channel (pilot tone), the E_t/N_0 value grows high because only two bits are carried in these high SNR band. The simulation results show that the modified ML algorithm performs better than the conventional one, especially at the tone carrying more bits. The E_t/N_0 of the modified ML algorithm is greater than the original one, which indicates that the decoded values after FFT and FEQ blocks are closer to the original constellation points. Therefore, the precursor ISI is reduced and BER is improved. The SNR differences between the two algorithms are shown in Fig. 4.3. The simulation is applied to all the VDSL test loops, including a simple loop with length varying from 100 m to 1500 m. Since the SNR curve of a pure loop without any bridged- tap decreases smoothly and the corresponding bit-loading curve is similar to that shown in Fig. 4.3. Therefore, it is easier to see the relationship between E_t/N_0 and bit-loading. For the loops shorter than 500 meters, the bit-loading maintains above 12 bits for most tones, and therefore, the SNR differences are high for all tones. For the longer loops, the bit-loading are lowered in high frequency, and the SNR difference is reduced, as shown in Fig. 4.4.
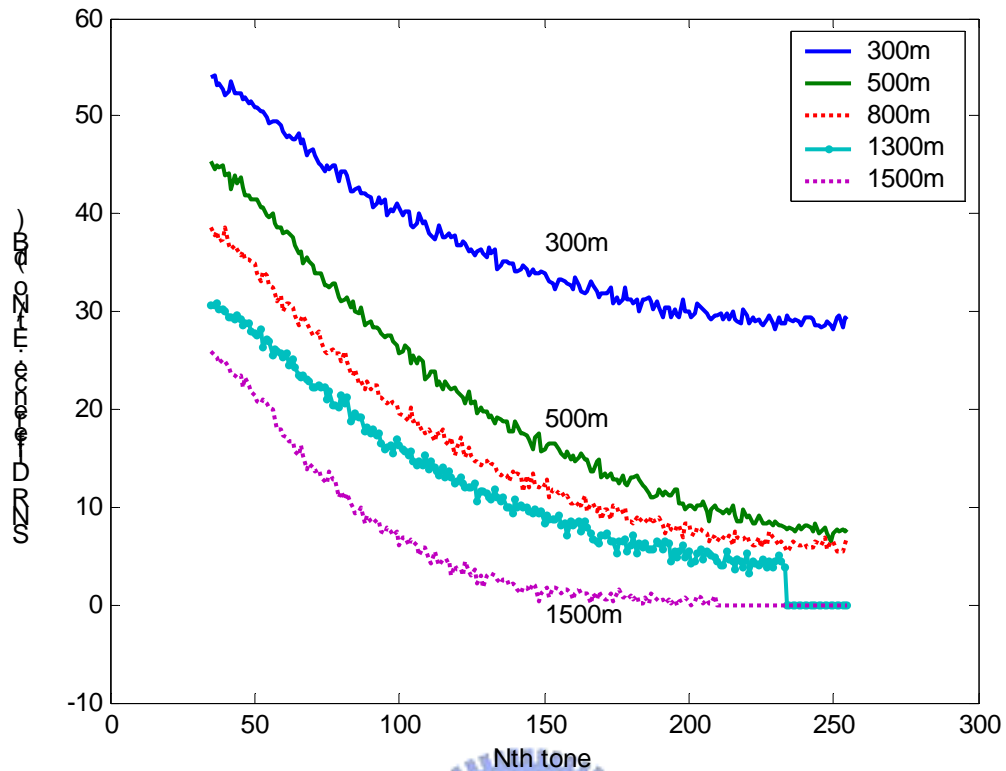
Figure 4.4 SNR difference of various loops.

Although the SNR difference is affected by the bit-loading, it also depends on the original SNR curve of the tested loop. In other words, the absolute value of SNR differences cannot indicate the exact bit-loading value, however, it increases at high bit-loading tones. From the simulations, we can see that the performance of the modified ML algorithm is better than the conventional one, especially for the DMT VDSL system with high-level QAM.

4.3.3 Loop Length and Channel Characteristics

The VDSL system limits its loop length up to 1500 m. Therefore, a set of test loops with simple topology and length from 100 m to 1500 m are simulated to show the relationship between channel characteristics and loop length.

It can be seen that the longer the loop, the broader the response will be. In addition, the delay becomes greater while the loop length gets longer. The impulse channel responses of these loops have long tails and their lengths are much longer than that of cyclic prefix. Therefore, the TEQ should be applied in the receiver system to get the SIR of each channel. The original channel response and its corresponding SIR are shown in Fig. 4.5.
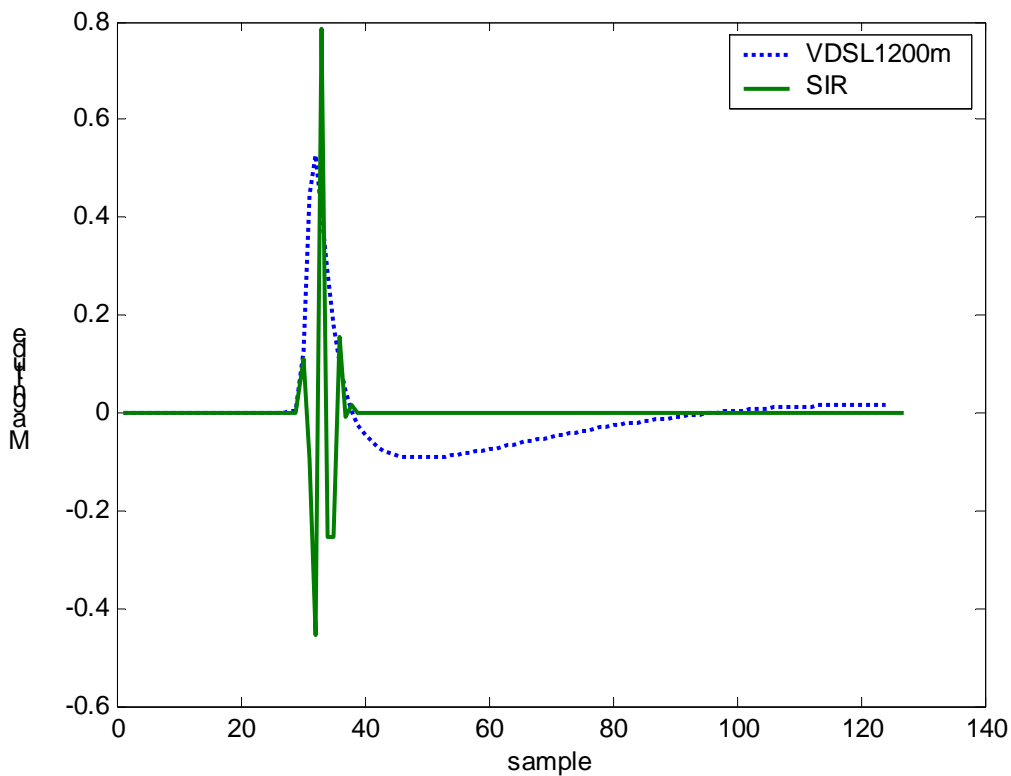
Figure 4.5 Channel response and its SIR of loop VDSL 1200 m.

Fig. 4.5 shows that the length of SIR, an output from TEQ functional block, is reduced to smaller than 20, i.e., M < 20. However, the length of the original impulse response is

over 100.

To search the optimal solution of summation window length for the frame synchronization, the magnitude of M varies from 1 to L, the corresponding averaged Et/N_0 of some tested loops are shown in Fig. 4.6. If the length of channel response is shorter than that of cyclic prefix, the choice of window length has more than one optimal choices. From Fig. 4.6, the Et/N_0 maintains at the same level during the window length (L-M) varying from 2 to 22. If the variable M is large enough to cover the main energy band of the SIR, the estimator can deliver a proper solution without precursor ISI. The conventional ML estimator can be viewed as a special case of the modified ML algorithm with M equal to zero. Since the channel responses of VDSL test loops are sharp after TEQ, the summation window length can be set under 20.

In real application system, the exact length of a SIR is difficult to estimate; therefore, the magnitude of M is assigned a reasonable value by the program, such as 20. However, if the assigned value M can cover the main energy band of the SIR, the ISI caused by the residual tail is negligible. On the other hand, if M is larger than the length of the SIR, the output of equation (4.5) has more than one solution. In other words, the maximum value θ is a continuous band instead of a sharp peak value. To obtain the correct solution in our system, the largest value in the continuous band should be selected.
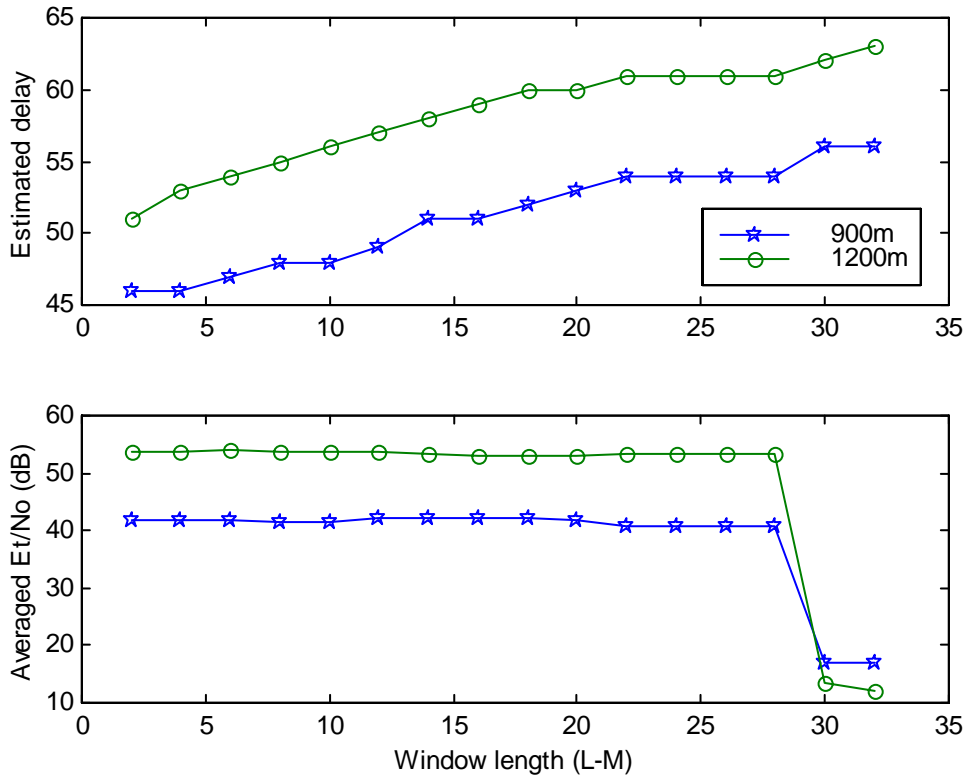
Figure 4.6 Estimated delays and their Et/N_0 vs. window length.
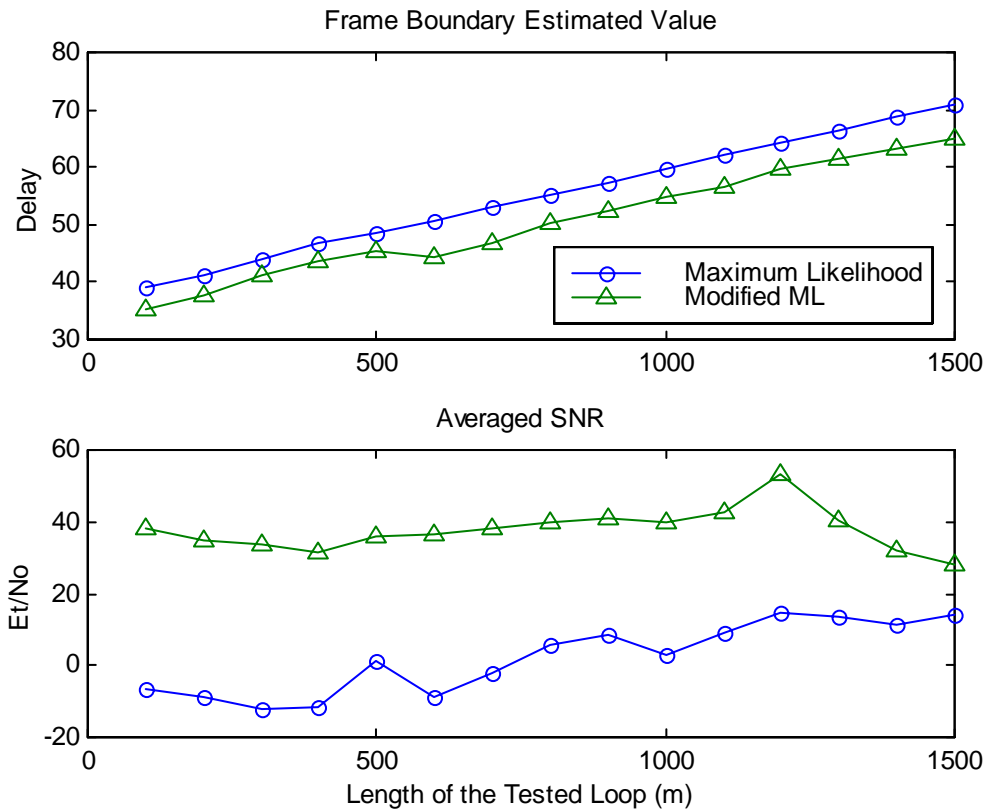
Figure 4.7 θ and Et/N_0 of VDSL test loops.

The estimated frame boundary θ and the averaged E_t/N_0 of all used tones for 8 kHz DMT VDSL downstream over a loop with various lengths are listed in Fig. 4.7.

The length of test loops is arranged from 100 m to 1500 m, and their index numbers are from 1 to 15, respectively. The estimated delays by ML and Modified ML algorithms are about 2 to 8. The delay indicates the distance between the original rising edge and peak position of the shortened channel response. The bit-loading of each tone for short loop is high, and therefore the performance of the modified ML algorithm is much better than the conventional one.

4.3.4 VDSL Test Loops with Complex Topologies

The above procedure can be applied to other test loops with complex topologies as listed in the VLSI draft standard [35]. The estimated frame boundary θ and the averaged E_t/N_0 of all used tones for 8 kHz DMT VDSL downstream are listed in Table 1 and Fig. 4.8. The first row in Table 1 contains the results from the conventional ML algorithm while the lower ones are from the modified ML algorithm.

Table 4.1 (θ, Et/N$_0$) of VDSL test loops.

Loop No.	VDSL1	VDSL2	VDSL3	VDSL4	VDSL5, 6, & 7
Short	(43,-12)	(42, -5)	(43,-4.5)	(43, -5)	(42, -4)
(300 m)	(37,35)	(39,36)	(37, 36)	(40,30)	(38,32)
Medium	(59, 2)	(58, 8)	(58,-0.5)	(58,26)	(58, 2)
(1000 m)	(50,41)	(48,32)	(49,35)	(55,38)	(49,38)
Long	(70,17)	(69, 3)	(69, -4)	(70,19)	(70,10)
(1500 m)	(61,24)	(60,23)	(60,20)	(64,21)	(61,33)
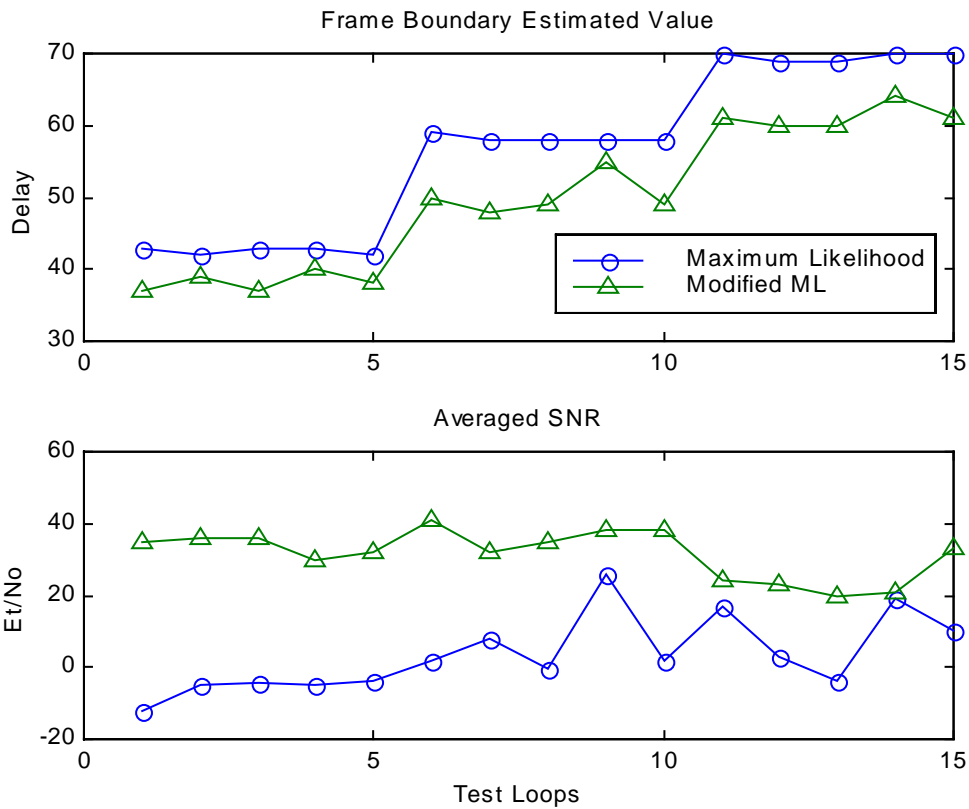
Figure 4.8 θ and Et/N$_0$ of VDSL test loops.

The order of test loops is arranged from short to long, with the index numbers from 1 to 15, respectively. In other words, VDSL1 to VDSL4 of 300 m long are indexed from 1 to

4, VDSL5 is 5, while VDSL1 to VDSL4 of 1000 m long are 6 to 9, VDSL6 is 10, etc. Since the topologies of these test loops contain various types of wires and some of them have bridged-taps, the performance differences of these two algorithms do not have smooth transition as the previous test cases. However, the bit-loading of each tone for short loop is high, and therefore the performance of the modified ML algorithm is much better than the conventional one, especially for short test loop.

4.4 Summary

In this chapter, a low-complexity modified ML algorithm for frame boundary estimation is developed. Its performance is better than the conventional one over the dispersive channel. A test environment is built to analyze the performance of DMT-based VDSL system. The analysis in this dissertation takes the AWGN noise into consideration and the transmission power is -60 dBm/Hz in the amateur radio bands. Simulation results show that the modified ML algorithm has better performance so that the Et/N_0 of each tone is raised, especially for those carrying data of high-level QAM. The modified algorithm improves the VDSL system performance significantly because most of its sub-channels are loaded with a large number of bits.

Chapter 5

ISI Cancellation Algorithm for DMT-based VDSL

System

For the traditional DMT-based VDSL system, there are still two drawbacks remained: un-cancelled residual ISI outside the cyclic prefix and deterioration of channel capacity by TEQ. In this chapter[3][43], we propose a algorithm to enhance the performance of the DMT-based VDSL system by minimizing the ISI effect.

Several techniques have been proposed to reduce or even remove the cyclic prefix in the OFDM system [43][44][45][46]. In [44], the residual ISI cancellation (RISIC) technique was first introduced to mitigate the residual ISI in an OFDM system with channel response longer than the guard interval. The corresponding receiver structure is shown in Fig. 5.1. Recently, there are some further studies to the RISIC algorithms. In [45], the author proposed a modified algorithm, denoted as Kim's approach in this dissertation, with multiple processing iterations and the performance is better than the RISIC algorithm especially over the channel with a deep spectral null. However, it can be applied only in a low-level QAM system, such as 16-QAM constellations. Another method proposed in [46]

---

[3] Part of the content in this chapter will be published in:

S. T. Lin and C. H. Wei, "Iterative ISI Cancellation for DMT-based VDSL Systems," to appear in *International Journal of Electrical Engineering.*

improves the performance of RISIC algorithm by adding soft in and soft out (SISO) decision feedback to the whole system. It does improve the whole system performance slightly, with a tremendous increase in system complexity. In this chapter, we first apply the RISIC algorithm to the DMT-based VDSL system with reduced guard interval and compare its performance with traditional cyclic prefix system. Then we propose an iterative ISI cancellation with zero-padded (IIC-ZP) algorithm, a modification of RISIC algorithm with reasonable complexity, for DMT-based VDSL system to improve its performance, especially for the system without guard interval. There is another approach [47][48] using perfect equalization for DMT system without guard interval, however, it process the data in frequency domain instead of time domain.

5.1 System Model

In this section, a typical DMT-based VDSL system is introduced first, then the procedures of RISIC algorithm and Kim's approach are derived. Finally, the proposed algorithm of IIC-ZP algorithm is discussed.

5.1.1 DMT-based VDSL System

The i-th transmitted DMT symbol in frequency domain can be expressed as $X_{i,k}$. The corresponding IFFT $x_{i,n}$ is the time domain signal after DMT modulation:

$$x_{i,n} = \frac{1}{\sqrt{N}} \sum_{k=0}^{N-1} X_{i,k} e^{j2\pi kn/N}, \ 0 \le n \le N-1 \ \text{..(5.1)}$$

Cyclic prefix is added to $x_{i,n}$ before transmission:

$$s_{i,n} = \left\{ x_{i,N-L}, \cdots, x_{i,N-1}, x_{i,0}, \cdots, x_{i,N-1} \right\}, \quad 0 \le n \le N+L-1 \quad \ldots\ldots\ldots\ldots\ldots\ldots\ldots\ldots\ldots\ldots(5.2)$$

Let the VDSL channel response $\mathbf{h}$ of length $M+1$ be

$$\mathbf{h} = \left\{ h_0, h_1, \cdots h_M \right\} \ldots\ldots\ldots\ldots\ldots\ldots\ldots\ldots\ldots\ldots\ldots\ldots\ldots\ldots\ldots\ldots\ldots\ldots(5.3)$$

If the channel length is shorter than the cyclic prefix, i.e., $M \le L$, the received signal $\mathbf{r}$ can

be represented as:

$$r_{i,n} = \sum_{m=0}^{M} h_m x_{i,((n-m))_N}, \quad 0 \le n \le N-1 \ldots\ldots\ldots\ldots\ldots\ldots\ldots\ldots\ldots\ldots\ldots\ldots\ldots(5.4)$$

where $(\cdot)_N$ denotes modulo by N.
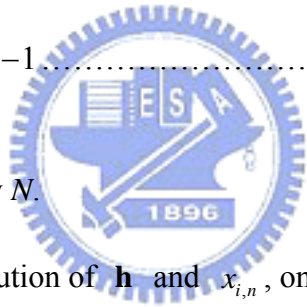
Signal $r_{i,n}$ is a circular convolution of $\mathbf{h}$ and $x_{i,n}$, only when $M \le L$. Otherwise, the

residual ISI outside the cyclic prefix will degrade the system performance.

5.1.2 RISIC Algorithm

The RISIC algorithm [44], was originally proposed for the fixed and low bit-loading

wireless OFDM application. The algorithm containing two major steps, tail cancellation

and cyclic reconstruction, can be described as follows.

Step (1) : Previous symbol ISI tail cancellation:

$$\tilde{r}_{i,n}^0 = r_{i,n} - \zeta_{i-1,n}^I, \quad 0 \le n \le N-1 \dots\dots\dots\dots\dots\dots\dots\dots\dots\dots\dots\dots\dots\dots(5.5)$$

where $\zeta_{i-1,n}^I$ is the previous symbol ISI tail after I-th iteration, as defined in Step (6),

equation (5.9)

Step (2) : Current symbol estimation:

$$\hat{X}_{i,k}^0 = FFT\{\tilde{r}_{i,n}^0\}/H_k \dots\dots\dots\dots\dots\dots\dots\dots\dots\dots\dots\dots\dots\dots\dots(5.6)$$

where H_k is k-th channel response in frequency domain.

Step (3) : Cyclic reconstruction tail calculation:

Perform IFFT to current symbol $\hat{X}_{i,k}^0$ to get $\hat{x}_{i,k}^0$, then calculate its tail portion $t_{i,n}^0$

$$t_{i,n}^0 = \sum_{m=L}^{M} h_m \hat{x}_{i,((n-m))_N}^0 \cdot (1 - u(n-m+L)) \dots\dots\dots\dots\dots\dots\dots\dots\dots(5.7)$$

where $u(k)$ is a step function at k=0
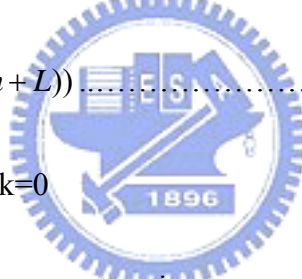
Step (4) : Current symbol cyclic reconstruction:

$$\tilde{r}_{i,n}^I = \tilde{r}_{i,n}^0 + t_{i,n}^{I-1}, \quad 0 \le n \le N-1 \dots\dots\dots\dots\dots\dots\dots\dots\dots\dots\dots\dots(5.8)$$

Step (5) : Repeat Step (2) to Step (4) I times to obtain $\hat{X}_{i,k}^I$ and $t_{i,n}^I$.

Step (6) : ISI tail calculation:

$$\zeta_{i,n}^I = \sum_{m=1}^{M} h_m \hat{x}_{i-1,((n-m+L))_N}^I \cdot (1 - u(n-m+L)) \dots\dots\dots\dots\dots\dots\dots\dots\dots(5.9)$$

The above RISIC algorithm can be employed to the OFDM system with insufficient

cyclic prefix length, even there is no guard interval between two symbols [44]. For

DMT-based VDSL system, each sub-channel contains high-level QAM, the performance of

RISIC algorithm is shown to be better than the traditional DMT system after one iteration

except when the system has no guard interval.
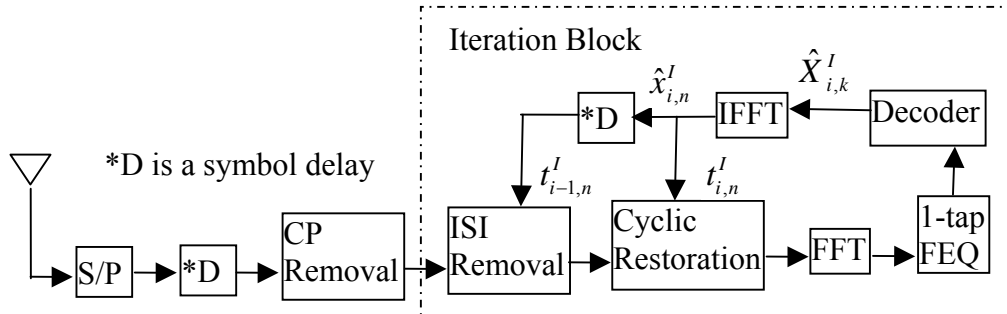
Figure 5.1 Receiver block for iterative ISI cancellation.

5.1.3 Kim's Approach

In this section, the Kim's approach [45], which is improved from the RISIC algorithm, is described. Fig. 5.2 shows the block diagram of the proposed approach which proceeds as:

Step (1) : Optimal delay is estimated:

$$D = \arg \max_{d \in \{0,1,\cdots,N-2L\}} \left\{ \sum_{n=0}^{N-2L} \left| z_{(N-d+n)N} \right| \right\} \quad \text{...(5.10)}$$

where $z_n = IFFT\{1/H_k\}, \ 0 \le n \le N-1$ ....(5.11)

Step (2) : Cyclic prefix portion of the current block is recovered:

$$\hat{X}'_{i,k} = FFT\left\{r_{i,D}, r_{i,D+1}, \cdots r_{i,N-1}, r_{i+1,0}, \cdots r_{i+1,D-1}\right\}\big/H_k \quad \text{.............................}(5.12)$$

$\hat{X}'_{i,k}$ is converted back to time domain giving $\hat{x}'_{i,n}$, $0 \le n \le N-1$

Step (3) : Previous symbol ISI cancellation and cyclic prefix reconstruction are performed

simultaneously:

$$\tilde{r}_{i,n} = r_{i,n} + h_n * \left(\hat{x}_{i,n-D} - \hat{x}_{i,n-D}\right) \quad \text{..}(5.13)$$

where * stands for linear convolution.

Step (4) : $\tilde{r}_{i,n}$, $0 \le n \le N-1$, are then converted to the frequency domain, and the

frequency domain equalization is done and decisions are made to obtain $\hat{X}_{i,k}$.

Although one block delay is introduced in Step (2), no intermediate decisions are used in
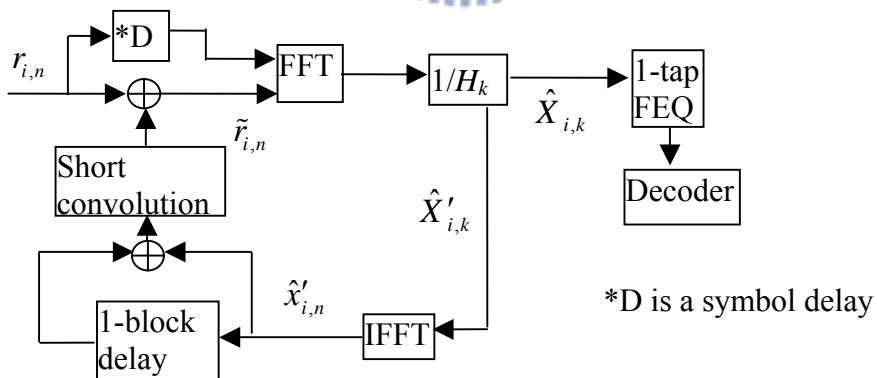
this scheme.

Figure 5.2 Block diagram of the Kim's approach.

5.1.4 IIC-ZP Algorithm

The IIC-ZP algorithm is derived from RISIC algorithm to improve the system performance, especially in the system without guard interval.

Modification 1: Select a peak delay Δ for initial symbol estimation in Step (2) of RISIC algorithm. This concept is similar to reference [45], but the peak is defined in [49] as the highest energy of the channel response, which can be located by maximum likelihood (ML) algorithm for frame synchronization.

If the peak of the twisted-pair channel response is located at D delays from the beginning of the response, the selected data used for the zero-th iteration in equation (5.5) of current symbol estimation in the FFT operation is replaced by:

$$\tilde{r}_{i,n}^0, \quad D \leq n \leq N+D-1 \dots\dots\dots\dots\dots\dots\dots\dots\dots\dots\dots\dots\dots\dots\dots(5.14)$$

Selecting the peak delay at the initial estimation will improve the performance of the RISIC algorithm when there is no guard interval, as shown in Fig. 5.9. If the length of guard interval exists, this peak delay technique cannot be applied to the cyclic prefix system but it can be applied to the zero-padded system [50] instead.

Modification 2: Padding zeroes in guard interval between two symbols instead of cyclic prefix is used for reducing complexity in tail calculation process.

$$s_{i,n} = \left\{ x_{i,0} \cdots, x_{i,N-1}, 0, ..., 0 \right\}, \quad 0 \leq n \leq N+L-1 \dots\dots\dots\dots\dots\dots\dots\dots\dots\dots(5.15)$$

The received signal **r** is expressed as:

$$r_{i,n} = t_{i-1,n+L}^I + \sum_{m=0}^{M} h_m \hat{x}_{i-1,((n-m))_N}^I \dots\dots\dots\dots\dots\dots\dots\dots\dots\dots\dots\dots\dots\dots(5.16)$$

Then the previous symbol's ISI tail in the Step (1) of RISIC is:

$$t_{i-1,n+L}^I = \sum_{m=1}^{M} h_m \hat{x}_{i-1,((n-m+L))_N}^I \cdot (1 - u(n-m+L)) \dots\dots\dots\dots\dots\dots\dots\dots\dots\dots(5.17)$$

And Step (4) of RISIC, current symbol cyclic reconstruction, should be modified:

$$\tilde{r}_{i,n}^{I} = \begin{cases} \tilde{r}_{i,n}^{0} + r_{i,n+N}, & 0 \le n \le L-1 \\ \tilde{r}_{i,n}^{0} + t_{i,n+L}^{I-1}, & L \le n \le M-1 \\ \tilde{r}_{i,n}^{0}, & M \le n \le N-1 \end{cases} \quad \text{(5.18)}$$

One advantage of the IIC-ZP algorithm is that ISI tail and cyclic reconstruction tail are identical, as shown in equations (5.16) to (5.18).

5.2 Computer Simulations

In this section, an example to illustrate the impact of the residual ISI on a DMT-based system is discussed first. Then the simulation results of the RISIC algorithm, Kim's approach, and our proposed IIC-ZP algorithm are illustrated to observe their performances.
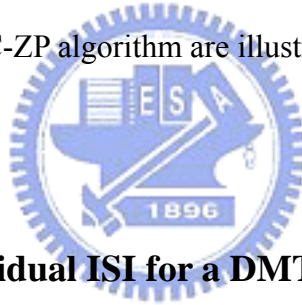
5.2.1 Influence of the Residual ISI for a DMT-based System

To see the influence caused by the ISI, an example is illustrated to demonstrate the relationship between the original information signals $X_{i,k}$, its corresponding IFFT signal $x_{i,n}$, and the transmission signal with cyclic prefix $s_{i,n}$. The sizes of both FFT and IFFT are set to N=128 and the cyclic prefix length L=8 in this proposed example. The original signals $X_{i,k}$ is set zero except the 4th and the 124th components to be 1+i and 1-i. The corresponding IFFT signal $x_{i,n}$ will form as three sine waves in one period N=128, as shown in Fig. 5.3 with small dots. The transmission signal with cyclic prefix $s_{i,n}$, with circle point in Fig. 5.3, are formed by adding last 8 component in front of $x_{i,n}$. The received data, $r_{i,n}$, is the results of convolution of transmission signal with the channel response H=[0.03

0.06 0.7 0.1 0.01 0.09 0.01], i.e., $M \leq L$ (L=8), is plotted in Fig. 5.4. The signals plotted by the '*' points are the convolution results of $x_{i,n}$ and H, while the circle points are the convolution results of $s_{i,n}$ and H. From the simulation results, the received data is distorted by the channel effect, however, if the cyclic prefix is added, the perfect reconstructed is possible by using the N points of information from the received (N+L) points.
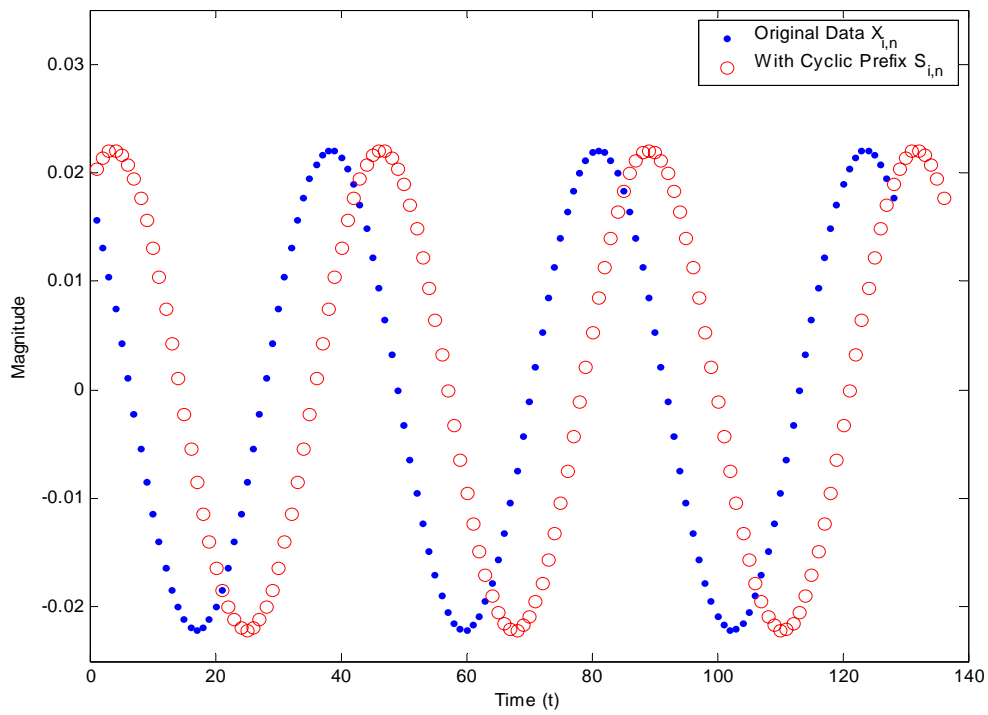
Figure 5.3 DMT signal in time domain with one active tone.
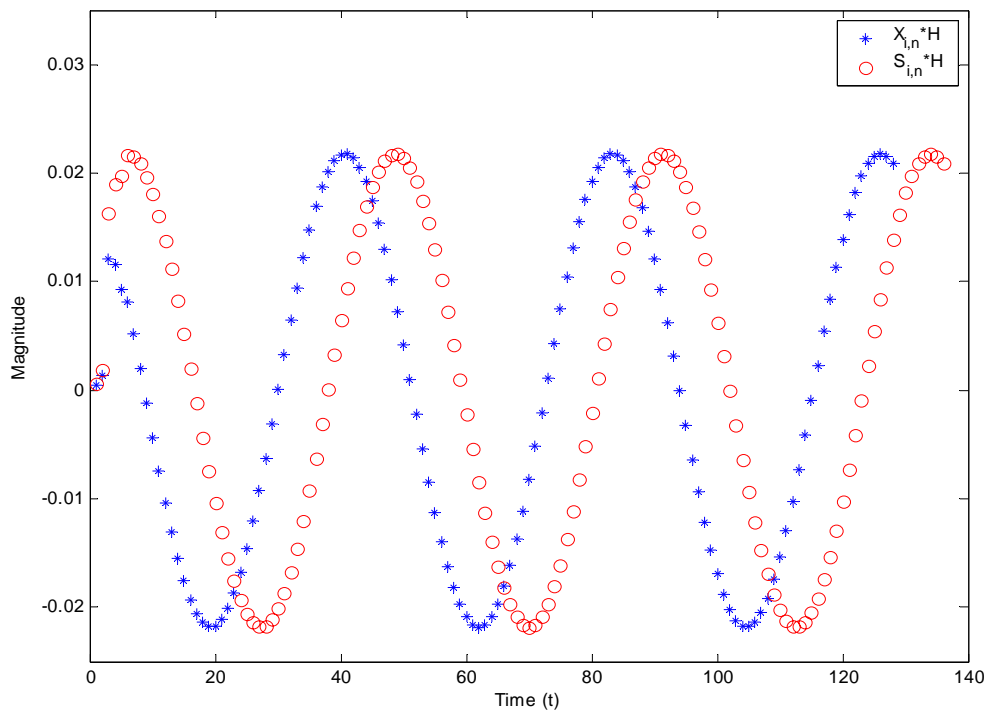
Figure 5.4 Received signal with channel length shorter than that of cyclic prefix.

However, if the channel length is longer than that of the cyclic prefix, the received data may be distorted seriously such that the perfect reconstruction is not possible no matter cyclic prefix is added or not, as shown in Fig. 5.5. In this example, the channel response H=[0.09 0.01 0.2 0.05 0.25 0.15 0.05 0.02 0.08 0.03 0.01 0.03 0.02 0.01], whose length is greater than L. Both the received data are distorted no matter the cyclic prefix is added or not.
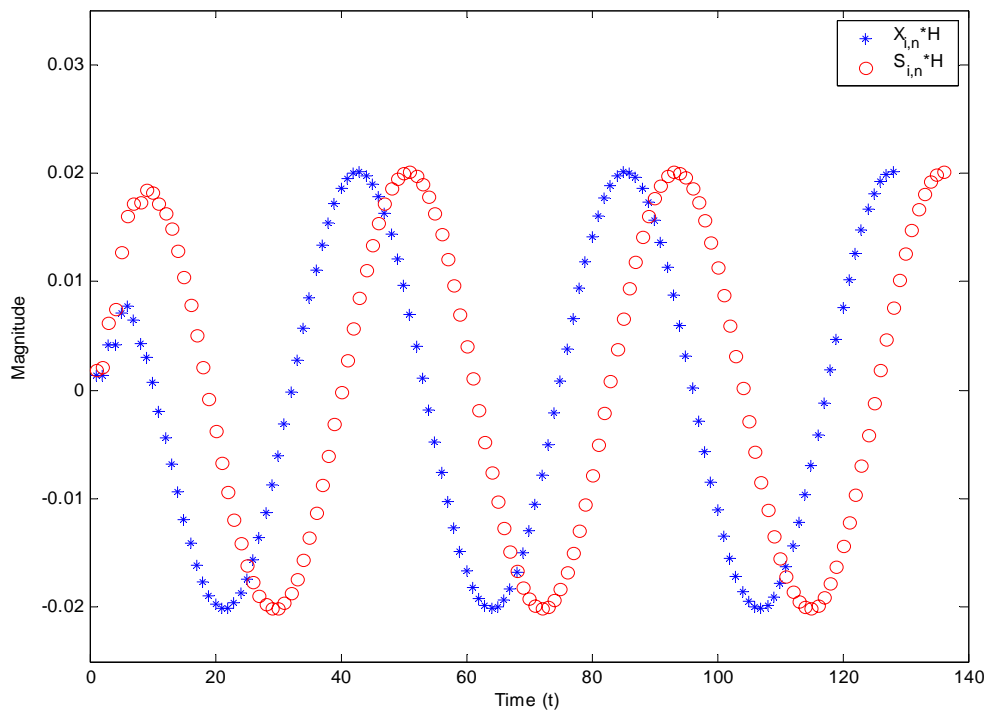
Figure 5.5 Received signal with channel length longer than that of cyclic prefix.

5.2.2 Kim's Approach and RISIC Performance in DMT-based VDSL

System

In this sub-section, the Kim's approach is applied to the DMT-based DSL system to observe that if it can be applied to this system. At first, a normal bit-loading number calculated according to the SNR parameter of each sub-channel are applied to the system, however, the symbol error rate performance of this system is not acceptable. By reducing the maximum allowed bit number in each sub-channel, the performance could be improved as shown in Fig. 5.6. Since the Kim's approach was proposed for the OFDM system with low-level QAM at each sub-channel, it is not suitable for our proposed DMT-based VDSL system with high-level QAM.
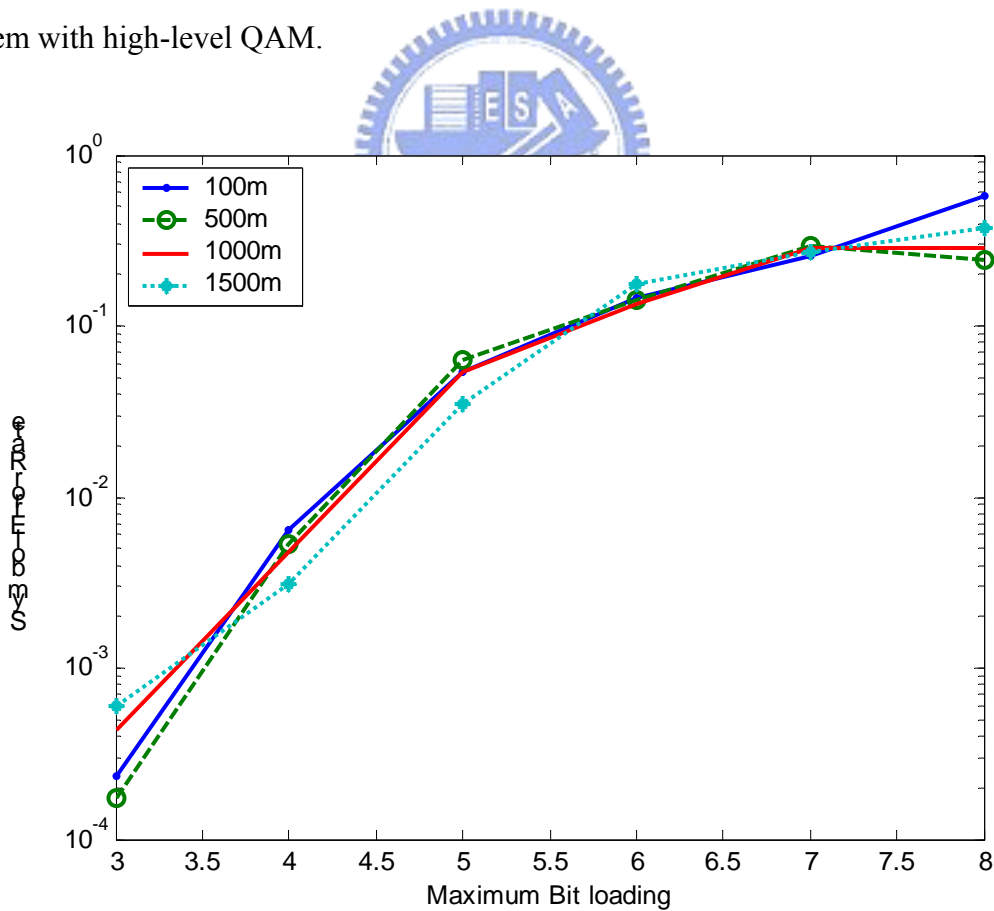
Figure 5.6 Bit loading vs. symbol error rate for Kim's approach.

Then, the RISIC algorithm is applied to the DMT-based VDSL system to see its performance. At first, if there is no cyclic prefix adding to the system, its performance is similar to the Kim's approach. However, since this algorithm can be applied to the system with different lengths of the cyclic prefix and its number of iterations can also be adjusted. Actually, the BER performance of the RISIC algorithm without iteration will be closed to that of traditional DMT-based system. For comparison, the simulation-results of the RISIC algorithms of the zeroth iteration are compared with the traditional DMT-based system, as shown in Fig. 5.7.

Figure 5.7 Performance comparison of RISIC (iteration 0) and traditional DMT technology.

However, the BER performance of the RISIC algorithm can be improved by increasing the iteration number except that if the guard interval length is zero, as shown in Fig. 5.8. On the other hand, if there is no cyclic prefix, the BER performance is greater than

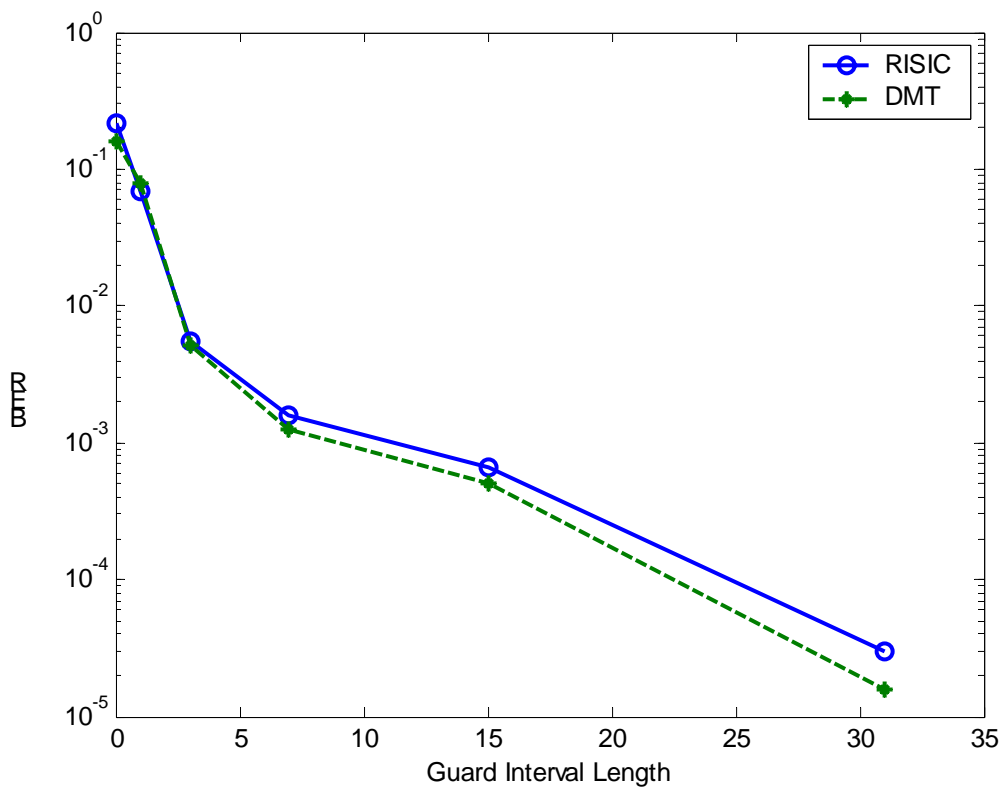one tenth no matter how many iterations are calculated, as shown in Fig. 5.8. Therefore, a new approach, IIC-ZP algorithm is proposed in this dissertation to improve the BER performance of the system without cyclic prefix. And its performance is discussed in the following sub-section.
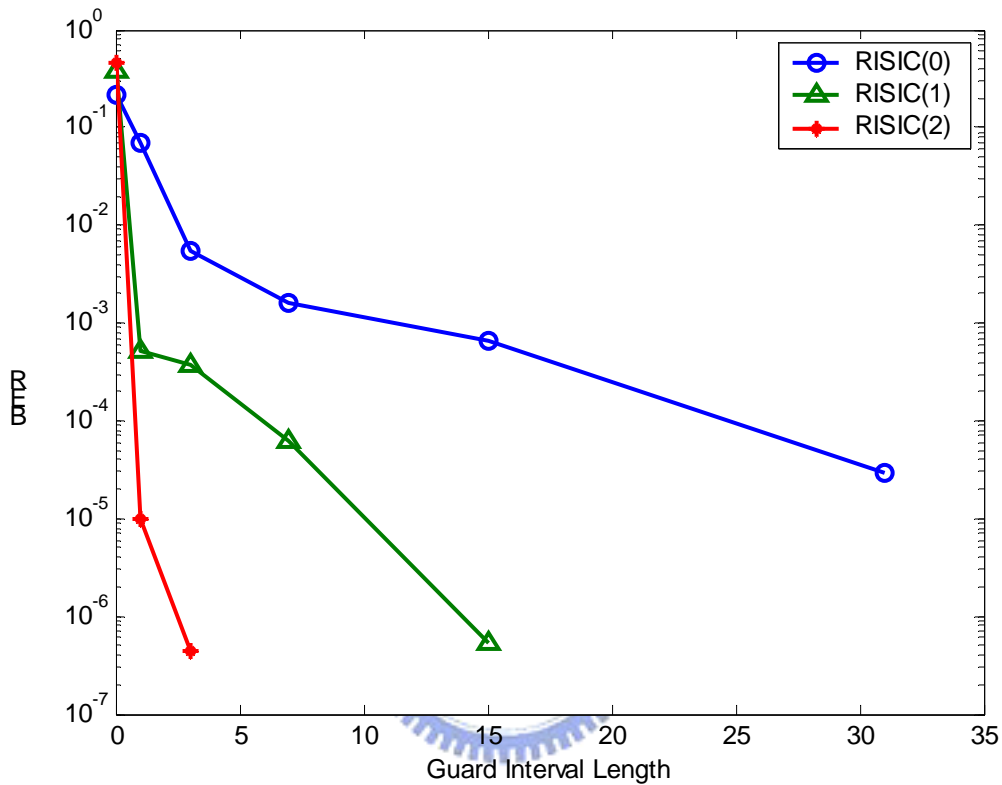
Figure 5.8 Performance comparison of RISIC algorithm with different iterations.

5.2.3 Performance Comparison of IIC-ZP and RISIC Algorithms

To evaluate the performances of the proposed IIC-ZP scheme, a 200-m gauge #26 test loop with -140 dBm/Hz AWGN have been simulated and compared to the traditional DMT and RISIC scheme. All the following simulations are based on the assumption that channel response at the receiver side is known. A 1024-QAM (10 bits) is used in each sub-channel. In simulations, the shorten impulse response type of TEQ [3] is used in the traditional DMT

system, and the energy ratio of the channel response power in the guard interval is 44 dB higher than outside the guard interval. While in RISIC and IIC-ZP system, the TEQ function is turned off during in this simulation. We simulated the systems with various guard interval lengths, from 0 to 32, and compare their BERs, as shown in Fig. 9. The performance of the IIC-ZP algorithm with two iterations, shown as IIC-ZP(2) in Fig. 9, is better than the traditional DMT system, which is plotted in dashed line. The value inside the parentheses means the number of iterations. For RISIC algorithm, the performances are plotted in dotted line for comparison. The performance of the IIC-ZP algorithm is close to that of the RISIC when the guard interval is greater than one but its performance is much better at zero guard interval case. If the recursive number is three, the guard interval length, L, can be reduced from 32 to 0 and the throughput can be increased to 6% (L/N+L, where N=512 and L=32).

The RISIC algorithm and IIC-ZP algorithm are able to process the received signals if the channel delay span is less than half of the symbol duration, and therefore the TEQ function block can be eliminated at the receiver block. To see the deterioration of channel capacity by TEQ, the performances of IIC-ZP after the second iteration with/ or without TEQ are illustrated in Fig. 5.10, and the performance of conventional DMT is also plotted for comparison. From the simulation results, we can see that the system without TEQ module has better performance. This is because the TEQ module is used to shorten the channel, but it also changes channel characteristics at the same time, and that may degrade the system performance.

From the above simulations, both the RISIC and our proposed IIC-ZP algorithms can be applied to a DMT VDSL system to improve the performance without decreasing the channel capacity by adding TEQ module and extend the usable bandwidth by reducing the length of guard interval. In addition, for the system without guard interval, our proposed IIC-ZP algorithm performs much better than the RISIC algorithm.

In summary, the RISIC algorithm and its modification IIC-ZP algorithm are applied to the high bit-loading DMT VDSL system. Their performances are compared with the traditional DMT system. These algorithms provide a more complete ISI cancellation scheme because they try to cancel all the ISI, including those outside the guard interval, i.e., residual ISI. Both the system performance and throughput can be improved at a reasonable cost of complexity increase.
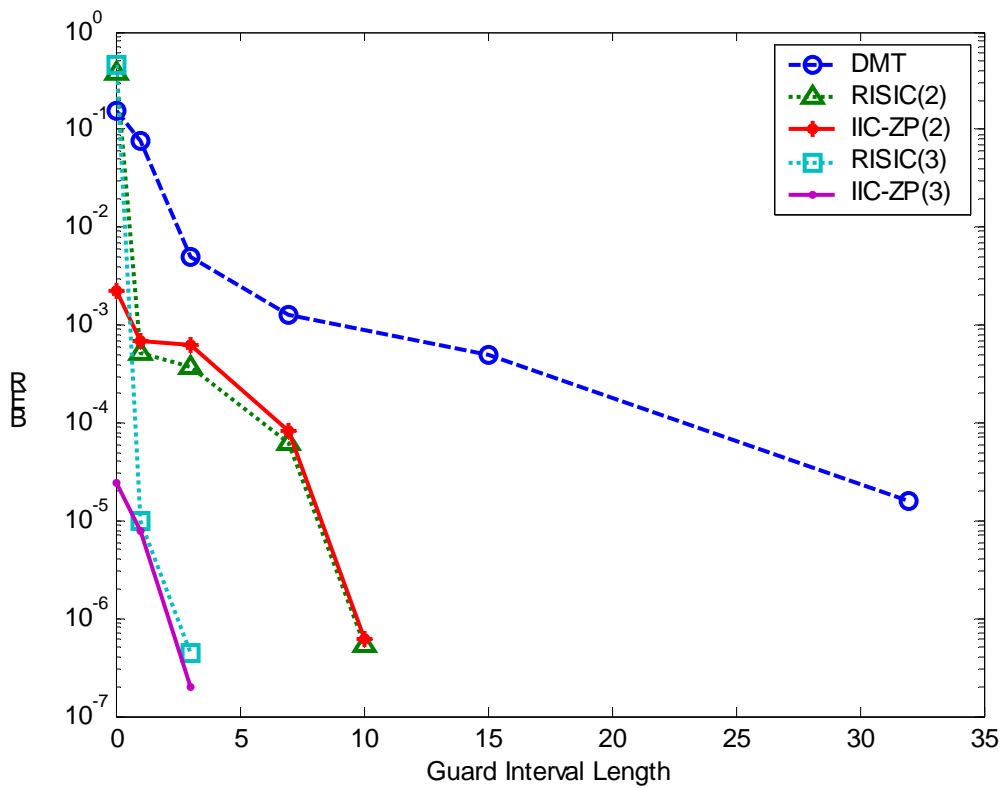
Figure 5.9 Performance comparison of DMT, RISIC and IIC-ZP receiver.
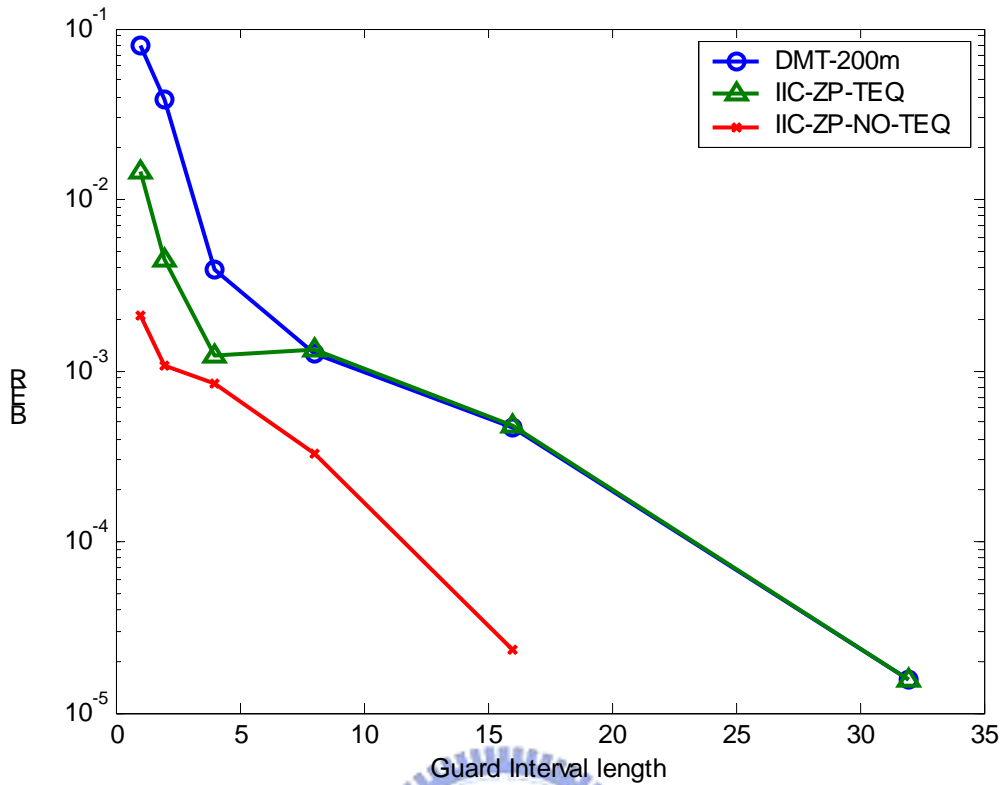
Figure 5.10 Performance comparison of IIC-ZP receiver with or without TEQ.

5.2.4 Residual ISI and Symbol Error Rate

From the previous derivations and simulations, it is clear that the ISI can degrade the BER performance of the DMT-based VDSL system. In this section, the effects of the ISI to the BER performance are discussed. First, a channel model is formulated with long tail of channel impulse response with length M such that it can create different level of residual ISI. For example, both a sine and reciprocal functions are selected to create the channel modeling as in equation (5.19). The corresponding waveform of this channel response is plotted in Fig. 5.11 with channel length equals to 80, i.e., M=80.

$$H(n) = \begin{cases} 0 & n = 1 \\ 0.1 \cdot \sin\left(2.5 \cdot \pi \cdot (n-2)\big/M\right) & 2 \le n \le 7 + M/5 \\ H(n) = 0.64\big/\left(0.8 \cdot (n - M/5)\right) & 8 + M/5 \le n \le M \end{cases} \quad \dots\dots\dots\dots\dots\dots(5.19)$$
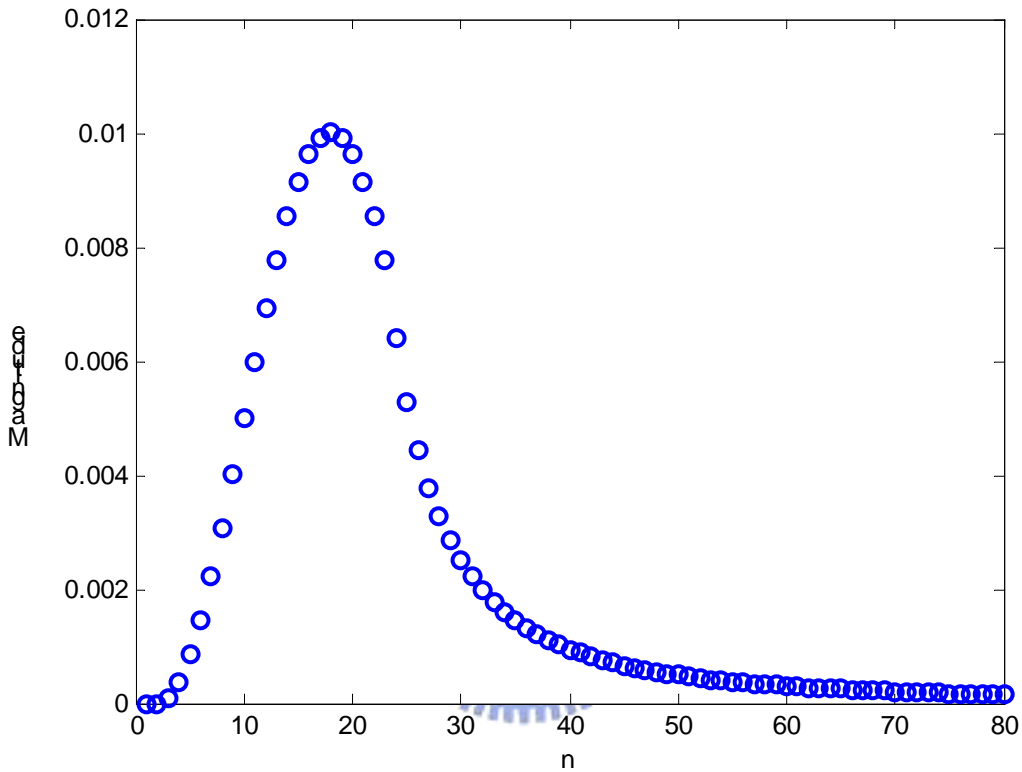
Figure 5.11 Channel response for residual ISI influence study.

The residual ISI is caused by the tail of channel response outside the guard-interval. To study the relationship of the residual ISI and the BER performance, the tail inside the guard interval energy ratio to the total channel is calculated first, as shown in Fig. 5.12. For clearly observation, the illustration is divided into four sections. The x-axis 'n' is the length of the guard interval while the y-axis is the ratio.
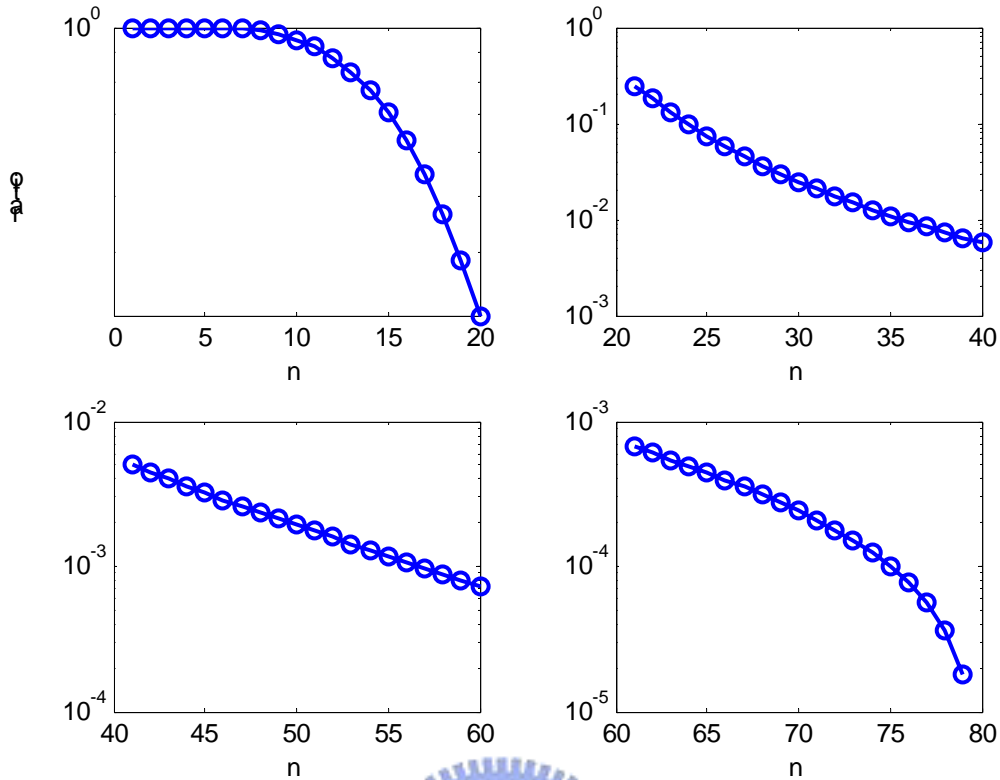
Figure 5.12 Energy ratio over various cyclic prefix lengths.

At first, the IIC algorithm is applied on the DMT-based system to show the BER performance with various guard interval length from 1 to M as well as different iteration times.

Fig. 5.13 shows part of the simulation results of the first iteration IIC algorithm with guard interval length from 48 to 76. In Fig. 5.14, the corresponding energy ratio outside the guard interval is plotted for reference. It can be seen from the simulation that if the energy ratio outside the guard interval is less than 8.0×10^{-4}, the BER is greater than 10^{-1}. Then the BER is improved from 10^{-1} to 10^{-7} as the energy ratio is changed from 2.1×10^{-3} to about 5.5×10^{-5}.
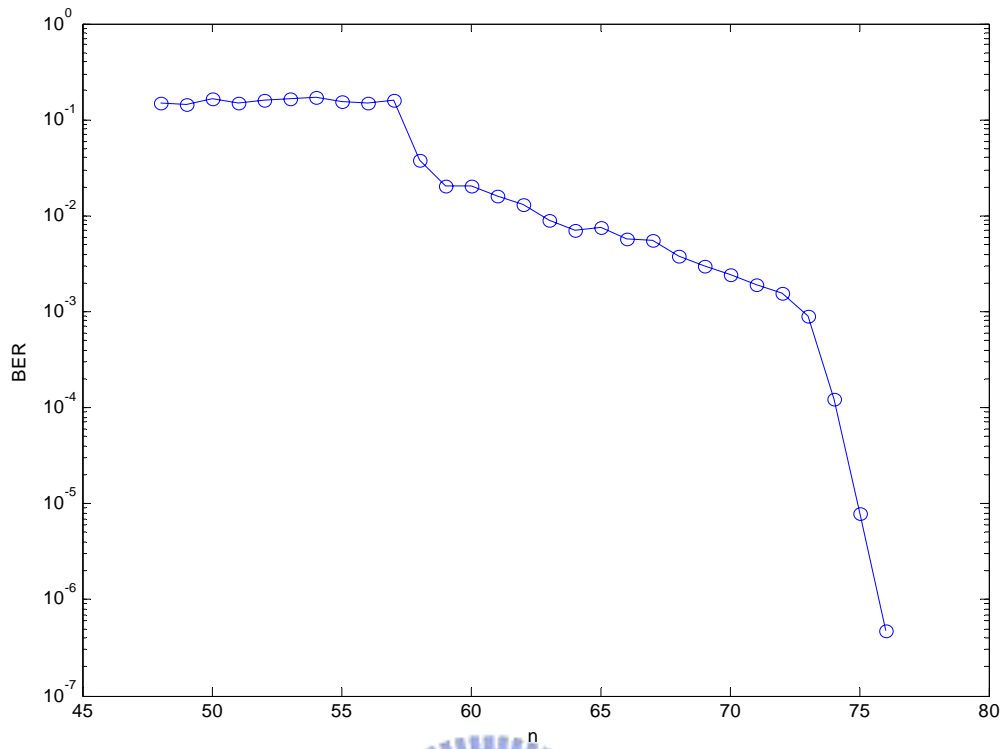
Figure 5.13 BER performance of the first iteration IIC algorithm.
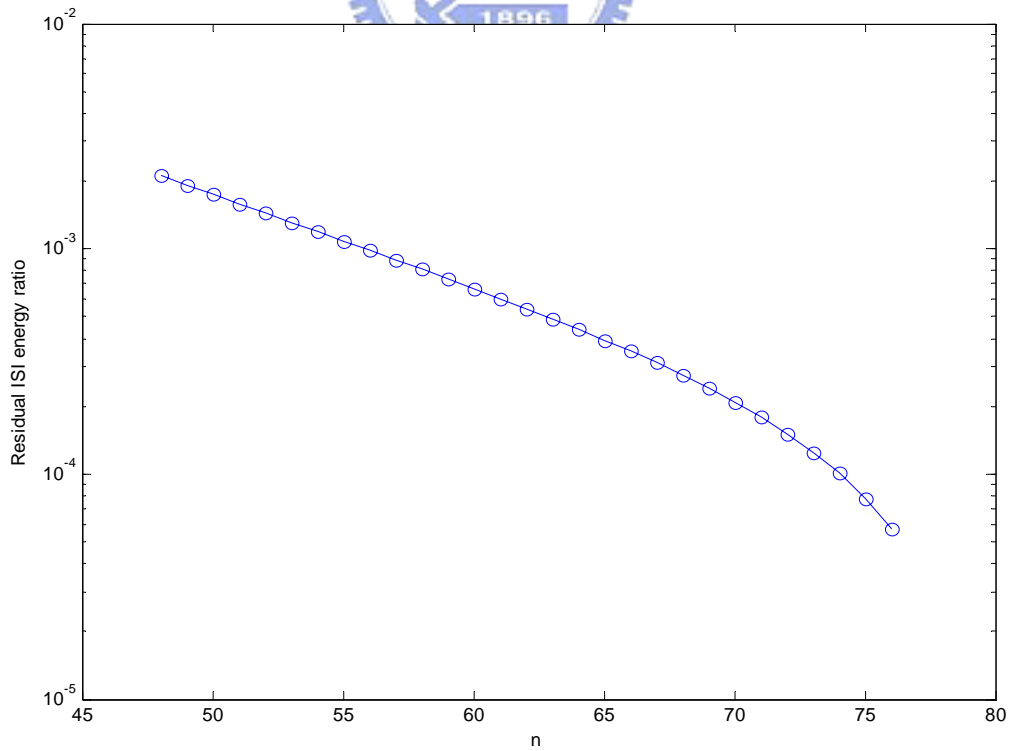
Figure 5.14 Corresponding residual ISI energy ratio.

Similarly, Fig. 5.15 shows part of the simulation results of the second iteration IIC algorithm with guard interval length from 27 to 36. In fig 5.16, the corresponding energy ratio inside the guard interval is plotted for reference. The BER is improved from 2×10^{-3} to 10^{-6} as the residual energy ratio is changed from 3.7×10^{-2} to about 8×10^{-3}.
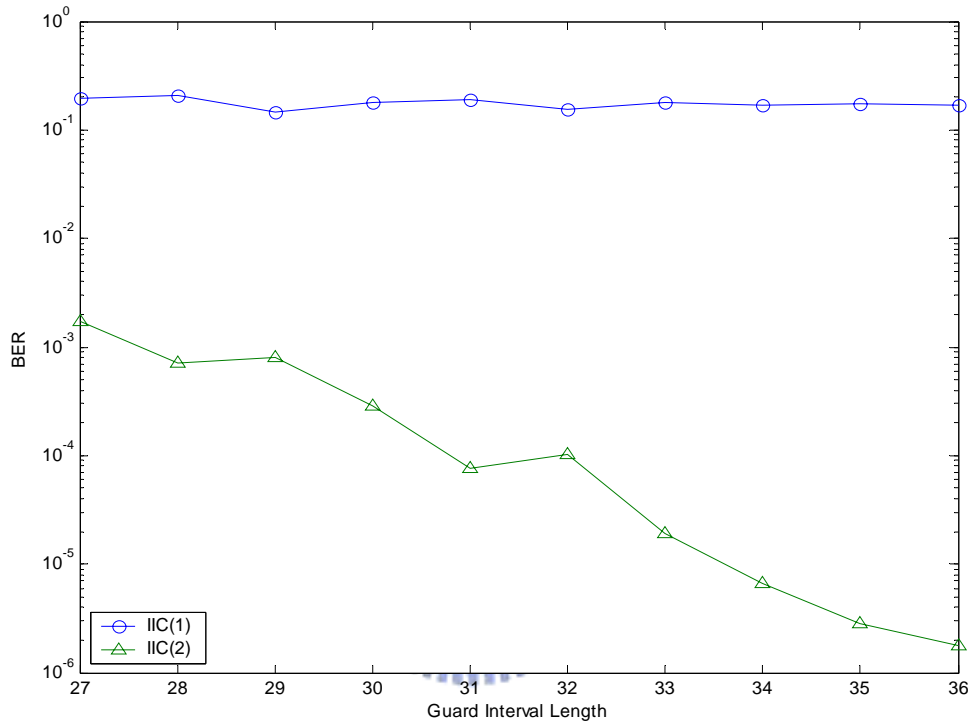
Figure 5.15 BER performance of the IIC algorithm with one and two iterations.
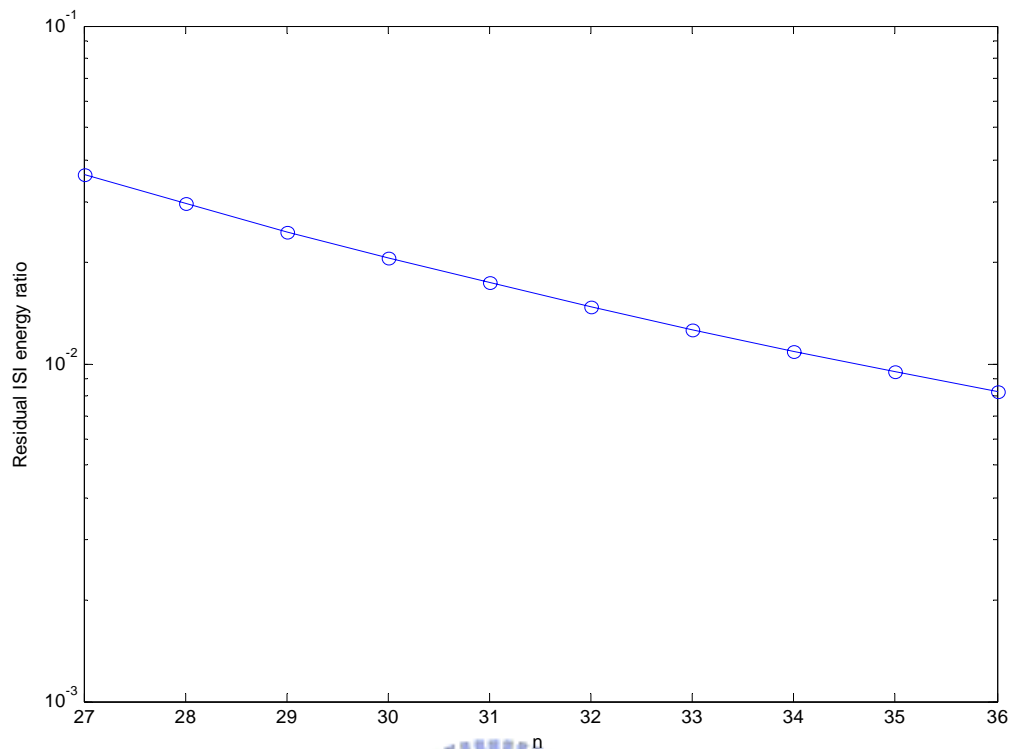
Figure 5.16 Corresponding residual ISI energy ratio.

5.3 Summary

In this chapter, the RISIC algorithm and its modification, IIC-ZP algorithm, are applied to the high bit-loading DMT VDSL system. Their performances are compared with the traditional DMT system. These algorithms provide a more complete ISI cancellation scheme than that only using cyclic prefix approach. Both the system performance and throughput can be improved at a reasonable cost of complexity increase. Also, the relationship between the residual ISI and the BER performance are studied by simulations.

Chapter 6

Conclusions and Future Works

In this dissertation, basing on the architecture of traditional DMT-based ADSL system, the DMT-based VDSL system is proposed. To upgrade the ADSL system to achieve the VDSL range of transmission throughput, the transmission bandwidth should be extended according to the channel capacity formula [1]. To utilize more transmission bandwidth, either the FFT size or the symbol rate of each sub-channel should be enlarged, and both of these two approaches involve raising the sampling rate. In other words, the throughput of this system can be increased by upgrading the sampling rate. From the simulation results, it is also observed that raising the sampling rate can improve the system throughput, especially when the loop length is short. We proposed this idea at the very beginning [9] and currently the development of advanced DMT-based ADSL and VDSL system drive towards the same direction.

From the study of the channel characteristic of the twisted-pair loop, the loop's SNR decreases at high frequencies; therefore, extending the transmission bandwidth has its limitations. To observe the relationship between the sampling rate and the throughput, we perform a series of simulations by sweeping the sampling rate from low to high on several twisted-pair loops and obtain the optimal throughputs. The optimal throughputs under various interference and noise environments of this DMT-based VDSL system are also

studied. From those simulations, it can be seen that if the length of the twisted-pair line becomes shorter, the optimal throughput becomes larger. To achieve the optimal throughput, high-level QAM for each tone should be applied. For these high-level QAM applications, some algorithms that can improve the system performance are proposed.

A modified low-complexity ML frame boundary detection algorithm is proposed to reduce the influence of the precursor ISI effect. We derive some formula to prove that the maximum likelihood algorithm [38] introduces precursor ISI if it is applied to the DMT-based VDSL system. We propose a modification approach of the low-complexity ML algorithm to avoid the influence of precursor ISI. From the simulation results and the mathematical derivations, optimizing the frame boundary detection can raise the SNR of each tone at the receiver side, and thus improves the system performance, especially for high-level QAM system.

Since the precursor ISI will reduce the performance of the DMT-based VDSL system, then the residual ISI also has similar effect. We apply the RISIC algorithm to this DMT-based VDSL system and compare its performance with the traditional DMT technology. Since the influence of residual ISI effect can be reduced through the iteration processes, the BER performance can be improved by increasing the iteration number. We also propose a modified IIC algorithm which can improve the BER performance in a system without guard interval. To see the influence of the residual ISI, we also introduce a special channel model and simulate the relationship between the magnitude of the residual ISI and the BER performance. It is found that the residual ISI energy ratio should be under 10^{-3} to 10^{-4} if the BER performance at the range of 10^{-3} for the first iteration of the IIC algorithm. For better BER performance such as 10^{-6}, the residual ISI energy ratio should be no more than 6×10^{-6}. However, for the second iteration of the IIC algorithm, the residual ISI energy ratio can be raise to about 8×10^{-3} to reach the BER performance to 10^{-6}.

Although the DMT-based VDSL system has been commercialized today, most of our idea proposed before the ITU-T or ANSI standards and some of them are similar to the final standardizations. We hope that reducing the influence of ISI effect to improve the BER performance of the DMT-based VDSL system will be helpful to the overall system performance.

References

[1] W. Y. Chen, *DSL Simulation Techniques and Standards Development for Digital Subscriber Line Systems*. Indianapolis, IN: Macmillan Technical Publishing, 1998.

[2] *Standards Project for Interfaces Relating to Carrier to Customer Connection of Asym. Digital Subscriber Line (ADSL) Equipment*, ANSI Standard T1.413 Issue 2, Dec. 1998.

[3] B. R. Saltzberg, "Comparison of single-carrier and multitone modulation for ADSL applications," *IEEE Commun. Mag.*, vol. 36, no. 11, pp. 114-121, Nov. 1998.

[4] J. M. Cioffi, ed., "Very-high-speed digital subscriber lines - System requirements," *ANSI Contribution T1E1.4/98-043R6 Draft Technical Document*, Nov. 1998.

[5] V. Oksman and J. J. Werner, "Single-carrier modulation technology for very high-speed digital subscriber line," *IEEE Commun. Mag.*, vol. 38, no. 5, pp. 82-89, May 2000.

[6] F. Sjoberg, M. Isaksson, R. Nilsson, P. Odling, S. K. Wilson, and P. O. Borjesson, "Zipper – A duplex method for VDSL based on DMT," *IEEE Trans. Commun.*, vol. 47, no.8, pp. 1245-1252, Aug. 1999.

[7] K. S. Jacobsen, "Synchronized DMT (SDMT) for very high-speed digital subscriber line (VDSL) transmission," in *IEEE Global Telecommun. Conf. GLOBECOM'98*, vol. 2, 8-12 Nov. 1998, pp. 856-861.

[8] J. M. Cioffi, "A symmetrical digital subscriber lines," in the Communications Handbook, J. D. Gibson (Ed.), CRC Press Inc., pp. 450-479, 1997.

[9] W. Y. Zou and Y. Wu, "COFDM: An overview," *IEEE Trans. Broadc.*, vol. 41, no. 1, pp.1-8, 1995.

[10] S.-T. Lin and C.-H. Wei, "Optimal channel capacity analysis for DMT VDSL system of various symbol rates," in *IEEE Global Telecommun. Conf. GLOBECOM'01,* vol. 1, 25-29 Nov. 2001, pp.389-393.

[11] AWARE Inc., "ADSL2 and ADSL2+: The new ADSL standards," [online]. Available: http://www.aware.com/products/dsl/whitepapers04.htm

[12] "Some transmission characteristics of telephone cables used in the loop plant," *IBM T1D1 Contribution*, T1D1.3/86-003, 24 Jan. 1986.

[13] *Asymmetric Digital Subscriber Line Transceivers 2 (ADSL2)*, ITU-T Recommendation G.992.3, Jan. 2005.

[14] W. Y. Chen, "Twisted-pair channel models for VDSL," *Texas Instruments T1E1 contribution*, T1E1.4/96-134, 9 April, 1986.

[15] D. G. Messershmitt, "A Transmission Line Simulator Written in C," *IEEE Transcript on Selected Area in Communications*, Jan. 1984.

[16] "A technical report on high-bit-rate digital subscriber lines (HDSL)," *Texas Instruments T1E1 contribution*, T1E1.4/96-006, Working Draft, 22 April, 1986.

[17] K. Szechenyi, "On the NEXT and impulse noise properties of subscriber loops," in *IEEE Global Telecommun. Conf. GLOBECOM'89*, vol. 3, 27-30 Nov. 1998, pp. 1569-1573.

[18] J. H. W. Unger, "Near-end crosstalk model for line code studies," *Bellcore T1D1 Contribution*, T1D1.3/85-244, 12 Nov., 1985.

[19] M. Elder and W. Y. Chen, "Effects of NEXT and FEXT in the same cable," *BNR and Bellcore Joint T1E1 Contribution*, T1E1.4/93-220, Aug. 1993.

[20] J. Bingham and W. Y. Chen, "NEXT from T1 to ADSL and Vice Versa," *Amati and Bellcore Joint Contribution*, T1E1.4/93-178, Aug. 1993.

[21] I. P. Auer, "Channel Capacity of Subscriber Loops Considering Near-End Crosstalk as the Dominant Source of Noise," *Bellcore internal memorandum,* June 1988.

[22] J. T. Aslanis Jr. and J. M. Cioffi, "Achievable information rates on digital subscriber loops: Limiting information rates with crosstalk noise," *IEEE Trans. Commun.*, vol. 40, no. 2, pp. 361-372, Feb. 1992.

[23] J. W. Cook, R. H. Kirkby, M.G. Booth, K. T. Foster, D. E. A. Clarke and G. Young,

"The noise and crosstalk environment for ADSL and VDSL systems," *IEEE Commun. Mag.*, vol. 37, no. 5, pp. 73 -78, May 1999.

[24] J. J. Werner, "Impulse noise in the loop plant," in *IEEE Intl. Conf. Commun. ICC '90*, 16-19 April 1990, pp. 1734-1737.

[25] R. A. McDonald, "Report on Bellcore impulse noise study," *Bellcore T1D1 Contribution*, T1D1.3/87-25, 27 July, 1987.

[26] K. Kerpez and C. Valenti, "Impulse Noise Testing for ADSL Transceiver," *Bellcore T1E1 Contribution*, T1E1.4/93-034, 10 Mar. 1993.

[27] I. Kalet and S. Shamai, "On the capacity of a twisted-wire pair: Gaussian model," *IEEE Trans. Commun.*, vol. 38, no. 3, pp. 379-383, Mar. 1990.

[28] A. Wang, J. J. Werner and S. Kallel, "Effect of bridged taps on channel capacity at VDSL frequencies," in *IEEE Intl. Conf. Commun. ICC '99*, vol.1, 6-10 June 1999, pp. 236-245.

[29] G.-H. Im, "Performance of 51.84-Mb/s VDSL transceiver over the loop with bridge taps," *IEEE Trans. Commun.*, vol. 50, no. 5, pp.711-717, May 2002.

[30] S. V. Ahamed, P. P. Bohn, and N. L. Gottfried, "A tutorial on two-wire digital transmission in the loop plant," *IEEE Trans. Commun.*, vol. 29, no. 11, pp. 1554-1564, Nov. 1981.

[31] W. Y. Chen and D. L. Waring, "Applicability of ADSL to support video dial tone in the copper loop," *IEEE Commun. Mag.*, vol. 32, no. 5, pp. 102-109, May 1994.

[32] C. C. Chang, M. S. Wang and T. D. Chiueh, "Design of a DMT-based baseband transceiver for very-high-speed digital subscriber lines," in *IEEE Asia-Pacific Conf. Commun.*, 6-8 Aug. 2002, pp. 367-370.

[33] M. D. Nava and C. Del-Toso, "A short overview of the VDSL system requirements," *IEEE Commun. Mag.*, vol. 40, no. 12, pp. 82 –90, Dec. 2002.

[34] D. M. Krinsk, D. E. Veeneman and R. Olshansky, "Bandwidth selection for the very high-rate digital subscriber line (VDSL) system," in *IEEE Intl. Conf. Commun.*, vol. 3, June 1996, pp. 1432 –1436.

[35] *Test Procedures for Digital Subscriber Line (DSL) Transceivers*, ITU-T Recommendation G.996.1, Feb 2001.

[36] K. Vanbleu, G. Ysebaert, G. Cuypers, M. Moonen, and K. Van Acker, "Bitrate-maximizing time-domain equalizer design for DMT-based systems," *IEEE Trans. Comm.*, vol. 52, no. 6, pp. 871- 876, June 2004.

[37] S.-T. Lin and C.-H. Wei, "Precursor ISI-free frame synchronization for DMT VDSL system," *IEICE Trans. Comm.*, vol. 85-B, no. 8, pp. 1447-1454, Aug. 2002.

[38] J.-J. van de Beek, M. Sandel and P. O. Borjesson, "ML estimation of time and frequency offset in OFDM systems," *IEEE Trans. Signal Processing*, vol. 45, no.7, pp.1800-1805, July 1997.

[39] M.-H. Hsieh and C.-H. Wei, "A low-complexity frame synchronization and frequency offset compensation scheme for OFDM systems over fading channels," *IEEE Trans. Veh. Technol.*, vol. 48, no.7, pp.1596 -1609, Sept. 1999.

[40] J.-J. van de Beek, M. Sandel, M. Isaksson and P. O. Borjesson, "Low-complex frame synchronization in OFDM systems," in *Proc. IEEE Int. Conf. Universal Personal Commun.*, 6-10 Sept. 1995, pp. 982-986.

[41] R. Negi and J. Cioffi, "Blind OFDM symbol synchronization in ISI channels", in *Proc. IEEE GLOBECOM'98*, 8-12 Nov. 1998, pp. 2812-2817.

[42] T. Pollet and M. Peeters, "Synchronization with DMT Modulation," *IEEE Commun. Mag.*, vol. No. 4, pp 80-86, April 1999.

[43] S.-T. Lin and C.-H. Wei, "Iterative ISI cancellation for DMT-based VDSL systems," to be appeared in *International Journal of Electrical Engineering. 中國電機工程學刊.*

[44] D. Kim and G. L. Stuber, "Residual ISI cancellation for OFDM with applications to HDTV broadcasting," *IEEE J. Select Areas in Common.*, vol. 16, no. 8, pp. 1590-1599, Oct. 1998.

[45] J. Kim, J. Kang, and E. J. Powers, "A bandwidth efficient OFDM transmission

scheme," *IEEE Intl. Conf. on Acoustics, Speech, and Signal Processing ICASSP'02*, vol. 3, 13-17 May 2002, pp. 2329-2332.

[46] C. J. Park and G.-H. Im, "Efficient cyclic prefix reconstruction for coded OFDM systems," *IEEE Commun. Letters*, vol. 8, no. 5, pp. 274-276, May 2004.

[47] S. Trautman and N. J. Fliege, "Perfect equalization for DMT systems without guard interval," *IEEE J. Select Areas in Common.,* vol. 20, no. 8, pp. 987-996, June 2002.

[48] C. J. Park and G.-H. Im, "DMT/OFDM transmission with insufficient cyclic prefix," *IEEE Commun. Letters*, vol. 8, no. 9, pp. 576-578, Sept. 2004.

[49] S.-T. Lin and C.-H. Wei, "Precursor ISI-free frame synchronization for DMT VDSL system," in *Proc. APCC 2001*, Tokyo, Japan, 2001.

[50] B. Muquet, M. de Courville, P. Duhamel, G. B. Giannakis, and P. Magniez, "Turbo demodulation of zero-padded OFDM transmissions," *IEEE Trans. Comm.*, vol. 50, no. 11, pp. 1725-1728, Nov. 2002.

簡歷

姓名： 林尚亭

籍貫： 高雄市

出生： 中華民國 五十七 年 三 月 七 日

學歷：

國立交通大學電子工程學系學士 (75 年 9 月~79 年 6 月)

美國俄亥俄州立大學電機工程研究所碩士 (79 年 9 月~81 年 12 月)

國立交通大學電子研究所博士班 (84 年 9 月入學)

博士論文:

提升高速用戶迴路系統性能之研究
Performance Enhancement for DMT-based VDSL System: Precursor ISI-Free
Frame Synchronization, ISI Cancellation and Optimizing Throughput

Publication List

Journal Papers:

1. S. T. Lin and C. H. Wei, "Precursor ISI-Free Frame Synchronization for DMT VDSL System," *IEICE Trans. Comm.*, vol. 85-B, no. 8, pp. 1447-1454, 2002.

2. S. T. Lin and C. H. Wei, "Iterative ISI Cancellation for DMT-based VDSL Systems," *accepted for publication* in *IJEE*.

Conference Papers:

1. S. T. Lin and C. H. Wei, "Precursor ISI-Free Frame Synchronization for DMT VDSL System," *Proc. APCC 2001*, Tokyo, Japan, pp. 413-416, 2001.

2. S. T. Lin and C. H. Wei, " Optimal channel capacity analysis for DMT VDSL system of various symbol rates," *Proc. IEEE Globecom'01, San Antonio, U.S.A.*, pp.389- 393, Nov. 2001.

3. S. T. Lin and I. C. Hwang, "Analysis of hybrid fibers in high bit rate optical transmission system" *Proc. IEEE CLEO/Pacific Rim 2003*. Vol.1, pp. 213, Dec. 2003.